Title

Profiling and Targeting Surface Biomarkers in Cellular Senescence, Hypoxic PDAC, MEKi-Treated Melanoma, and Antigen-Presenting Cells

Author

Rettko, Nicholas Joseph

Publication Date

2022

Peer reviewed|Thesis/dissertation

Profiling and Targeting Surface Biomarkers in Cellular Senescence, Hypoxic PDAC, MEKi-Treated Melanoma, and Antigen-Presenting Cells

by
Nicholas Joseph Rettko

DISSERTATION
Submitted in partial satisfaction of the requirements for degree of
DOCTOR OF PHILOSOPHY

in

Chemistry and Chemical Biology

in the

GRADUATE DIVISION
of the
UNIVERSITY OF CALIFORNIA, SAN FRANCISCO

Approved:

DocuSigned by:
James Wells
5F2F4D1A06164C2...

James Wells
Chair

DocuSigned by:
Davide Ruggero
[illegible]

Davide Ruggero

DocuSigned by:
Judith Campisi
[illegible]

Judith Campisi

DocuSigned by:
Kole Roybal
D4E558B3B71948B...

Kole Roybal

Committee Members

This work is dedicated to my science teachers and mentors Mrs. Betty Olszewski, Mrs. Jamie Lemminger, and Dr. James Checco, who have inspired me and ignited my passion for the chemical sciences – and to all the science teachers who inspire future scientists.

Acknowledgements

There have been several individuals who have played roles in impacting both my professional and personal development throughout the course of completing this work. “It takes a village” is a gross understatement. Without the support of these individuals, it is difficult to imagine that I would have grown into the scientist I am today. They have pushed me to think more creatively and critically, to question the boundaries of what is scientifically possible, and to work diligently in producing convincing data to support my hypotheses.

First, I thank my partner Jake who has supported me from 2,000 miles away for almost 4 years while I worked towards my goal of attaining a Ph.D. Without your endless love and support, I could not have made it as far as I have today. To say you have been a rock is a vast understatement and no recognition will ever be enough to express my gratitude. Second, I would like to thank my family, who has supported me throughout my entire education and never once questioned my ambitions in the sciences. From a young age you’ve always cheered me on and helped me every step of the way. I could not have done this without you.

I’ve been graced with so many amazing teachers and mentors throughout my life that have inspired me and molded me into the scientist I am today. To my science teachers Mrs. Betty Olszewski and Mrs. Jamie Lemminger, to whom this thesis is dedicated, thank you for your dedication and tireless effort to educate and inspire. Because of you I found my place and passion for science, and I’m confident I’m just one of the many scientists you’ve inspired. To Dr. Sam Gellman, my undergraduate research advisor, thank you for taking a chance on me and allowing me to join your lab my sophomore year. It was here I found my passion for scientific research and I would not be writing this thesis without your commitment to younger students and providing them with amazing opportunities. Lastly, to Dr. James Checco, my graduate student

mentor in the Gellman Lab to whom this thesis is also dedicated, thank you for taking me under your wing and teaching me the scientific rigor and creativity necessary to conduct research. It was the confidence you had in me as an undergraduate to be independent enough perform on my own and even mentor others that gave me the confidence in myself to go on to continue a doctorate in chemical biology.

There are many people to specifically thank who have been part of the UCSF community. To Dr. Jim Wells, my advising professor and dissertation chair, thank you for taking a chance on me and allowing me to join your lab. The lab you've created is one in a million, with unlimited creativity and endless support. Thank you for creating a lab environment that encourages coming up with ideas. I would also like to thank you for your limitless optimism and support. Without that, this work surely would not have been possible. I look forward to many more years working together. To Drs. Judith Campisi, Kole Roybal, and Davide Ruggero, my thesis committee members – thank you for all your support, invaluable insight, and thought-provoking questions that have propelled these projects forward. I can't thank you all enough. I would also like to thank members of my qualifying exam committee, Drs. Davide Ruggero, Martin Kampmann, and Lewis Lanier.

Alongside the professors that have supported me, I am grateful to the various members of the Wells lab that have helped me along the path of obtaining my PhD. This list is long and speaks to the unique environment that has been created in our lab – Dr. Zach Hill, my rotation mentor; Dr. Alex Martinko, who not only taught me everything I know about phage display, but also was an amazing friend and colleague my first 4 years of graduate school; Dr. Sam Pollock, who gave sage life advice and kept me in check; Dr. Kevin Leung, who taught me how to perform surfaceomics; Dr. Jamie Byrnes, who gave countless pointers on mass spectrometry and

experimental set up, and especially helped me learn how to craft a paper; Susanna Elledge, Irene Lui, Paige Solomon, and Kata Pance, whose friendship made me excited to go to lab every day and kept me sane throughout my years in graduate school; and to all the members of the Wells Lab who I couldn't fit here who helped me and answered my endless questions. Words can't express my gratitude to you all.

Outside of my labmates, there were many peers at UCSF that made this a fun environment to pursue our PhDs in. In particular, my CCB cohort: Dr. Emily Kang, Dr. Ryan Tibble, Sergei Pourmal, Fatima Ugur, and Peter McTigue. Although we were neither seen nor heard, you'll never be forgotten. I can't wait to have you as my friends as we continue our futures in the sciences.

Finally, I'd like to thank the institutions who believed in my work enough to provide funding for it - specifically, National Science Foundation Graduate Research Fellowship. Additionally, I'd like to thank the UCSF Grad Division who awarded me a travel award that helped make it possible for me to give an oral presentation at the International Cellular Senescence Association's conference in Athens, Greece. It is something I will truly never forget.

Contributions

Chapter 1: Unpublished work that has not yet been submitted for publication. Nicholas J. Rettko designed and executed the experiments. Nicholas J. Rettko, Judith Campisi, and James A. Wells conceptualized the project and experiments. James A. Wells oversaw the project.

Chapter 2: Adapted version of unpublished work that has been submitted for publication: Rettko NJ, Camisi J, and Wells JA. Engineering Antibodies Targeting p16 MHC-peptide complexes.

Chapter 3: Unpublished work that has not yet been submitted for publication. Nicholas J. Rettko and Lisa L. Kirkemo designed and executed the experiments. Nicholas J. Rettko, Lisa L. Kirkemo, and James A. Wells conceptualized the project and experiments. James A. Wells oversaw the project.

Chapter 4: Adapted version of unpublished work that has been submitted for publication: Stopfer LE*, Rettko NJ*, Leddy O, Mesfin JM, Brown E, Winski S, Bryson B, Wells JA, White FM. MEK inhibition enhances presentation of targetable MHC-I tumor antigens in mutant melanomas. *Denotes equal contribution to this work. Stopfer LE performed all mass spectrometry analysis, target triage, and viability assays. Rettko NJ performed all antibody selections, characterization, development, and downstream engineering and design.

Chapter 5: Unpublished work that has not yet been submitted for publication. Nicholas J. Rettko designed and executed the experiments. Nicholas J. Rettko, Miguel Álvaro-Benito, James A. Wells, and Christian Freund conceptualized the project and experiments. James A. Wells oversaw the project.

Profiling and Targeting Surface Biomarkers in Cellular Senescence, Hypoxic PDAC, MEKi-Treated Melanoma, and Antigen-Presenting Cells

Nicholas J. Rettko

Abstract

Cells are constantly encountering damaging reagents and undergoing damaging processes, all of which compromise the integrity of the cell. Luckily, our cells are equipped with repair mechanisms that can combat the damage and return the cell to a healthy state. However, these mechanisms are not fully efficient and over time cells will accumulate damage until they become pro-tumorigenic. These cells can then go on to become cancerous and lead to tumors. Fortunately, our cells have back up mechanisms to prevent these potentially cancerous cells from dividing, which ultimately manifest in a phenotype termed cellular senescence. Cells that have undergone senescence are put under permanent cell-cycle arrest, and secrete a number of factors to initiate removal through immune cell clearance. Yet, over time senescent cells will accumulate and with sustained secretion of inflammatory molecules drive a host of aging phenotypes. Therefore, discovering biomarkers for senescence that can be used to target senescent cells is important for both senescent cell identification and potential senolytic strategies. Monoclonal antibodies have been useful tools in distinguishing cell populations by binding to disease-associated extracellular biomarkers on the surface of cells. In this thesis, we look at a number of membrane proteins, in particular MHC-peptide complexes, that could serve as biomarkers for cellular senescence and those cells that have bypassed senescence to become cancer. In Chapter 1, we perform surface proteomics of senescent fibroblasts and identify the membrane protein GGT1 as a potential marker for senescence. In Chapter 2, we develop antibodies against MHC-

peptide complexes containing the senescence-associated protein p16. In Chapter 3, we design a novel secreted HLA Fc-fusion construct that can be coupled with mass spectrometry to profile the immunopeptidome of disease-phenotypes, including senescence and hypoxia. In Chapter 4, we use MEKi-modulation of the immunopeptidome in melanoma to identify targetable MHC-peptide complexes that can be leveraged to increase cytotoxicity of melanoma cells. In Chapter 5, we expand our antibody development into class II MHC-peptide complexes and engineer antibodies that can recognize MHC-peptide complexes with differential orientations in the peptide binding groove.

Table of Contents

List of Figures

List of Tables

List of Abbreviations

ADC – Antibody-drug conjugate

ADCC – Antibody-dependent cellular cytotoxicity

APC – Antigen presenting cell

BiTE – Bispecific T cell engager

BLI – Biolayer interferometry

BRAF – Serine/Threonine-protein kinase B-raf

BRAFi – BRAF inhibitor

CAR – Chimeric antigen receptor

CCPG1 – Cell cycle progression protein 1

CD3 – Cluster of differentiation 3

CD44 – Cluster of differentiation 44

CDK4 – Cyclin-dependent kinase 4

CDK6 – Cyclin-dependent kinase 6

CLIP – Class Ii-associated invariant chain peptide

DDA – Data dependent acquisition

DCT – Dopachrome tautomerase

Dox - Doxycycline

DPP4 – Dipeptidyl peptidase 4

DYH11 – Dynein axonemal heavy chain 11

EGFR – Epidermal growth factor receptor

ELISA – Enzyme-linked immunoassay

ER – Endoplasmic reticulum

ERK – Extracellular signal-regulated kinases

FBS – Fetal bovine serum

FDR – False discovery rate

FOXO4 – Forkhead box protein O4

GDF15 – Growth differentiation factor 15

GGT1 – Gamma-glutamyltransferase 1

GFP – Green fluorescent protein

Gp100/PMEL – Premelanosome protein

GSTM2 – Glutathione S-transferase mu 2

HA - Human influenza hemagglutinin

HER2 – Human epidermal growth factor receptor 2

hipMHC – Heavy isotope-labeled peptide MHC's

HLA – Human leukocyte antigen

HLA-DM – human leukocyte antigen DM

ICI – Immune checkpoint inhibitor

IEDB – Immune epitope database

IF44L – Interferon induced protein 44 like

IFN - Interferon

IGF2R – Insulin like growth factor 2 receptor

IgG – Immunoglobulin G

IL-6 – Interleukin 6

IL-8 – Interleukin 8

irAEs – Immune related adverse events

IS-PRM/SureQuant – Internal-standard triggered parallel reaction monitoring data acquisition

ITGB3 – Integrin beta-3

KAD4 – Adenylate kinase 4

K_D – Binding affinity

K_{off} – Dissociation rate

K_{on} – Association rate

MAGE – Melanoma antigen

MAPK – Mitogen-activated protein kinase

MEK – Mitogen-activated protein kinase kinase

MEKi – Mitogen-activated protein kinase kinase inhibitor

MHC – Major histocompatibility complex

MICA – MHC class I polypeptide-related sequence A

MLANA – Protein melan-A

MME – Membrane metallo-endopeptidase

NFAT – Nuclear factor of activated T cells

NRAS – Neuroblastoma RAS

P16 – Cyclin-dependent kinase inhibitor 2A

P21 – Cyclin-dependent kinase inhibitor 1A

P53 – Tumor protein 53

PBMC – Peripheral blood mononuclear cell

PDAC – Pancreatic ductal adenocarcinoma

PFS – Progression-free survival

PGH2 – Prostaglandin H2

PI3K – Phosphoinositide 3-kinase

PKT7 – Tyrosine-protein kinase-like 7

pMHC – Peptide MHC or MHC-peptide complex

PVR – Polio virus receptor

RTN4 – Reticulon 4

SASP – Senescence-associated secretory phenotype

scDb – Single-chain diabody

scFab – Single-chain Fab

scFv – Single-chain variable fragment

SEC – Size exclusion chromatography

sEV – Small extracellular vesicle

sHLA – Secreted HLA

SILAC – Stable isotype labeling by amino acids in cell culture

SPAG4 – Sperm associated antigen 4

STAT1 – Signal transducer and activator of transcription 1

TAA – Tumor-associated antigen

TCR – T cell receptor

TEV – Tobacco etch virus

TMEM132A – Transmembrane protein 132A

TMEM2 – Transmembrane protein 2

TNF-α – Tumor necrosis factor alpha

TNFRSF10D – Decoy receptor 2

TRYP1 – Tyrosinase related protein 1

TXNIP – Thioredoxin-interacting protein

TYR - Tyrosinase

uPAR – Urokinase plasminogen activator surface receptor

WT1 – Wilms tumor 1

Chapter 1

Characterizing the surface proteome of senescent cells for novel biomarkers

Abstract

Accumulation of senescent cells, or cells under permanent proliferation arrest, has long been linked to aging and tissue dysfunction. Therefore, identifying protein targets on senescent cells has great therapeutic potential for aging and improving quality of life. Despite extensive study into the proteome of senescent cells, a specific surface biomarker has remained elusive, thereby limiting study of senescence *in vivo*. Through a LC-MS/MS analysis of membrane proteins pulled down from isotopically labeled fibroblasts, we have identified a number of surface proteins up-regulated in cellular senescence. Utilizing our phage display technology, we were able to generate >30 unique Fabs in total specific to the extracellular domains of 8 membrane proteins up-regulated in senescent cells. We engineered Doxycycline-inducible over-expression cell lines for each of these antigens and showed that our antibodies are capable of binding to their respective antigens on cells. When staining the surface of growing and senescent A549 cells, GGT1 showed up-regulation and appeared to be a specific marker for cellular senescence. Hence, GGT1 may be a valuable marker for senescence and warrants further study, including if antibodies targeting GGT1 can be used in senolytic strategies.

Introduction

Cellular senescence, defined as permanent cell-cycle arrest, is an anti-tumor mechanism evolved to halt the progression of premalignant cells from expanding and progressing to cancer[1,2]. A number of stresses induce senescence, including critically short or dysfunctional telomeres (often termed replicative senescence)[3,4], physical DNA damage such as double-strand breaks[5], the expression of certain oncogenes[6], and mitochondrial dysfunction[7]. Upon initiation of cell-cycle arrest, senescent cells secrete numerous cytokines, chemokines, growth factors, and metalloproteases collectively known as the senescence-associated secretory phenotype

(SASP)[8,9]. The SASP further solidifies the senescent phenotype via autocrine and paracrine mechanisms[8,10,11], and ultimately can attract natural killer cells[12,13], macrophages[14], and $CD8^+$ T cells for clearance[15]. Once the senescent cell is cleared, the surrounding cells can propagate and return the tissue to a normal, healthy state, effectively eliminating the pro-tumorigenic threat[16]. However, these mechanisms are not fully efficient, and over time senescent cells accumulate, leading to sustained secretion of inflammatory molecules such as IL-6, IL-8, and TNF-α[7,8]. This chronic inflammation, coined inflammaging, both desensitizes the immune system and results in pronounced tissue dysfunction[17,18]. As such, senescence is associated with a host of age-related diseases including diabetes[16,19], Alzheimer's disease[18,20], glaucoma[16], and cardiac dysfunction[21]. Hence, novel strategies to eliminate senescent cells, also known as senotherapy or senolytics, are of great interest to the anti-aging field[2].

Although senescent cells commonly share several features such as increased lysosomal beta-galactosidase activity, increased size, activation of damage-sensing signaling pathways, upregulation of pro-survival pathways, and a secretory phenotype, senescence is notorious for lacking a single universal biomarker[22–24]. Therefore, identification of senescent cells, particularly *in vivo*, has remained a challenge. Antibodies targeting surface proteins enriched in senescent cells could not only fill this void, but also potentially provide scaffolds for further senolytic strategies.

Here, we describe a surface proteomics analysis of senescent IMR90 fibroblasts induced through senescence through irradiation and mitochondrial dysfunction. This proteomics analysis identified several previously identified and novel up-regulated membrane proteins in senescent cells. From this list, we pursued a phage display campaign to generate antibodies targeting a collection of senescence-associated membrane proteins. Using a Doxycycline-inducible over-

expression cell line for each antigen, we show our antibodies to be specific and able to recognize their respective antigen on the surface of cells. Staining of growing and senescent A549 lung cancer cells revealed the membrane protein GGT1 to be up-regulated in senescence, indicating the potential of this protein as a novel biomarker for cellular senescence.

Results

Surface Proteomics of Senescent IMR90 Fibroblasts

While senescent cells share the common feature of cell-cycle arrest, differential SASP signatures can manifest depending on how the senescent phenotype was induced[7,8]. For example, recent studies have revealed that senescence induced via mitochondrial dysfunction has a unique, yet overlapping, SASP profile as that driven by a DNA-damage response[7]. Given this trend, we hypothesized the surface proteome of senescent cells would be reflected similarly, but that cells differentially induced into senescence may share common proteins that could serve as reliable biomarkers for the senescent phenotype.

To generate our cell models, we chose IMR90 fibroblasts as these are a commonly used and accepted cell line in the study of cellular senescence. Using stable isotope labeling with amino acids in cell culture (SILAC), we labeled IMR90 fibroblasts in "light" or "heavy" media. In order to identify biomarkers of senescence rather than just a non-proliferative state, we serum-starved "heavy" IMR90 fibroblasts for 3 days to drive them into quiescence, or a temporary cell-cycle arrest (**Figure 1.1A**). "Light" IMR90 fibroblasts were driven into senescence through irradiation (10 Gy) or 50 nM Antimycin A. Irradiated cells received a singular treatment while Antimycin A-treated cells were continuously cultured in media with drug (**Figure 1.1A**). After 10 days, senescent cells were harvested and pooled with quiescent cells. Senescence was confirmed by staining for beta-galactosidase activity (**Figure 1.2**). Surface proteins were labeled

through oxidation of glycans and subsequent tethering of biotin with biocytin-hydrazide. Proteins were captured with streptavidin beads and enzymatically processed with trypsin and PNGaseF. Processed peptides were purified and analyzed via mass spectrometry. Identified peptides were filtered for proteins containing transmembrane domains and quantified in SkyLine using an established pipeline[25].

Relative quantification revealed a number of proteins that were up-regulated in cellular senescence vs. quiescence (**Figure 1.1B**). Excitingly, this list included several proteins previously reported to be up-regulated in senescence, including DPP4[26], IGF2R[27], TNFRSF10D[28,29], MICA[2,13,28], PVR[30], and ITGB3[31]. Interestingly, there were proteins found to be up-regulated in senescence regardless of means of induction. MICA is a ligand for receptors on natural killer cells, indicating this protein may be universally expressed in senescent cells as a means of initiating immune cell clearance[13]. However, several of these proteins have no established role in cellular senescence, making them interesting candidates for further investigation. Of these proteins, TMEM2 and TMEM132A were biologically interesting as they are typically expressed in response to stress and could play important roles in the initial onset and/or maintenance of the senescent phenotype[32,33]. In the end, we chose to 9 proteins to further pursue in a phage display campaign (in bold, **Figure 1.1B**).

Interestingly, there were several proteins down-regulated in senescent cells that have previously been reported to be expressed in cancers, such as MME, PKT7, and EGFR (**Figure 1.1C**)[34]. As cancer is typically defined as uncontrolled cell proliferation, it is intriguing that several markers for aggressive cell growth were shown to be down-regulated in cells under permanent cell-cycle arrest. These striking differences highlight potential roles these proteins

play under different biological contexts and further demonstrate how senescent cells may establish the phenotype.

Generating and Validating Antibodies Against Potential Markers for Senescence

For each of the nine proteins of interest, Fc-fusion proteins were engineered by fusing the extracellular domain of the membrane protein to a human IgG1 Fc domain with a TEV protease site in the linker connecting them. All Fc-fusions contain a C-terminal AviTag to biotinylate and immobilize constructs on streptavidin beads throughout the phage display process (**Figure 1.3A**). Using a Fab-phage library, we first performed a negative clearance using a biotinylated human IgG1 Fc fragment, thereby removing any Fab-phage that bound elsewhere on the protein other than the extracellular domain region. Taking the remaining phage, we performed a positive selection against the Fc-fusion and eluted any bound phage with TEV protease cleavage to be amplified in *E.coli* (**Figure 1.3A**). After multiple rounds of selection, individual phage clones were screened via ELISA to determine specific binding to the extracellular domain and not the Fc domain. Antibodies that appeared to be specific and have a predicted affinity of <20 nM were carried forward (**Figures 1.4).** Upon sequencing, we identified 33 unique Fab-phage clones specific to their respective antigen (CPM: 2, DCBLD2: 4, GGT1: 4, MICA: 1, PVR: 5, TMEM132A: 11, TMEM2: 5, TNFRSF10D: 1). RTN4 did not return any suitable Fabs to carry forward.

To validate all antibodies were able to bind their respective antigen on cells, we engineered a Dox-inducible over-expression FlpIn line for each antigen. These constructs were engineered to display a HA tag and the extracellular domain of the protein of interest on the surface while anchoring it to the membrane with a transmembrane domain (**Figure 1.5A**). Extracellular staining for the HA tag revealed all cell lines properly express and traffic the

construct to the surface as intended (**Figure 1.5B**). If more than one Fab was identified for a specific antigen, the Fab with the best SEC profile and flow cytometry staining was carried forward (data not shown). Top performing Fabs for each antigen were converted into full length IgG's and used in live cell staining of each respective FlpIn line with or without Doxycycline-treatment (**Figure 1.3B**). All but one antibody (targeting TNFRSF10D) were successfully able to recognize the target extracellular domain on the surface of cells, confirming that our antibodies can be useful tools in the evaluation of surface presentation of these 7 proteins.

GGT1 is a Marker for Senescence in A549 Lung Cancer Cells.

We next sought to validate the proteins identified from our surface proteomics analysis with the antibodies we generated. We induced senescence in five cell lines (MCF7 breast cancer, PC3 prostate cancer, HCT116 colon cancer, A549 fibroblasts, IMR90 fibroblasts) using a 24 hour treatment of 250 nM doxorubicin followed by a 9 day recovery period. Senescent cells were stained and imaged on Day 10 post-treatment while growing cells were evaluated after 24 hours of DMSO treatment. Unfortunately, no cell line other than the A549 cell line was successfully able to be stained and imaged (data not shown).

Senescence was confirmed in A549 cells by staining for β-galactosidase activity and p21 expression (**Figure 1.6A & 1.6B**). Excitingly, our antibody targeting GGT1 showed robust staining in the senescent samples but not the growing sample (**Figure 1.6C**). A western blot analysis demonstrated in parallel the up-regulation of GGT1 in A549 senescent cells (**Figure 1.6B**). More so, an antibody targeting GFP did not stain in either sample, indicating that there were no contributions from off-target secondary binding. Therefore, these data indicate that GGT1 is indeed up-regulated in senescent A549 cells and that antibodies can sufficiently bind GGT1 on senescent cells. This provides clear evidence and rationale that further investment

should be made into GGT1 both as a biomarker for cellular senescence, but also as a potential therapeutic target for antibody-based therapeutics and senolytic strategies.

Discussion

Cellular senescence has been shown to drive a host of age-related diseases. While senescent cells have been targets for anti-aging strategies, properly identifying them has been challenging due to the lack of a universal biomarker. Here, we perform a surface proteomics campaign on senescent IMR90 fibroblasts that have been driven into senescence through DNA-damage and mitochondrial dysfunction. We identified several previously seen up-regulated membrane proteins, and also several novel markers that were up-regulated in senescence in both methods of induction. Using phage display, we generated specific and functional antibodies against several of these targets. Our antibody against GGT1 demonstrated clear up-regulation of this protein in senescent A549 lung cancer cells and opens the door for future investigation.

GGT1, otherwise known as Gamma-Glutamyltransferase 1, degrades the extracellular antioxidant glutathione into glutamate and cysteinylglycine[35]. Interestingly, recent findings have shown that small extracellular vesicles (sEV's) from young cells contained high amounts of the GSTM2, a protein involved in combating oxidative stress. When these sEV's were introduced to old mice senescence was ameliorated[36]. Hence, while we show that senescent cells likely degrade the antioxidant glutathione through GGT1, glutathione is ironically important in senescent cell removal. Therefore, we propose that senescent cells up-regulate GGT1 as a means of solidifying the senescent phenotype, possibly through increased oxidative stress and degradation of important antioxidants. More work needs to be done to uncover the role of GGT1 and its role in senescence; however, inhibiting GGT1 may be a promising senolytic strategy.

Methods

Cell lines

IMR90 primary fibroblasts were purchased from ATCC. HEK293-FlpIn and Expi293F cell lines were from frozen stocks maintained by the Wells lab. A549 lung cancer cells were a gift from the Rosenberg lab (UCSF). IMR90 fibroblasts were grown in DMEM+10% FBS+1% Pen/Strep. Engineered FlpIn cell lines were grown and maintained in DMEM+10% Tetracycline-negative FBS+1% Pen/Strep+100 μg/mL Hygromycin B+2 μg/mL blasticidin. A549 lung cancer cells were grown in RPMI+10% FBS+1% Pen/Strep. For growing and senescent samples, A549 cells were incubated in media containing either 250 nM Doxorubicin (Sigma Aldrich) or the equivalent volume of DMSO for 24 hours. For the senescent samples, media was replaced and then subsequently replaced every other day for 9 days post-doxorubicin treatment.

Cell culture/SILAC labeling and treatment

IMR90 cells were grown in DMEM for SILAC (Thermo Fisher) with 10% dialyzed FBS (Gemini) and 1% Pen/Strep. Media was also supplemented with either light L-[12C6,14N2] lysine/L-[12C6,14N4] arginine (Sigma Aldrich) or heavy L-[13C6,15N2] lysine/L-[13C6,15N4] arginine (Cambridge Isotope Laboratories). Cells were maintained in SILAC media for five passages to ensure complete isotopic labeling. IMR90 cells that were grown in "heavy" media were serum-starved (0.2% dialyzed FBS instead of 10%) for 3 days to generate the quiescent samples, replacing media on Day 2. IMR90 cells that were grown in "light" media were used for the senescent samples. Irradiated cells were treated with 10 Gy and allowed to recover for 10 days post-treatment to allow the phenotype to develop. Cells treated with Antimycin A (Sigma Aldrich) were cultured in media containing 50 nM Antimycin A for 10 days, with media being

replaced every day to maintain drug integrity. Quiescent and senescent cells were collected and heavy/light-labeled cells pooled together.

Mass spectrometry sample preparation

Cell surface glycoproteins were captured as previously described[25]. Briefly, cells were first washed in PBS, pH 6.5 before the glycoproteins were oxidized with 1.6 mM $NaIO_4$ in PBS, pH 6.5 for 20 minutes at 4°C. Cells were then biotinylated via the oxidized vicinal diols with 1 mM biocytin hydrazide (Biotium) in the presence of 10 mM aniline (Sigma Aldrich) in PBS, pH 6.5 for 90 minutes at 4°C. Cell pellets were washed three times with PBS, pH 6.5 and snap frozen and stored at -80°C.

Frozen cell pellets were lysed with a commercial RIPA buffer (Millipore) supplemented with 1X Protease Inhibitor Cocktail (Sigma Aldrich) and 2 mM EDTA for 30 minutes at 4°C. Cells were further disrupted with probe sonication and the cell lysates were then incubated with NeutrAvidin coated agarose beads (Thermo Scientific) for 1 hour at 4°C to isolate biotinylated glycoproteins. After this incubation, beads were transferred to Poly-Prep chromatography columns (Bio-Rad) and washed sequentially with RIPA wash buffer (0.5% DOC, 0.1 % SDS, 1% NP40, 1 mM EDTA in PBS, pH 7.4), high salt PBS (PBS pH 7.4, 1 M NaCl), and denaturing urea buffer (50 mM ammonium bicarbonate, 2 M Urea). Proteins on the beads were next treated with 5 mM TCEP for 30 minutes at 55°C in the dark, and subsequently treated with 11 mM IAM for 30 minutes at room temperature in the dark. Beads were washed twice with denaturing buffer and resuspended in 1 mL denaturing buffer and digested with 20µg trypsin (Promega). Tryptic peptides were collected and cells were washed twice with denaturing buffer.

To release the remaining trypsin digested N-glycosylated peptides bound to the neutravidin beads, we performed a second on-bead digestion using 2500U PNGase F (New

England Biolabs) at 37°C for 4.5 hours. Similarly, the "PNGase F" fraction was eluted using a spin column. Both tryptic and PNGase F fractions were then desalted using SOLA HRP SPE column (Thermo Fisher) using standard protocol, dried, and dissolved in 0.1% formic acid, 2% acetonitrile prior to LC-MS/MS analysis.

Mass spectrometry

Approximately 1 µg of peptides was injected to a pre-packed 0.75mm x 150 mm Acclaimed Pepmap C18 reversed phase column (2 µm pore size, Thermo Fisher Scientific) attached to a Q Exactive Plus (Thermo Fisher Scientific) mass spectrometer. For the "tryptic" fraction, peptides were separated using a linear gradient of 3-35% solvent B (Solvent A: 0.1% formic acid, solvent B: 80% acetonitrile, 0.1% formic acid) over 180 minutes at 300 µL/min. Similarly, the "PNGase F" fraction was separated using the same gradient over 120 minutes. Data were collected in data dependent mode using a top 20 method with dynamic exclusion of 35 s and a charge exclusion setting that only samples peptides with a charge of 2, 3, or 4. Full (ms1) scans spectrums were collected as profile data with a resolution of 140,000 (at 200 m/z), AGC target of 3E6, maximum injection time of 120 ms, and scan range of 400-1800 m/z. MS-MS scans were collected as centroid data with a resolution of 17,500 (at 200 m/z), AGC target of 5E4, maximum injection time of 60 ms with normalized collision energy at 27, and an isolation window of 1.5 m/z with an isolation offset of 0.5 m/z.

Data analysis/Statistics

Peptide search for each individual dataset was performed using ProteinProspector against human proteins (Swiss-prot database, obtained August 3, 2017). Enzyme specificity was set to trypsin with up to two missed cleavage; cysteine carbamidomethyl was set as a fixed modification;

methionine oxidation, N-terminal acetylation, N-terminal acetylation and oxidation, pyroglutamic acid, methionine loss with N-terminal acetylation, lysine and arginine SILAC labels were set as variable modifications; asparagine deamidation was also set as variable modification for the PNGase F fraction; peptide mass tolerance was 6 ppm; fragment ion mass tolerance was 0.4 Da; peptide identification was filtered by peptide score of 15 in Protein Prospector, resulting in a false discovery rate (FDR) of <1% calculated by number of decoy peptides included in the database. To estimate the efficiency of the surface proteome enrichment method, a list of surface proteins was generated by searching for "membrane" but not "mitochondrial" or "nuclear" using Uniprot subcellular localization annotations.

Quantitative data analysis was performed using Skyline (UWashington) software with a ms1 filtering function. Specifically, spectral libraries from forward and reverse SILAC experiments were analyzed together such that ms1 peaks without an explicit peptide ID would be quantified based on aligned peptide retention time. An isotope dot product of at least 0.8 was used to filter out low quality peptide quantification, and a custom report from Skyline was then exported for further processing and analysis using R. In the tryptic fraction, only peptides with two or more well quantified peptides were included. In the PNGase F fraction, only peptides with N to D deamidation modification were included. Forward and reverse SILAC datasets were reported as median $\log_2$ enrichment values normalized to a mean of zero for the senescent cells.

B-gal Staining

β-galactosidase activity staining was performed using a Senescence β-Galactosidase Staining Kit (Cell Signaling) following the manufacturer's protocol.

Cloning

Fc-fusion proteins were cloned into a pFUSE (InvivoGen) vector with a human IgG1 Fc domain as previously described.[26] Fabs were subcloned from the Fab-phagemid into an *E. coli* expression vector pBL347. The heavy chain of the IgG was cloned from the Fab plasmid into a pFUSE (InvivoGen) vector with a human IgG1 Fc domain. The light chain of the IgG was cloned from the Fab plasmid into the same vector but lacking the Fc domain. FlpIn constructs encoding each extracellular domain fused to the transmembrane anchoring domain of platlet-erived Growth Factor (for Type I membrane proteins) and the Gamma-Glutamyltransferase 1 (for Type II membrane proteins) with a HA tag were cloned in the pcDNA5/FRT/TO Mammalian Expression vector (ThermoFisher). All constructs were sequence verified by Sanger sequencing.

Protein expression and purification

Fabs were expressed in E. coli C43 (DE3) Pro+ as previously described using an optimized autoinduction medium and purified by protein A affinity chromatography[37]. Fabs were subsequently buffer exchanged into PBS pH 7.4 and stored in 10% glycerol at -80°C and assessed by SDS-PAGE.

IgGs were expressed and purified from Expi293F-BirA cells using transient transfection (Expifectamine, Thermo Fisher Scientific). Enhancers were added 20 hrs after transfection. Cells were incubated for 5 days at 37ºC and 8% CO_2. Media was then harvested by centrifugation at 4,000xg for 20 min. IgGs were purified by Ni-NTA affinity chromatography and buffer exchanged into PBS pH 7.4 and stored in 10% glycerol at -80°C and assessed by SDS-PAGE.

Phage display selection

All phage selections were done according to previously established protocols. Briefly, selections with antibody phage library were performed using biotinylated Fc-fusion antigens captured with streptavidin-coated magnetic beads (Promega). Prior to each selection, the phage pool was incubated with 1 μM of biotinylated Fc-domain immobilized on streptavidin beads in order to deplete the library of any binders to the beads or Fc-tag. In total, four rounds of selection were performed with decreasing amounts of ECD-Fc-fusion antigens (100 nM, 50 nM, 10 nM and 10 nM). To reduce the deleterious effects of nonspecific binding phage, we employed a 'catch and release' strategy, where ECD-Fc-fusion binding Fab-phage were selectively eluted from the magnetic beads by the addition of 50 μg/mL TEV protease. Individual phage clones from the fourth round of selection were analyzed for binding by ELISA.

Fab-phage ELISA

For each phage clone, four different conditions were tested – Direct: Fc-fusion of interest, Competition: Fc-fusion with an equal concentration of Fc-fusion in solution, Negative selection: Fc-biotin, and Control: PBSTB. 384-well Nunc Maxisorp flat-bottom clear plates (Thermo Fisher Scientific) were coated with 0.5 μg/mL of NeutrAvidin in PBS overnight at 4°C and subsequently blocked with PBSTB. Plates were washed 3x with PBS containing 0.05% Tween-20 (PBST) and were washed similarly between each of the steps. 20 nM biotinylated Fc-fusion or Fc-biotin was diluted in PBSTB and immobilized on the NeutrAvidin-coated wells for 30 minutes at room temperature, then blocked with PBSTB + 10 μM biotin for 10 minutes. For the competition samples, phage supernatant was diluted 1:5 into PBSTB with 20 nM Fc-fusion 30 minutes prior to addition to the plate. For the direct samples, phage supernatant was diluted 1:5 in PBSTB. Competition and direct samples were added to the plate for 30 minutes at room

temperature. Bound phage was detected by incubation with anti-M13-horseradish peroxidase conjugate (Sino Biologics, 1:5000) for 30 minutes, followed by the addition of TMB substrate (VWR International). The reaction was quenched with the addition of 1 M phosphoric acid and the absorbance at 450 nm was measured using a Tecan M200 Pro spectrophotometer. Clones with high binding to Fc-fusion, low binding to PBSTB/Fc-biotin, and competition signal <0.5*direct binding signal were carried forward.

FlpIn T-REx Cell Line Generation

FlpIn cells were grown to 70% confluence in the presence of 100 μg/mL zeocin and 10 μg/mL blasticidin in a well of a 6-well plate. Growth media replaced with Opti-MEM for >15 minutes to transfection. Mixed 1.5 μg pCDNA5/FRT/TO plasmid, 1.5 μg pOG44 plasmid, and 9 μL 1 mg/mL polyethylenimine (PEI) in 200 μL of Opti-MEM and incubated at room temperature for 15 minutes. Replaced media in cells with Opti-MEM and added DNA/PEI mixture. Incubated for 6 hours at 37°C, 5% CO_2, and replaced transfection media with 1:1 Opti-MEM/DMEM+10% Tetracycline-negative FBS+1% Pen/Strep and incubated at 37°C, 5% CO_2. After 24 hours, media was replaced and drug selection for stable cell lines was initiated by the addition with 100 μg/mL Hygromycin B and 2 μg/mL blasticidin.

Cell imaging

FlpIn cell lines were seeded 10k cells/well in a black, PDL-coated, CellCarrier-96 Ultra Microplates (PerkinElmer). Doxycycline-treated samples were cultured in media containing 2 μg/mL Doxycycline. Media was replaced after 24 hours. After 48 hours post-seeding, cells were incubated for 20 minutes in serum-free DMEM with 1 μM CellTracker™ Violet BMQC Dye (Thermo Scientific). Cells were blocked with ice cold DMEM+3% BSA for 5 minutes at 4°C.

Cells were stained with anti-HA Tag rabbit IgG or 2 μg/mL IgG in DMEM+3% BSA for 30 minutes at 4°C, and then washed three times with DMEM+3% BSA. Cells were then stained with anti-rabbit Alexa Fluor® 647 or 1 μg/mL Protein A, Alexa Fluor® 647 conjugate (Life Technologies) for 30 minutes at 4°C, and then washed three times with DMEM+3% BSA followed by a washed one time in cold PBS pH 7.4. Samples were fixed in 4% Formalin at room temperature for 10 minutes, and then washed three times with PBS pH 7.4. Samples were imaged using an InCell Analyzer 6500.

A549 cells were seeded at 20k cells/well and treated directly on plate. A549 cells were imaged similarly but stained and washed in RPMI+3% BSA.

Western Blot

Cells were washed twice on plate with PBS prior to lysis. Lysis buffer contained 1x RIPA (EMD Millipore), 1% protease inhibitor cocktail (Sigma-Aldrich), and 1 mM EDTA. Cells were lysed for 20 minutes on ice prior to sonication (1 minute, 20% amp, 1 second on/off pulse). Cells were spun at 16000 x g at 4°C for 5 minutes, and lysate protein concentration was determined using a Pierce™ BCA Protein Assay (Thermo Scientific). Samples were run on a Bolt 4-12% Bis-Tris gel (Invitrogen), and transferred to a PVDF membrane (Thermo Scientific) using an Iblot™ (Thermo Scientific). Membranes were blocked in Odyssey® Blocking Buffer (TBS) (LiCOR) prior to staining. Membranes were stained with primary anti-human p21 (Abcam, ab109520), anti-human GGT1 (Abcam, ab109427), anti-human α-tubulin (Sigma-Aldrich, T6199), and anti-human β-actin (Cell Signaling, 8H10D10) antibodies in blocking buffer for 1 hour at room temperature. Secondary staining was performed using goat anti-rabbit IRDye® 800CW and goat anti-mouse IRDye® 680RD antibodies (LiCOR Biosciences) in blocking buffer for 1 hour at

room temperature. Membranes were washed with three 5 minute washes of TBST between each staining step. Membranes were imaged using an Odyssey® CLx (LiCOR Biosciences).

Figures and Tables

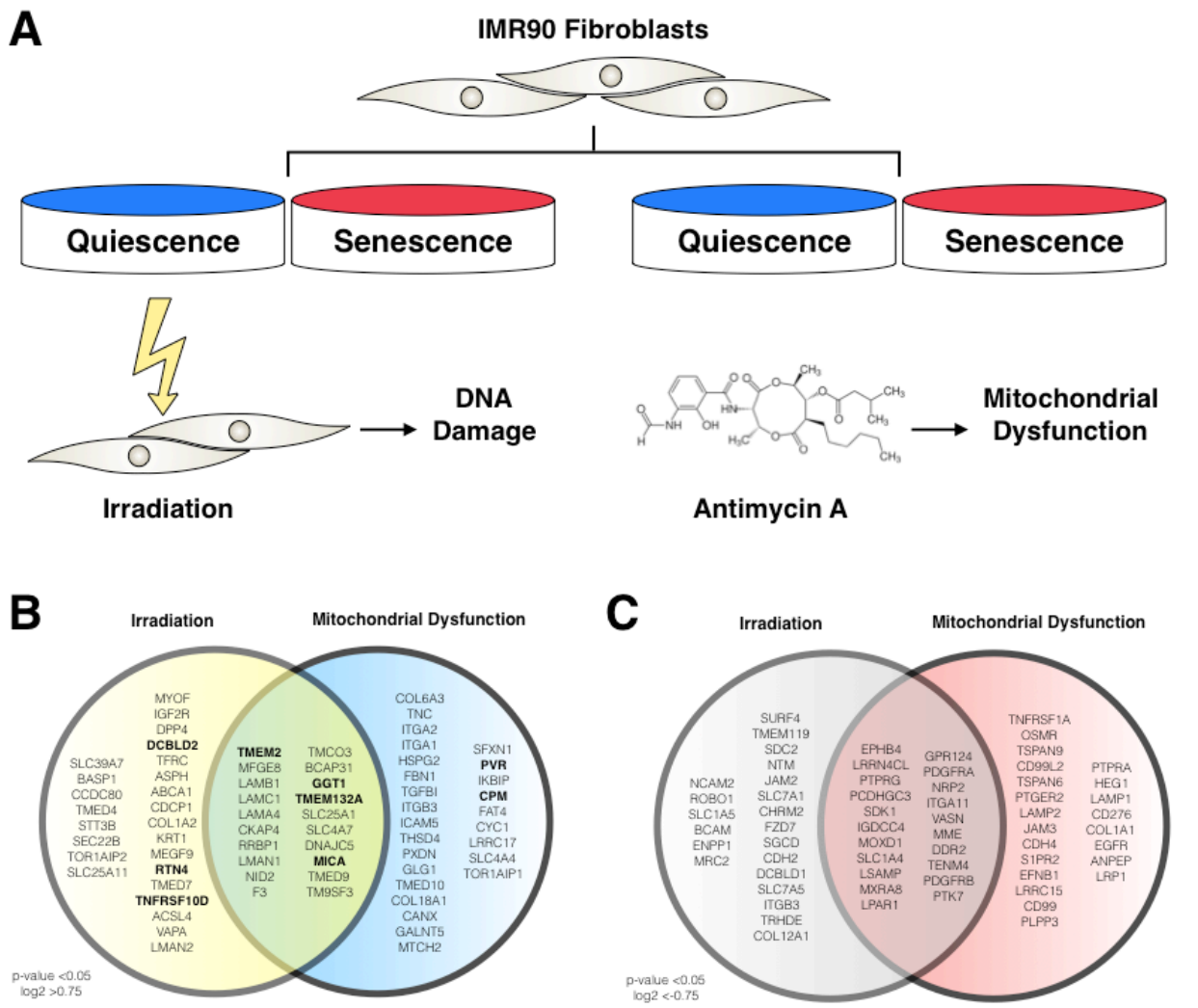

Figure 1.1: Surface proteomics of quiescent and senescent fibroblasts. A) The workflow for quantitative surface proteins using differential SILAC labeling of quiescent ("heavy" labeled, blue) and senescent ("light" labeled, red) IMR90 fibroblasts (n=2 for each condition). B) Up-regulated membrane proteins in senescence vs. quiescence identified from surface proteomics. Proteins in bold were considered proteins of interest and carried forward with as targets in a phage display campaign. C) Down-regulated membrane proteins in senescence vs. quiescence identified from surface proteomics.

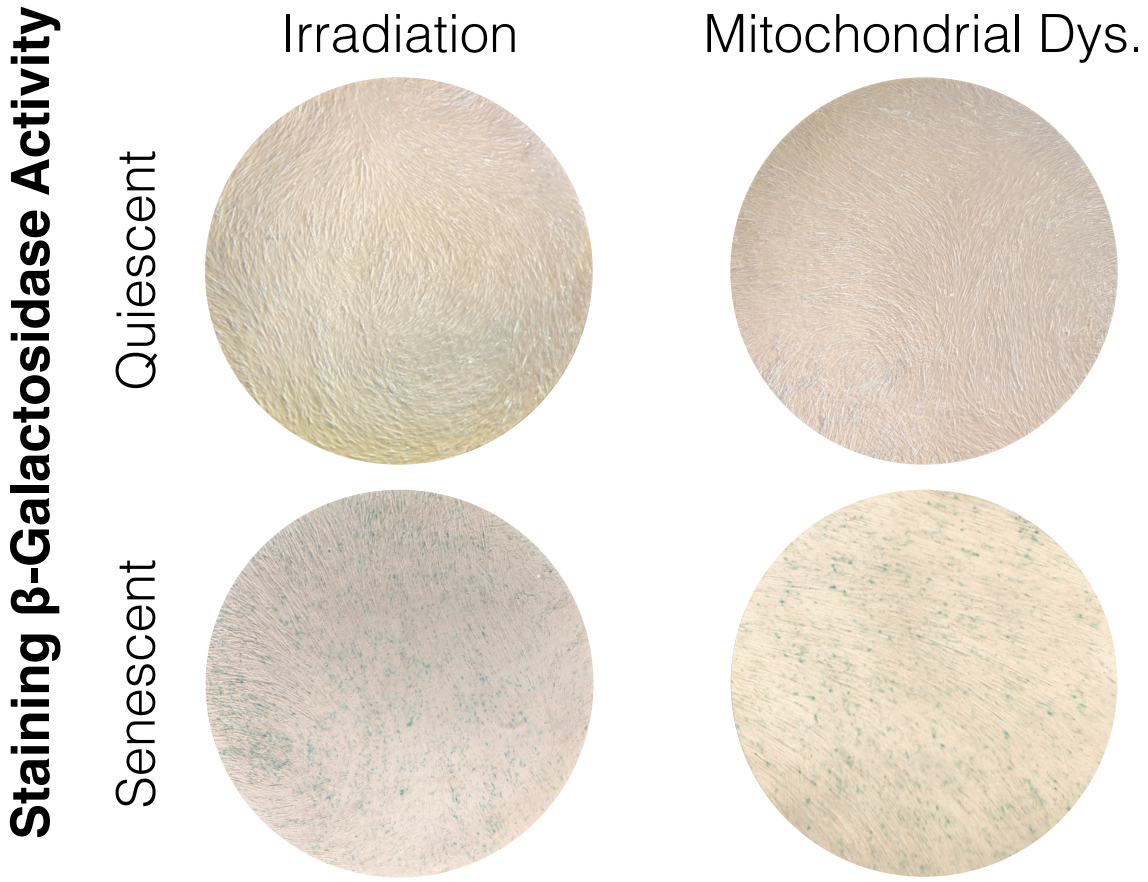

Figure 1.2: Staining of senescence-associated β-galactosidase activity in growing and senescent IMR90 fibroblasts.

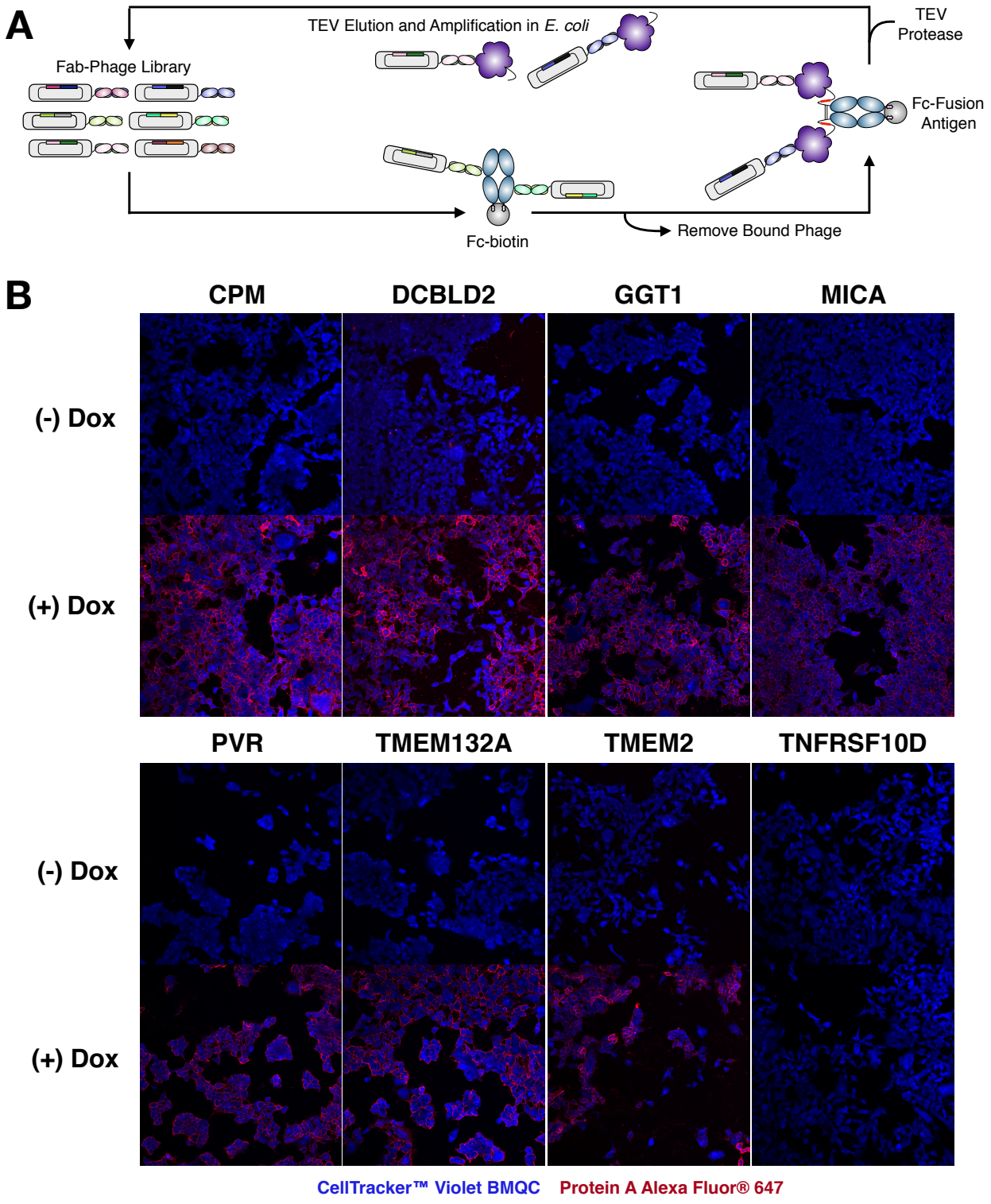

Figure 1.3: Phage display selection and on-cell binding validation of antibodies against each antigen. A) Differential phage display selection strategy to select for the extracellular domains of each membrane protein. B) Live cell staining of using the top performing IgG's on each antigen's respective FlpIn line, with and without Doxycycline treatment.

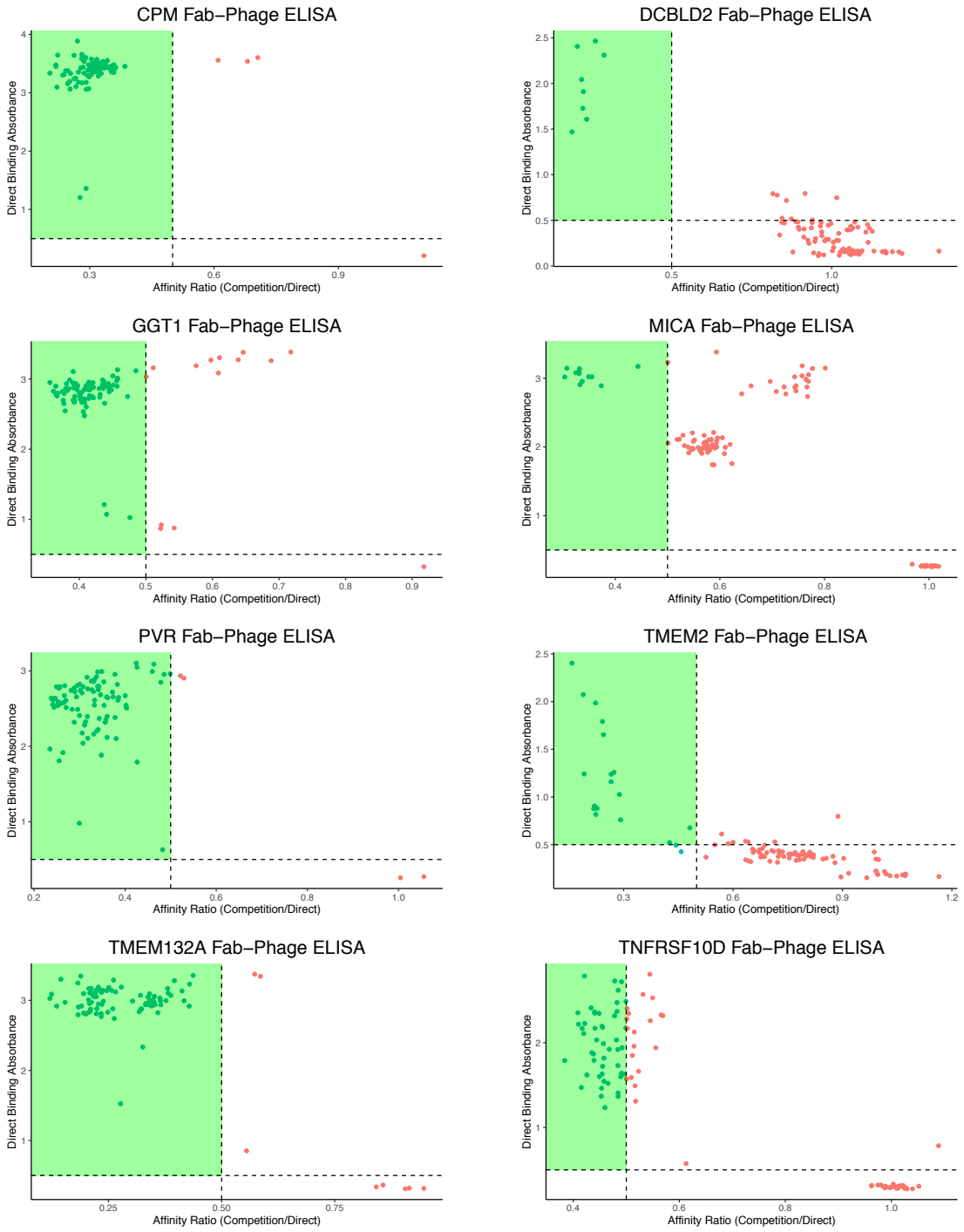

Figure 1.4: Single colony ELISA screening of Fab-phage clones against each antigen.

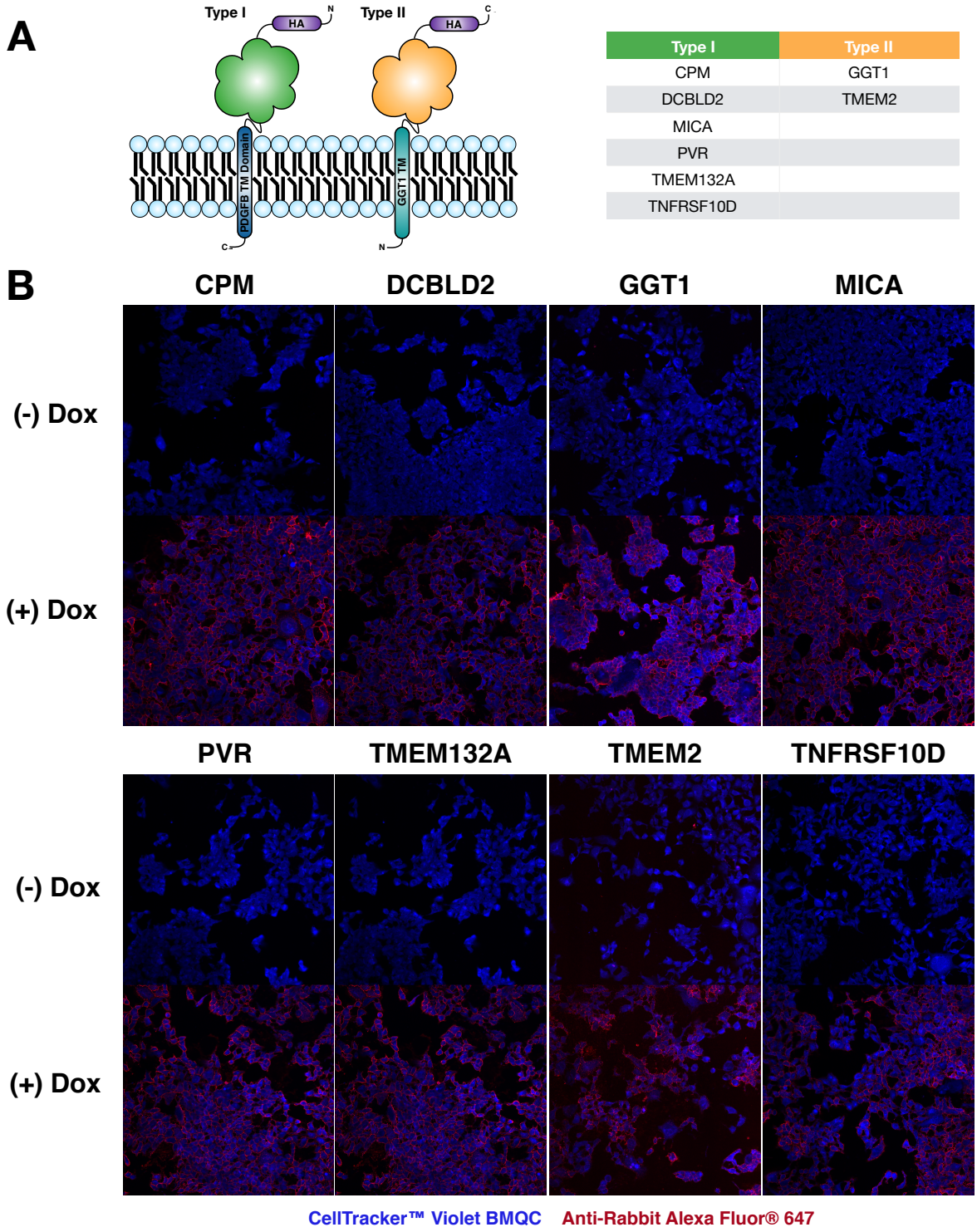

Figure 1.5: Engineering Dox-inducible antigen FlpIn cells. A) Antigen design for each of the 8 antigens. B) Live cell staining for HA-tag display on each engineered FlpIn line to confirm proper Doxycycline-induced expression and trafficking of the antigen.

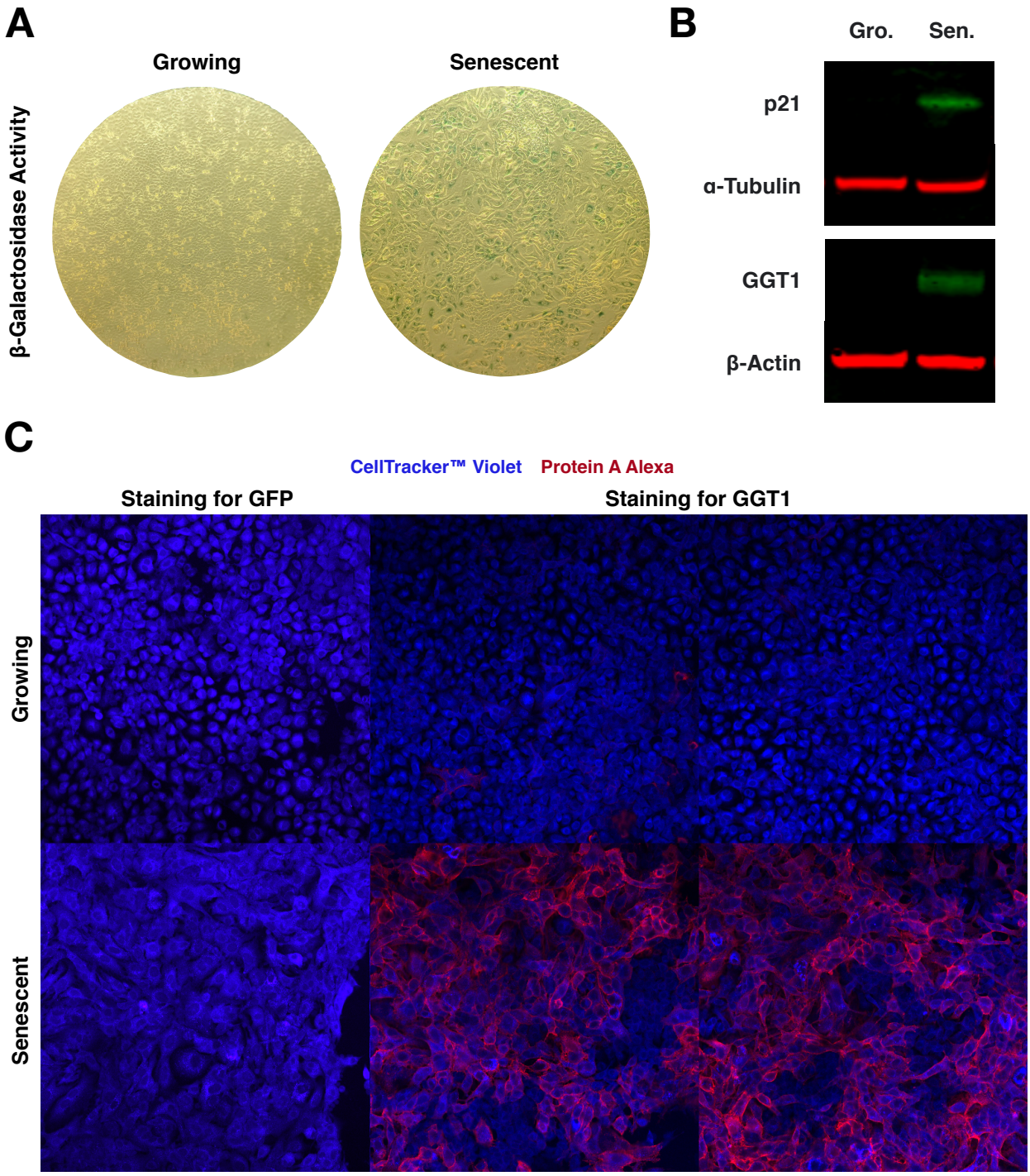

Figure 1.6: GGT1 is a biomarker for senescence in senescent A549 lung cancer cells. A) Staining of senescence-associated β-galactosidase activity in growing and senescent A549 cells. B) Western blot for p21 expression in growing (Gro.) and senescent (Sen.) A549 cells. C) Live cell staining using anti-GFP and anti-GGT1 IgG's on growing and senescent A549 cells.

Chapter 2

Engineering Antibodies Targeting p16 MHC-peptide Complexes

Abstract

Senescent cells undergo a permanent cell-cycle arrest and drive a host of age-related pathologies. Recent transgenic mouse models indicate that removing cells expressing the senescence marker p16Ink4a (p16) can increase median lifespan and delay the onset of many aging phenotypes. However, identifying and eliminating native human cells expressing p16 has remained a challenge. We hypothesize that senescent cells display peptides derived from p16 in MHC-peptide complexes on the cell surface that could serve as targetable antigens for antibody-based biologics. Using Fab-phage display technology, we generated antibodies that bind to a p16 MHC-peptide complex from the HLA allele HLA-B*35:01. When converted to single-chain Fab chimeric antigen receptor (CAR) constructs, these antibodies can recognize naturally presented p16 MHC-peptide complexes on the surface of cells and activate Jurkat cells. Furthermore, we developed antibodies against predicted p16 MHC-peptide complexes for HLA-A*02:01 that specifically recognize their respective antigen on the surface of cells. These tools establish a platform to survey the surface of senescent cells and provide a potential novel senolytic strategy.

Introduction

Although senescent cells commonly share several features such as increased lysosomal beta-galactosidase activity, increased size, activation of damage-sensing signaling pathways, upregulation of pro-survival pathways, and a secretory phenotype, senescence is notorious for lacking a single universal biomarker[22–24]. However, the tumor suppressor protein p16 is among the more reliable biomarkers for cellular senescence[38]. Acting as a CDK4 and CDK6 inhibitor, p16 prevents phosphorylation of the retinoblastoma protein thereby inhibiting the transcription of several pro-mitogenic genes, locking the cell in a G1 arrest[6,39]. As such, p16 levels are extremely low in proliferating cells[4]. Yet, p16 is not universally expressed in all non-proliferating cells – it

does not, for example, accumulate in quiescence[6,24], making its expression relatively specific to the senescent phenotype[24,40].

Recently, transgenic mouse models engineered with chemical-inducible suicide genes under the control of the p16-promoter have been used to study the role of senescent cells in disease[41,42]. Since their inception, these models have revealed a causal role of p16-expressing cells in driving sarcopenia[42], cataracts[42], impaired neurogenesis and cognitive decline[43,44], osteoporosis[45], metabolic syndromes[46], atherosclerosis[47], osteoarthritis[48], impaired adipogenesis[49], hepatic steatosis[50], Parkinson's disease[51], fibrotic pulmonary disease[52], anxiety[43], glomerulosclerosis/impaired renal filtering[53,54], cancer relapse[55], and loss of energy[42]. Remarkably, the selective removal of these cells ameliorated these diseases and phenotypes. Possibly most exciting, selective elimination of p16-expressing cells extended median healthy lifespan by up to 30% in mice[54], indicating these cells are prime therapeutic targets in combating aging-phenotypes.

Despite this profound therapeutic potential, targeting p16-expressing senescent cells has remained challenging as p16 is an intracellular protein with a desired, non-catalytic function[1]. One way these cells could be identified is through the presentation of a p16-derived peptide in a major histocompatibility complex (MHC). Class I MHC-peptide complexes are loaded with peptides roughly 8-12 residues in length from degraded intracellular proteins and are displayed on the cell surface[56,57]. Under infection or oncogenic transformation, these complexes can present peptides from viral or mutated proteins to $CD8^+$ T cells and initiate T cell activation and subsequent cellular clearance[57].

However, even with a primary role in immunosurveillance, MHC-peptide complex loading is unbiased as to protein origin. As a result, thousands of peptides derived from

endogenous proteins, termed "self-peptides," are presented at the cell surface in a pool that is collectively known as the immunopeptidome[58,59]. As the immunopeptidome typically reflects the protein population and biological context of the cell, MHC-peptide complexes can act as biomarkers for disease and oncogenic transformation by presenting peptides from phenotype-associated proteins[57,60–63]. Consequently, there has been growing therapeutic interest in engineering antibodies against MHC-peptide complexes as they provide an increased layer of specificity, and importantly, extracellular access to intracellular targets. Over the past two decades, we have seen the generation of TCR-like antibodies specific for MHC-peptide complexes of several tumor-associated antigens such as of HER2, gp100, and WT1[61,64,65]. Indeed, these antibodies demonstrate selective cytotoxicity against tumor cells expressing the target antigen and underscore the promise of MHC-peptide complexes as therapeutic targets[64–67].

In addition to the expression of p16 in senescent cells, senescent cells have also been shown to increase expression of MHC molecules at the cell surface[68]. Given this observation, along with the instability of p16 (half-life up to 3.5 hours) and a characterized proteasomal degradation pathway[69–71], we hypothesize there is an increased pool of p16-derived peptides in senescent cells that is displayed in MHC-peptide complexes. Herein, we describe the development of antibodies targeting p16 MHC-peptide complexes across multiple HLA-alleles. These antibodies, developed against a previously identified peptide for HLA-B*35:01 and predicted peptides for HLA-A*02:01, demonstrate high affinity and selectivity for the antigens in a peptide-dependent manner. Furthermore, use of a cell-based CAR platform revealed these new antibodies are useful tools in detecting naturally processed and displayed p16 peptides on the cell surface. These antibodies represent a promising, novel scaffold for further development of biologics and could contribute to the growing arsenal of senolytics.

Results

*Engineering Antibodies Against a p16 MHC-peptide Complex for HLA-B*35:01*

Class I MHC-peptide complexes are comprised of three components: the human leukocyte antigen (HLA) heavy chain, the invariant β_2-microglobulin (β_2M) light chain, and the peptide itself[72]. HLA molecules are the most polymorphic genes in the human genome with over 11,000 different class I allotypes identified across the human population[73]. With each allele having a specific peptide-binding motif determined by variations in the peptide-binding groove, different peptides will be displayed by different HLA molecules[57,58,74]. Given peptide loading is dependent on the peptide length and residue composition, not all peptides derived from a particular protein will be presented at the cell surface. Furthermore, since each cell is genetically encoded to express up to just six of the class I HLA alleles, not all cells will present the same MHC-peptide complexes[75]. Hence, identifying HLA-associated peptides for a given protein and their HLA counterpart is not trivial.

When searching for a potential candidate for a p16 MHC-peptide complex, we turned to the Immune Epitope Database (http://www.iedb.org) as it curates a comprehensive list of previously identified HLA-associated peptides. Excitingly, we discovered several peptides derived from p16 had been reported in the literature. In particular, the peptide LPVDLAEEL, noted to be presented by the HLA allele HLA-B*35:01, was a promising candidate as it was identified in multiple mass-spectrometry studies[76,77]. Additionally, HLA-B*35:01 is considered a fairly common allele, with a genotypic frequency of >5% in the global population according to the Immune Epitope Database coverage tool, increasing its potential impact. Thus, we chose this p16 MHC-peptide complex to move forward with in an antibody-selection campaign.

In constructing our antigens for catch-and-release phage selection[37], we engineered the extracellular domain of HLA-B*35:01 to feature a TEV protease cleavage site followed by a C-terminal AviTag (**Figure 2.1A**). Our HLA molecules were individually refolded in the presence of excess peptide and β_2M and were subsequently SEC-purified and biotinylated, producing pure MHC-peptide complexes of interest. Using a Fab-phage library, we first performed a negative clearance using a MHC-peptide complex containing a decoy peptide (in this case, derived from the viral protein B8R), thereby removing any Fab-phage that bound elsewhere on the complex other than the peptide epitope. Taking the remaining phage, we performed a positive selection against the p16 MHC-peptide complex and eluted any bound phage with TEV protease cleavage (**Figure 2.1B**).

After multiple rounds of selection, individual phage clones were screened via ELISA to determine specific binding to the p16 MHC peptide complex and not the B8R MHC-peptide complex (**Figures 2.1C & 2.2).** Upon sequencing, we identified 11 unique Fab-phage clones specific to the p16 MHC-peptide complex. After a preliminary kinetic screen and SEC profiling of the Fabs, we were left with 2 unique Fabs (henceforth referred to as PBE2 and PBG4) that demonstrated specificity and promising biophysical properties (**Figures 2.3 & 2.4**). An in-depth kinetic analysis of PBE2 and PBG4 revealed the Fabs bound to the p16 MHC-peptide complex with affinities of ~8 nM and ~3 nM, respectively (**Figure 2.1D**). Importantly, these Fabs demonstrated no binding to HLA-B*35:01 MHC-peptide complexes containing different peptides, indicating that PBE2 and PBG4 are highly specific for the p16 MHC-peptide complex.

To further evaluate selectivity, we assayed PBE2 and PBG4 binding a MHC-peptide complex containing a peptide derived from Importin-4. This peptide, only differing in sequence at two positions (L5→K5, E7→Q7) is the closest in homology in the human proteome to the

peptide derived from p16. Both Fabs did not demonstrate binding to the Importin-4 MHC-peptide complex, once again highlighting the specificity of PBE2 and PBG4 (**Figure 2.5**). Thus, we generated two Fabs that recognize a p16 MHC-peptide complex for HLA-B*35:01. Thus, we generated two Fabs that recognize a p16 MHC-peptide complex for HLA-B*35:01.

scFab CARs Recognize p16-MHC peptide Complex and Activate Jurkats

Historically, HLA-associated peptides have been suggested to be presented at extremely low copy numbers, with many quantitative analysis reporting well under 100 copies per cell – often times only reaching single digit levels[78,79]. In fact, recent quantifications of oncogenic RAS and p53 peptides revealed anywhere from ~9 to as little as ~1 peptide presented per cell[80,81]. In line with these trends, we expect low presentation levels of the p16-derived peptide on the surface of senescent cells. Because of sparse antigen quantities, targeting MHC-peptide complexes has typically required more sensitive antibody-based targeting constructs. Chimeric antigen receptor (CAR) T cells have classically shown exquisite sensitivity, eliciting cytotoxicity from low levels of target antigen[82]. Given the prior success of CAR T cells in targeting both senescent cells and MHC-peptide complexes, we hypothesize a CAR would be the most successful and relevant modality in targeting a p16 MHC-peptide complex[83,84].

To engineer our CARs, we converted PBE2 and PBG4 into single-chain Fabs (scFab) by fusing the light and heavy chains with a 60-aa linker[85]. We chose a scFab format over the traditional scFv as scFv's are less stable and can form diabodies, leading to tonic signaling. Moreover, a scFab is structurally closer to the parent Fab from which it was designed. The scFab was constructed with a CD8 transmebrane domain and respective cytosolic 4-1BB and CD3ζ signaling domains (**Figure 2.6A**). We transduced NFAT-GFP Jurkats, a transformed T cell reporter cell line in which GFP expression correlates with T cell activation, with our scFab CARs

to generate our model cell lines. In order to evaluate both the functionality and specificity of our scFabs in this CAR format, we incubated our scFab Jurkats with different MHC-peptide complexes immobilized through magnetic-streptavidin beads (**Figure 2.6B**). While the parental cell line without a CAR did not respond to beads with or without immobilized MHC-peptide complex, both the scFab PBE2 and scFab PBG4 CAR Jurkats showed robust expression of GFP only when incubated with beads containing the HLA-B*35:01 p16 MHC-peptide complex. Hence, these CARs maintained specificity for the p16 MHC-peptide complex as a scFab and illustrate the scFab CAR can recognize and activate T cells in the presence of this particular complex.

The HLA-B*35:01 p16 peptide was originally identified in the cell line B721.221[76,77]. This HLA-null cell line allows for the transduction and homogenous expression of a single HLA allele, providing a ubiquitous model to study peptide generation and MHC class I presentation. Further, these cells provide a controlled system under which we can evaluate scFab CAR efficacy in identifying naturally generated p16 MHC-peptide complexes on the surface of cells. We transduced B721.221 cells to constitutively express HLA-B*35:01, followed by a subsequent transduction of a Doxycycline-inducible p16 expression system. This strategy allows for the presentation of p16 peptides exclusively in HLA-B*35:01 molecules in a Doxycycline-dependent manner. In addition, we inserted the Doxycycline-induced p16 expression system into parental B721.221 cells to confirm p16 expression alone was not responsible for Jurkat activation (**Figure 2.6C**).

To examine scFab CAR sensitivity to naturally presented p16 peptides, we incubated our NFAT-GFP Jurkat cells with the B721.221 target cells with and without Doxycycline. Parental NFAT-GFP Jurkats with B721.221 cells showed no response under any condition, indicating that

any resulting activation was mediated through our scFab CARs (**Figure 2.6D**). As with the NFAT-GFP Jurkats without CARs, the scFab PBE2 and scFab PBG4 CAR Jurkats did not react to the B721.221 HLA-null cell lines with or without p16 expression. Hence, this confirms all CAR reactivity is via recognition of HLA-B*35:01 MHC-peptide complexes and not other surface molecules or any p16-induced antigens. However, when incubated with B721.221 cells expressing both HLA-B*35:01 and p16 we observed significant GFP expression, confirming that our scFab CARs can both recognize the p16 MHC-peptide complex on the surface of cells and consequently activate T cells. Importantly, these data provide further evidence that the p16 peptide, LPVDLAEEL, is indeed generated and presented by HLA-B*35:01.

We next sought to determine if our scFab CARs could sufficiently activate T cells when surveying target cells expressing p16 at levels similar to that of senescent cells. To generate growing and senescent samples, IMR90 primary fibroblasts were treated with either DMSO or 250 nM Doxorubicin for 24 hours and harvested after 0 or 9 days, respectively. Senescence was confirmed via β-galactosidase activity staining (**Figure 2.6E**). When our scFab CAR Jurkats were incubated with HLA-B*35:01-expressing B721.221 cells treated with decreasing doses of Doxycycline, we saw appreciable activation to cells that expressed p16 in a range comparable to senescent IMR90 fibroblasts (**Figure 2.6F**). The PBG4 scFab Jurkat, in particular, showed a dynamic range of activation and a large increase in signal over baseline within the p16 levels the senescent IMR90 fibroblasts fall. Hence, these data provide further evidence that our scFab CARs can be used to identify and target senescent cells expressing p16.

Interestingly, we saw lower but appreciable activation in our scFab CAR Jurkats when incubated with B721.221 cells expressing HLA-B*35:01 without induced-expression of p16 (**Figures 2.6D & 2.6F**). As forementioned, this is the cell line from which this p16-derived

peptide was identified so we suspect this activation is due to presentation of endogenously expressed p16. However, since the scFab CARs are allowed to sample the entire immunopeptideome of the cell, it is possible that the Fabs have off-target reactivity to other MHC-peptide complexes outside those described here. Further research will be required to determine the cause of this activity. Nonetheless, these findings reveal our scFab CAR Jurkats recognize and respond to p16 MHC-peptide complexes on the cell surface and provide rationale for further therapeutic development of this platform.

Engineering Antibodies Against a p16 MHC-peptide Complex for HLA-A*02:01

As previously mentioned, there are thousands of HLA alleles expressed across the human population that limits the pool of people expressing a specific allele. Therefore, we aimed to generate antibodies against p16 MHC-peptide complexes for HLA-A*02:01, as this is the most widely expressed HLA allele worldwide, being expressed in 50% of the Caucasian population[86]. However, to date, there have been no peptides derived from p16 reported to be presented by HLA-A*02:01. We therefore used the NetMHC4.0 server to predict potential p16 peptide candidates. While the mechanisms responsible for peptide processing are not fully understood, predictive algorithms such as NetMHC can predict which peptides from a protein could bind a HLA allele if said peptides were ever generated by the cell. Upon scanning the p16 protein sequence, two overlapping 9-mer peptides were identified with the potential to bind HLA-A*02:01: VMMMGSARV (a strong-binding peptide, with a predicted affinity of ~8 nM) and MMMGSARVA (a weak-binding peptide, with a predicted affinity of ~250 nM) (**Figure 2.7A**).

Following a similar design and selection rationale as for the HLA-B*35:01 complexes, we performed phage display selection on both the p16 strong-binding and weak-binding peptide complexes. After screening clones via ELISA (**Figure 2.8**), promising candidates were carried

forward and expressed as Fab protein. We performed flow cytometry with these Fabs on the T2 lymphboblast cell line. This HLA-A*:02:01^{+} cell line, deficient for the TAP transporter responsible for shuttling peptides into the ER, has an increased pool of apo-MHC-peptide complexes, allowing for the exogenous loading of a particular peptide of interest at the cell surface[55]. Excitingly, one Fab (SB5D) bound exclusively to T2 lymphoblasts loaded with the p16 strong-binding peptide, indicating this Fab can specifically recognize this MHC-peptide complex on the surface of cells (**Figure 2.7B**). Interestingly, while there were Fab-phage clones that bound specifically to the p16 weak-binding peptide via ELISA, flow cytometry analysis showed all respective Fabs were non-specific (**Figure 2.9**). We suspected this could be due to instability of the p16 weak-binding MHC-peptide complex itself as the peptide had a predicted affinity of ~250 nM to HLA-A*02:01, resulting in a failure to properly pull-down binding Fab-phage.

To circumvent this problem, we reengineered the p16 weak-binding peptide by replacing the anchor residues at positions 2 and 9 with the preferred residues of leucine and valine[58], respectively (hereafter referred to as p16-DR peptide) (**Figure 2.7A**). This strategy has been employed in the past to generate tetramers to stain reactive T cells, as it improves the peptide affinity but maintains the solvent-exposed TCR-reactive residues[62]. Upon replacing the anchor residues, the predicted affinity of the p16 weak-binding peptide was improved over 8-fold to ~30 nM. After repeating selections and screening clones via ELISA (**Figure 2.10**), promising Fabs were once again evaluated via flow cytometry using the T2 lymphoblast cells (**Figure 2.7B**). Excitingly, one Fab (WB9E) bound specifically to cells loaded with the p16-DR peptide.

Upon further kinetic characterization of SB5D and WB9E, we observed these Fabs specifically bound the p16 strong-binding peptide and p16 weak-binding peptide complexes, respectively (**Figure 2.7C**). Perhaps more impressive, SB5D and WB9E are able to distinguish

these overlapping peptides that differ by just one amino acid in register. WB9E binds to the p16 weak-binding peptide complex with an affinity of ~96 nM. Thus, the replacement of anchor residues in weak-binding peptides can successfully be used in phage display to design more stable MHC-peptide complex for selections. Interestingly, WB9E bound the p16-DR MHC-peptide complex with a higher affinity of ~21 nM (**Figure 2.11**). While we attribute this increase in affinity to the stability of the MHC-peptide complex, it is possible the new anchor residues cause a conformational shift in the complex landscape compared to its parental counterpart resulting in weaker binding. Nonetheless, SB5D and WB9E specifically bind and recognize their respective HLA-A*02:01 p16 MHC-peptide complexes on the surface of cells. Future work using these antibodies can determine if these peptides are generated and presented on the surface of senescent cells and open the door for senolytic potential across a broader population pool.

Discussion

Cellular senescence is a physiological response to stress and an anti-cancer mechanism employed to halt the expansion of pro-tumorigenic cells. Once the onset of senescence is initiated, cells will secrete a number of factors, including inflammatory molecules to recruit immune cells to clear them. However, over time senescent cells accumulate, resulting in persistent inflammation. This inflammation is suspected to drive several age-related pathologies and tissue dysfunction. Given the anti-proliferative cellular state, senescence is often a therapeutic end goal for radiation and several DNA-damaging chemotherapies to treat cancers[22,87]. However, the SASP is composed of several molecules, such as IL-6 and VEGF, that can ironically create a tumorigenic microenvironment and drive metastasis[5,55,88]. Consequently, lingering senescent cells can drive cancer relapse and more aggressive cancer phenotypes. Additionally, senescent cells have even been shown to engulf and consume surrounding healthy cells as a source of macromolecular

building blocks[89]. Hence, remaining senescent cells have negative consequences and must be cleared for senescence to be fully beneficial.

Senescence has been connected to a number of diseases, including Alzheimer's disease and arthritis. As such, identifying strategies capable of eliminating senescent cells is attractive. Over the years, an increasing diversity of senolytics has been discovered, ranging from FOXO4 inhibitors to repurposed cancer chemotherapies[53,90]. Some of the most effective senolytics have taken advantage of certain senescent cell upregulating of anti-apoptotic pathways[21], and thus include Bcl-xL and Bcl-2 inhibitors venetoclax and navitoclax[91–94]. Yet, navitoclax can result in toxic side effects, including thrombocytopenia and neutropenia, making its use challenging[93]. The combination of dasatinib, a tyrosine kinase inhibitor, and quercetin, a broad PI3K inhibitor, has shown promise and entered clinical trials in 2019[21,95]. Even this senolytic advancement is likely to be context-specific and multiple strategies will be necessary. Transgenic mouse models have shown clear benefits to removing senescent cells that express the tumor suppressor, p16. However, this strategy has yet to be translatable to humans.

Here, we describe a novel modality for identifying p16-expressing cells by targeting a p16 MHC-peptide complex. Using phage display, we generated a panel of antibodies that recognize p16 MHC-peptide complexes, both identified and predicted, across the alleles HLA-B*35:01 and HLA-A*02:01. When converted to a scFab CAR, antibodies targeting the HLA-B*35:01 complex showed successful recognition of presented p16-derived peptides and subsequent T cell activation. These antibodies could serve as useful tools in surveying senescent cells for p16 MHC-peptide complexes and targeting them for removal, providing a framework for future senolytic avenues.

It has been suggested age-related impairment can occur if just 0.01%-0.03% of overall cells are senescent[49]. Furthermore, preclinical studies have revealed removing just 30% of senescent cells is sufficient to alleviate the resulting dysfunction[95]. Therefore, although not all senescent cells express p16, complete senolytic clearance may not be required to reap the benefits[24,96]. Indeed, transgenic mouse models showed numerous benefits of specifically clearing p16-expressing senescent cells. Additionally, telomere attrition, which is a cause of replicative senescence and a contributing factor to aging-phenotypes, does not occur in mice[20,97]. As such, it has been speculated that the effects of removing p16-expressing cells may be even more profound in humans than what has been observed thus far in mice[20].

While removing p16-posititive senescent cells has been shown to be beneficial in ameliorating a number of age-related pathologies, there are scenarios in which senescent cells are desirable and constructive. For example, senescent cells play a beneficial role in wound healing and cellular plasticity[41,98,99], limiting fibrosis[16,100], and embryonic development (although this occurs through a p21-dependent pathway and does not involve p16)[22,101]. It has also been shown that senescent pancreatic beta cells secrete higher amounts of insulin, and removing these cells could have negative impacts for glucose homeostasis and diabetic individuals[102]. Additionally, recent reports have indicated that p16-positive senescent cells play an important structural role in vascular and liver endothelial cells, and that when removed but not sufficiently replaced by surrounding cells debilitating fibrosis develops[103]. Furthermore, despite its use as a senescence marker, there are additional cases in which p16 plays other biological roles, such as in macrophage polarization[104]. Hence, therapeutic strategies targeting p16-expressing cells may likely require localized and temporal execution.

Recent advances in CAR T therapies have seen the evolution of multi-circuited effector function. Through systems such as synthetic Notch (synNotch) receptors[99], split costimulatory domains[106], and split CARs[107], we have seen greater precision in target cell removal than single-domain CAR T cells alone. One could envision synNotch receptors against oft-expressed senescence-associated antigens, such as uPAR[83], CD44[22], MICA[13], and DPP4[26], be used to induce transcription of our scFab CARs to increase specificity for p16-positive senescent cells. Alternative approaches could utilize split costimulatory domains with one arm targeting a p16 MHC-peptide complex and the other targeting a tissue-specific biomarker to eliminate senescent cells in a tissue-directed manner. Additionally, reports that bispecific T cell engagers (BiTEs) secreted by CAR T cells create a relatively localized concentration of the effector molecule[108]. As single-chain diabodies (scDbs) have shown recent success in targeting MHC-peptide complexes at extremely low copy numbers[80,81], synNotch receptors driving the release of scDbs derived from the Fabs described here could also be an attractive strategy to kill senescent cells in a localized fashion. This approach is particularly attractive as senescent cells tend to induce senescence in neighboring cells via SASP, resulting in senescent "clusters.[18]" Regardless of approach, it is likely these senolytic strategies would need to be coupled with methods to propagate surrounding healthy tissue to avoid succumbing to debilitating fibrosis and tissue dysfunction[40,103].

In conclusion, we engineered antibodies against p16 MHC-peptide complexes across different HLA alleles. While future work moves to testing these molecules on senescent cells, this platform provides a general phage-display strategy for developing antibodies against class I MHC-peptide complexes. Furthermore, we show a general strategy for the selection of antibodies against weak-binding peptides that will be useful as immunopeptidomics identifies

novel targets. Above all, these antibodies demonstrate a novel way to identify p16-expressing cells and will be useful tools to surveying and ultimately eliminating select senescent cells.

Methods

Cloning

AviTag HLA-A*02:01 in the expression vector pMBio and β_2M in the expression vector pIN-III ompA2 were generous gifts from Dr. Ton Schumacher (Netherlands Cancer Institute). To generate our selection construct, we subcloned a TEV protease cleavage site in between HLA-A*02:01 and the AviTag. Subsequently, we replaced HLA-A*02:01 with the extracellular domain of HLA-B*35:01 to generate our HLA-B*35:01 selection construct. Fabs were subcloned from the phagemid into the expression vector pBL347. scFab CAR's and full-length HLA-B*35:01 were cloned into the lentiviral vectors pCDH-EF1-FHC-Puro and pCDH-EF1-FHC-Hygro, respectively. Full-length p16 was cloned into the lentiviral vector pLVX-TetOne-Puro. All constructs were sequence verified by Sanger sequencing.

Protein expression and purification

MHC-peptide complexes were expressed and refolded as previously described[109]. HLA-B*35:01 peptides were purchased from ELIM Biopharmaceuticals, Inc. and HLA-A*02:01 peptides were purchased from GL Biochem Shanghai Ltd. All peptides were >98% purity. MHC-peptide complexes were refolded at 10°C for 3 days and SEC-purified on a HiLoad 16/600 Superdex 75 pg column equilibrated in 10 mM Tris pH 8. After purification, MHC-peptide complexes were biotinylated using a BirA reaction kit (Avidity) per manufacturer's instructions in the presence of excess peptide and β_2M at 25°C for 4 hours. After biotinylation, MHC-peptide complexes were purified again via SEC to remove excess biotin. Proper folding was assessed by SDS-PAGE.

Biotinylation was assessed by pre-incubating MHC-peptide complexes with NeutrAvidin and subsequently assessed by SDS-PAGE.

Fabs were expressed in E. coli C43 (DE3) Pro+ as previously described using an optimized autoinduction medium and purified by protein A affinity chromatography[37]. Fabs were subsequently buffer exchanged into PBS pH 7.4 and stored in 10% glycerol at -80°C and assessed by SDS-PAGE.

Fab-phage selection

Phage selections were run as previously described[37]. Selections were performed on a KingFischer™ System (Thermo Fisher Scientific). Biotinylated antigens were immobilized using streptavidin-coated magnetic beads (Promega). In each round, phage was first cleared by incubation with beads loaded with MHC-peptide complexes loaded with decoy peptide. Unbound phage was next incubated with beads loaded with p16 MHC-peptide complex. Beads were washed and bound phage was eluted with 50 μg/mL of TEV protease. Four rounds of selection were performed with decreasing amounts of p16 MHC-peptide complex. Selections were performed in PBS+0.02% Tween-20+0.2% bovine serum albumin (PBSTB). Individual phage clones from the fourth round of selections were analyzed by ELISA.

Phage ELISA

For each phage clone, four different conditions were tested – Direct: p16 MHC-peptide complex, Competition: p16 MHC-peptide complex with an equal concentration of p16 MHC-peptide complex in solution, Negative selection: decoy MHC-peptide complex, and Control: PBSTB. 384-well Nunc Maxisorp flat-bottom clear plates (Thermo Fisher Scientific) were coated with 0.5 μg/mL of NeutrAvidin in PBS overnight at 4°C and subsequently blocked with PBSTB.

Plates were washed 3x with PBS containing 0.05% Tween-20 (PBST) and were washed similarly between each of the steps. 20 nM biotinylated p16 MHC-peptide complex or decoy MHC-peptide complex was diluted in PBSTB and immobilized on the NeutrAvidin-coated wells for 30 minutes at room temperature, then blocked with PBSTB + 10 μM biotin for 10 minutes. For the competition samples, phage supernatant was diluted 1:5 into PBSTB with 20 nM p16 MHC-peptide complex 30 minutes prior to addition to the plate. For the direct samples, phage supernatant was diluted 1:5 in PBSTB. Competition and direct samples were added to the plate for 30 minutes at room temperature. Bound phage was detected by incubation with anti-M13-horseradish peroxidase conjugate (Sino Biologics, 1:5000) for 30 minutes, followed by the addition of TMB substrate (VWR International). The reaction was quenched with the addition of 1 M phosphoric acid and the absorbance at 450 nm was measured using a Tecan M200 Pro spectrophotometer. Clones with high binding to p16 MHC-peptide complex and low binding to PBSTB/decoy MHC-peptide complex were carried forward. Clones were further filtered using the competition ELISA where appropriate.

Bio-layer Interferometry

BLI measurements were made using an Octet RED384 (ForteBio) instrument. MHC-peptide complex was immobilized on a streptavidin biosensor and loaded for 200 seconds. After blocking with 10 μM biotin, purified binders in solution were used as the analyte. PBSTB was used for all buffers. Data were analyzed using the ForteBio Octet analysis software and kinetic parameters were determined using a 1:1 monovalent binding model.

Lentivirus and cell line generation

HEK293T cells were cultured in DMEM+10% fetal bovine serum (FBS)+1% Pen/Strep. Cells were seeded $5x10^5$ per well of a 6-well plate a day prior to transfection. Plasmids at the designated concentrations (1.35 μg pCMV delta8.91, 0.165 μg pMD2-G, 1.5 μg insert plasmid) were added to OptiMEM media with 9 μL FuGENE HD Transfection Reagent (Promega) at a 3:1 FuGENE:DNA ratio, incubated for 30 minutes, and subsequently transfected into HEK293T cells. The supernatant was harvested and cleared by passing through a 0.45-μm filter 72 hours post transfection. Cleared supernatant was added to target cells (~1 million cells) with 8 μg/mL polybrene and centrifuged at 1000 x g at 33°C for 3 hours. 24 hours post-transduction, media was replaced with fresh RPMI+10% FBS (tetracycline-negative for B721.221 cells with Doxycycline-inducible p16)+1% Pen/Strep. After an additional 24 hours, drug selection for stable cell lines was initiated by the addition of 2 μg/mL puromycin and 300 μg/mL hygromycin B.

To expand successfully transduced cells, live cells were isolated using SepMate™-50 (IVD) tubes and Lymphoprep™ (Stemcell Technologies). For isolation, cell cultures were centrifuged at 300 x g for 5 minutes and resuspended in 5 mL of cell culture media. 15mL Lymphoprep™ was added to each SepMate™-50 (IVD) tube, and the 5 mL cell suspension was subsequently added. Tubes were centrifuged at 400 x g for 10 minutes, and then supernatant was quickly decanted into 30 mL cell media and the SepMate™-50 (IVD) tube was discarded. The cell culture was spun at 300 x g for 5 minutes and supernatant was removed. Pellets were resuspended in cell media containing appropriate drug and expanded. A total of 2 isolations occurred for each cell line. Once expanded, designated cells were analyzed for expression of scFab CAR or HLA-B*35:01. Jurkat cells displaying high levels of scFab CARs were enriched by flow cytometry by gating for anti-human Fab antibody staining using an anti-human Fab goat

mAb Alexa Fluor 647 conjugate (Jackson ImmunoResearch). B721.221 cells displaying high levels of HLA-B*35:01 were enriched by flow cytometry by gating for anti-human HLA-A,B,C antibody staining using a W6/32 Alexa Fluor 647 conjugate (BioLegend). All flow cytometry cell sorting was performed using a Sony SH800 FACS Cell Sorter.

Cell Culture

The NFAT-GFP reporter Jurkat cells used were a generous gift from Dr. Arthur Weiss (UCSF). Jurkats were cultured in RPMI+10% FBS+1% Pen/Strep+2 mg/mL G418. All scFab CAR containing Jurkat cell lines were maintained in 2 μg/mL puromycin in addition to G418. B721.221 cells were a generous gift from Dr. Lewis Lanier (UCSF). B721.221 cells with Doxycycline-inducible p16 were cultured in RPMI+10% tetracycline-negative FBS+1% Pen/Strep+2 μg/mL puromycin. All HLA-B*35:01 containing B721.221 cells were maintained in 300 μg/mL hygromycin in addition to puromycin. IMR90 primary fibroblasts were purchased from the UCSF cell culture facility. IMR90 cells were cultured in DMEM+10% FBS+1% Pen/Strep. T2 lymphoblasts were purchased from ATCC. T2 cells were cultured in RPMI+10% FBS+1% Pen/Strep with 1x 2-mercaptoethanol. All cell lines were cultured at 37 °C under 5% CO_2.

scFab CAR Jurkats with Immobilized Antigen Assay

Washed streptavidin-coated magnetic beads (Promega) 2x with PBS pH 7.4 for each MHC condition. Made 100 pM MHC-peptide complex solutions with excess β_2M and peptide for each complex. Incubated each solution with beads at room temperature for 30 minutes, and then washed 3x with PBS pH 7.4. Resuspended each in RPMI serum-free media containing excess β_2M and peptide. For beads alone, resuspended in RPMI serum-free media. In a 96-well plate,

added immobilized antigen and designated NFAT-GFP Jurkat line (50000 cells total, $5x10^5$/mL final concentration) to each respective well. Incubated at 37 °C under 5% CO_2 for 24 hours. Beads were removed and cells were analyzed on a CytoFLEX (Beckman Coulter). Data were processed using FlowJo.

scFab CAR Jurkats with B721.221 Cells Assay

48 hours prior to co-culturing, B721.221 cells were cultured in media with or without 2 μg/mL Doxycycline. Media was replaced after 24 hours. In a 48-well plate, cultured B721.221 target line with NFAT-GFP Jurkat effector line at a 3:1 ratio ($3x10^5$:$1x10^5$) in 500 μL. For the "Dox(+)" cultures, cells were cultured in media with 4 μg/mL Doxycycline. Cultures were incubated at 37°C under 5% CO_2 for 24 hours. Cells were washed 1x with PBS pH 7.4+3% bovine serum albumin (BSA), and then stained with anti-human CD3 mouse mAb APC conjugate antibody (Biolegend) for 30 minutes. Cells were washed 3x with PBS pH 7.4+3% BSA and resuspended in 200 μL sterile PBS pH 7.4 and analyzed on a CytoFLEX (Beckman Coulter). Jurkat cells were gated for staining of CD3. Data were processed using FlowJo. scFab CAR Jurkats with lowering Doxycycline-dosed B721.221 cells were analyzed similarly using the appropriate concentration of doxycycline during incubation.

Inducing and Assessing Senescence in IMR90 Fibroblasts

IMR90 cells were seeded at 50K cells/well in a 12-well plate one day prior to treatment. Cells were incubated in media containing either 250 nM Doxorubicin (Sigma-Aldrich) or the equivalent volume of DMSO for 24 hours. For the senescent samples, media was replaced and then subsequently replaced every other day for 9 days post-doxorubicin treatment. Cells were harvested for western blot analysis by washing cells twice with PBS and lysed directly on the

plate. β-galactosidase activity staining was performed using a Senescence β-Galactosidase Staining Kit (Cell Signaling) following the manufacturer's protocol.

Western Blot

Cells were washed twice with PBS prior to lysis. Lysis buffer contained 1x RIPA (EMD Millipore), 1% protease inhibitor cocktail (Sigma-Aldrich), and 1 mM EDTA. Cells were lysed for 20 minutes on ice prior to sonication (1 minute, 20% amp, 1 second on/off pulse). Cells were spun at 16000 x g at 4°C for 5 minutes, and lysate protein concentration was determined using a Pierce™ BCA Protein Assay (Thermo Scientific). Samples were run on a Bolt 4-12% Bis-Tris gel (Invitrogen), and transferred to a PVDF membrane (Thermo Scientific) using an Iblot™ (Thermo Scientific). Membranes were blocked in Odyssey® Blocking Buffer (TBS) (LiCOR) prior to staining. Membranes were stained with primary anti-human $p16^{INK4A}$ (Abcam, ab108349), anti-human HLA-B (Proteintech, 17260), and anti-human α-tubulin (Sigma-Aldrich, T6199) antibodies in blocking buffer overnight at 4°C. Secondary staining was performed using goat anti-rabbit IRDye® 800CW and goat anti-mouse IRDye® 680RD antibodies (LiCOR Biosciences) in blocking buffer for 1 hour at room temperature. Membranes were washed with three 5 minute washes of TBST between each staining step. Membranes were imaged using an Odyssey® CLx (LiCOR Biosciences).

Flow Cytometry of T2 Lymphoblasts

The day prior to Fab staining, T2 lymphoblasts were cultured in RPMI serum-free media containing 50 μg/mL peptide of interest at a concentration of 1 million cells/mL. Cells were spun down at 125 x g for 7 minutes and washed 1x in PBS pH 7.4+3% BSA. Each sample was resuspended in 10 μg/mL Fab for 30 minutes, and then washed 3x in PBS pH 7.4+3% BSA.

Each sample was then stained with an anti-human Fab goat mAb Alexa Fluor 647 conjugate (Jackson ImmunoResearch) for 30 minutes, and then washed 2x in PBS pH 7.4+3% BSA. Samples were resuspended in 200 µL sterile PBS pH 7.4 and analyzed on a CytoFLEX (Beckman Coulter). Data were processed using FlowJo.

Figures and Tables

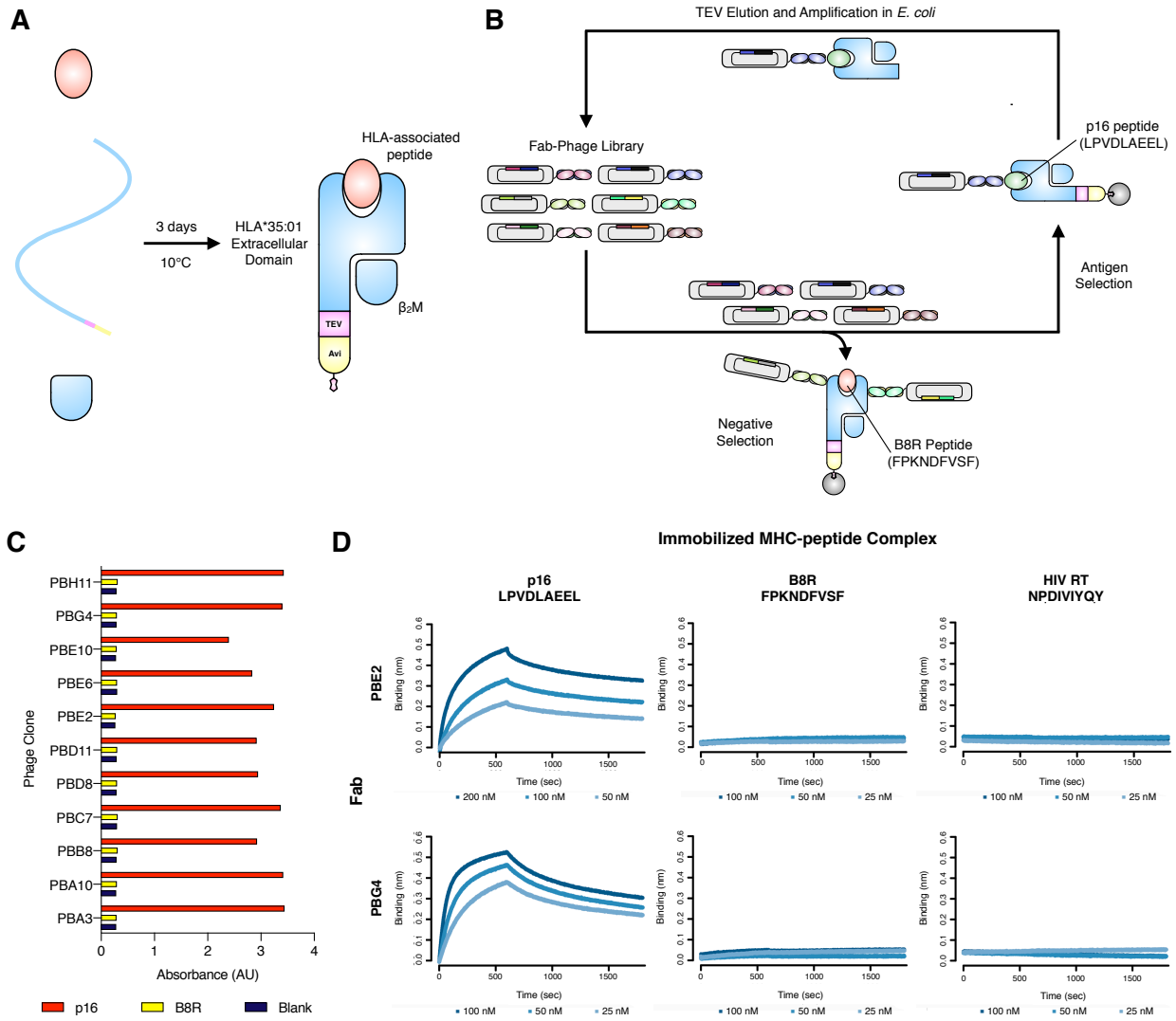

Figure 2.1: Differential selection of highly specific Fabs against HLA-B*35:01 p16 MHC-peptide complexes. A) Refolding and design of MHC-peptide complexes for catch-and-release phage display. B) Differential phage display selection strategy to select for HLA-B*35:01 p16 MHC-peptide complexes. C) ELISA results of the 11 Fab-phage clones identified to be specific for the p16 MHC-peptide complex. D) Octet analysis of PBE2 and PBG4 Fabs against different HLA-B*35:01 MHC-peptide complexes. PBE2 binds the p16 MHC-peptide complex with a $k_{on} \approx 4.13E4$ (1/Ms) and a $k_{off} \approx 3.20E-4$ (1/s). PBG4 binds the p16 MHC-peptide complex with a $k_{on} \approx 1.42E5$ (1/Ms) and a $k_{off} \approx 4.88E-4$ (1/s).

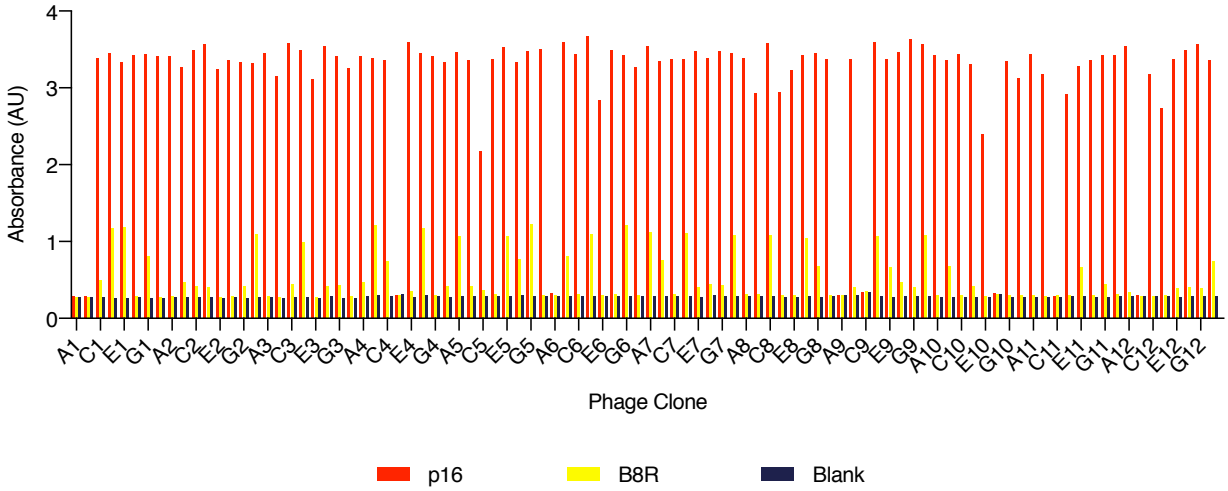

Figure 2.2: Full ELISA screen of Fab-phage clones against HLA-B*35:01 MHC-peptide complexes.

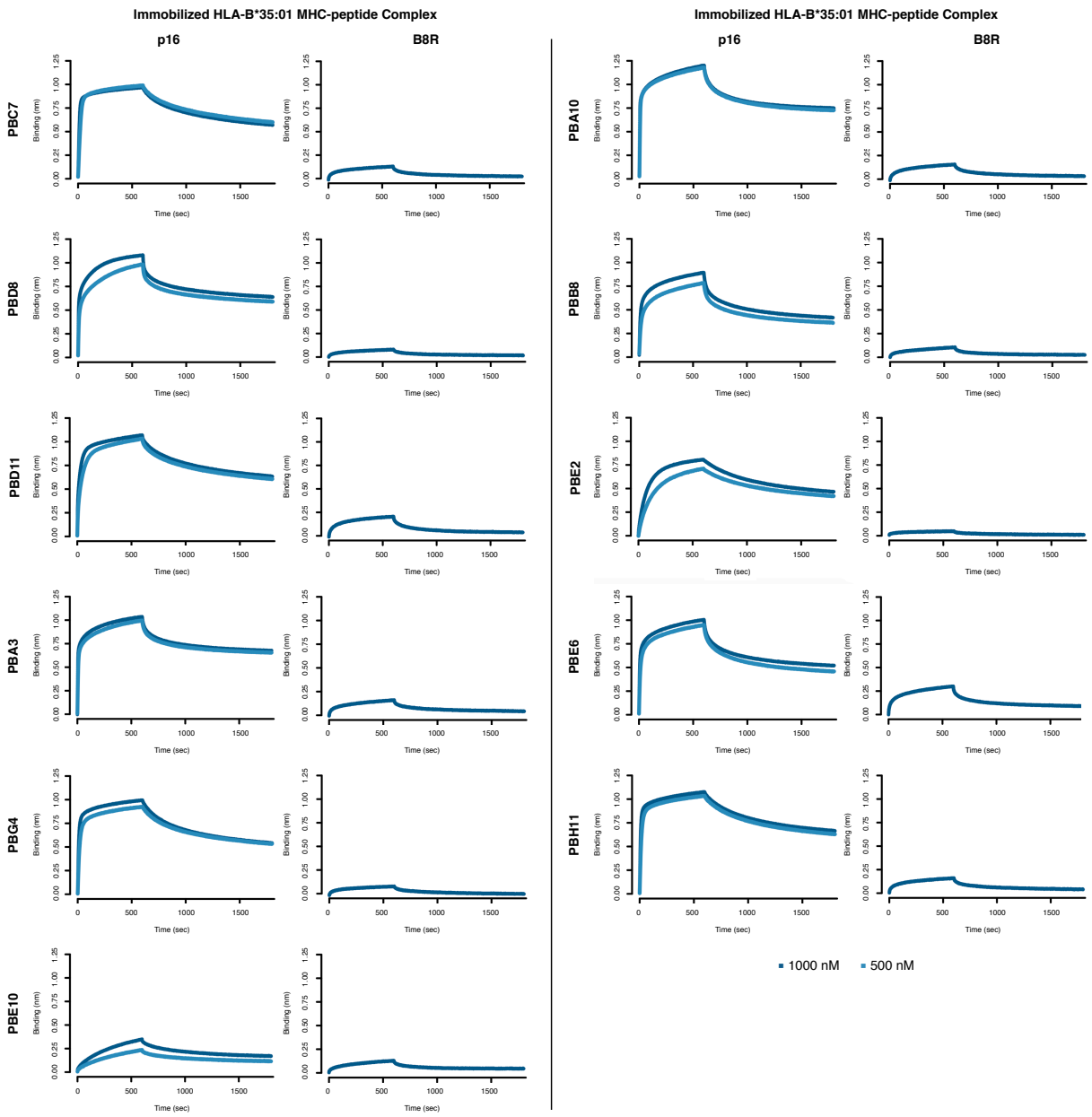

Figure 2.3: Octet binding to screen 11 unique Fab hits from our of our ELISA data in Figure 2.1C.

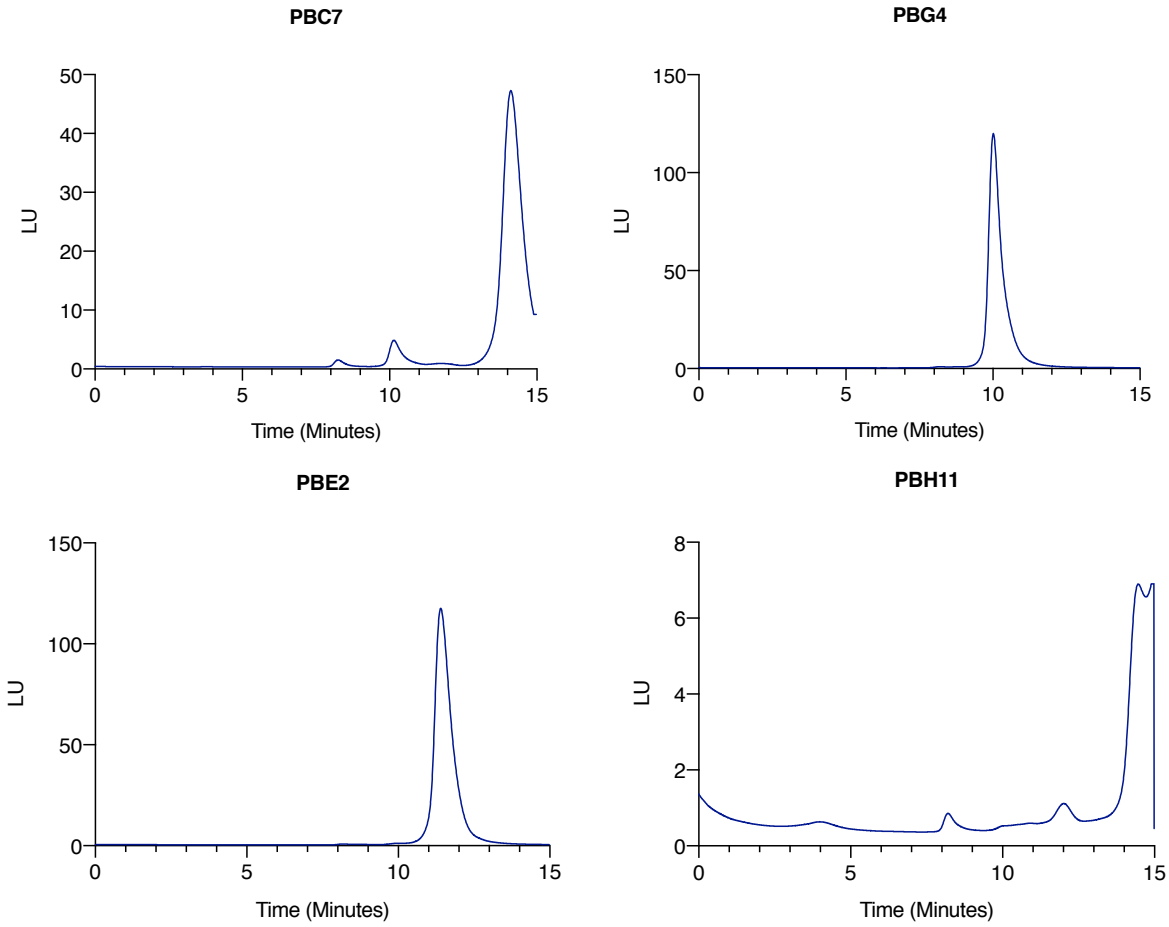

Figure 2.4: SEC traces of 4 Fabs we moved forward with from the Octet screen in Figure 2.3.

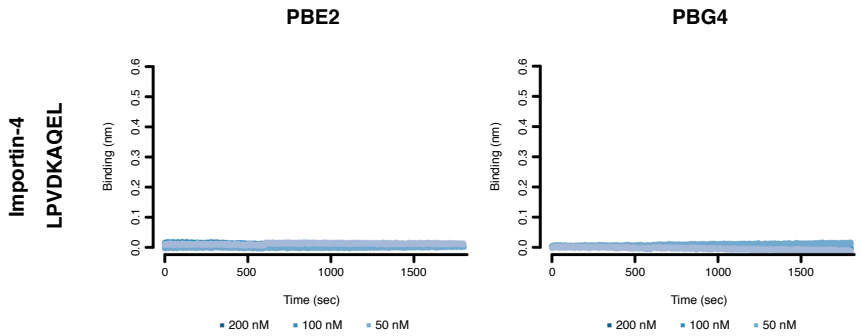

Figure 2.5: Octet binding of PBE2 and PBG4 with the Importin-4 MHC-peptide complex. The Importin-4 peptide (LPVDKAQEL) is the closest in homology in the human proteome to the p16 peptide (LPVDLAEEL), differing at just two positions.

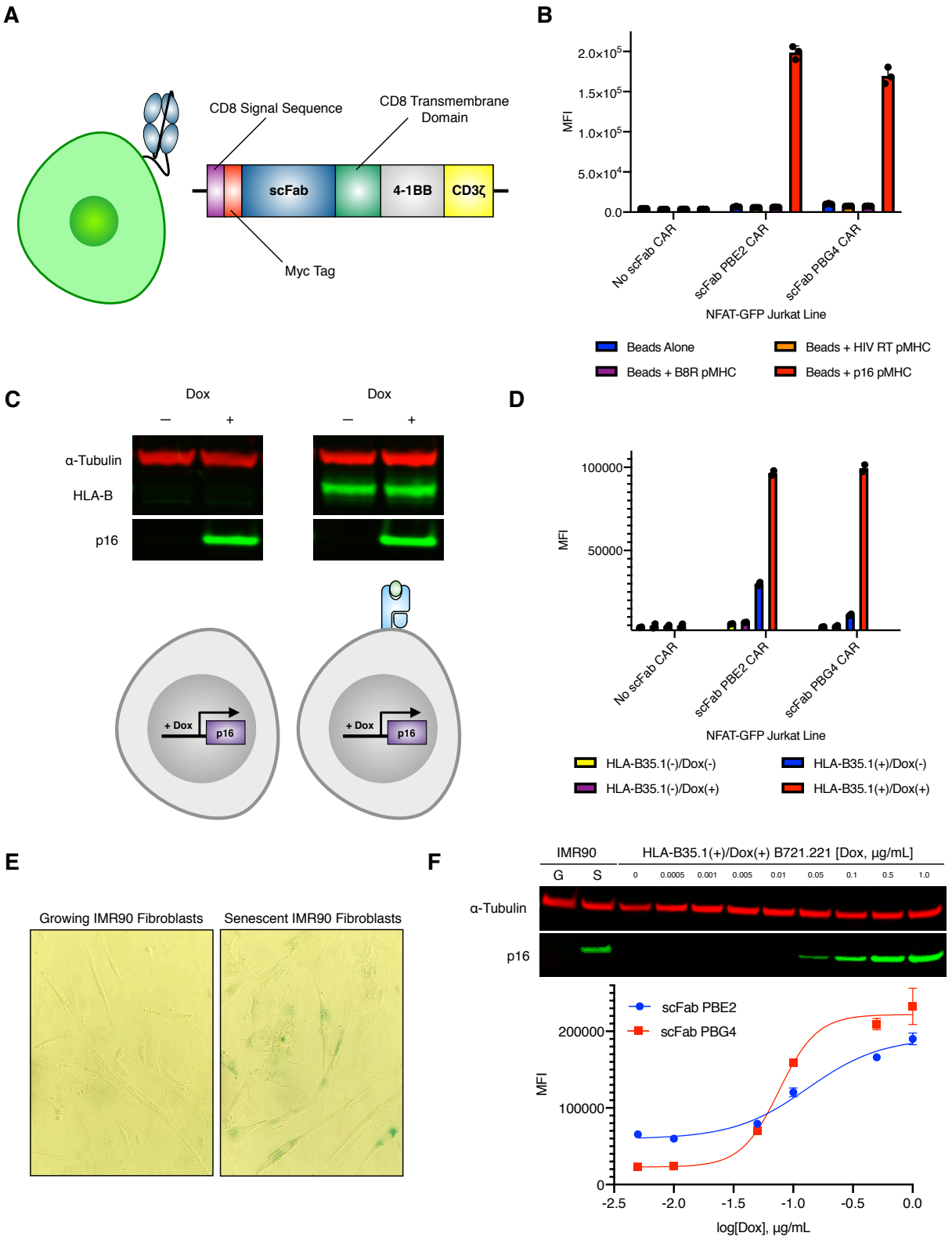

Figure 2.6: scFab CAR Jurkats recognize HLA-B*35:01 p16 MHC-peptide complex on the surface of cells. A) scFab CAR design in NFAT-GFP Jurkat cells. B) FITC-A intensity of scFab CAR Jurkat lines when incubated with streptavidin beads loaded with or without 100 pM

biotinylated HLA-B*35:01 MHC-peptide complexes. C) Engineering of B721.221 cell lines with Doxycycline-inducible expression of p16. D) FITC-A intensity of scFab CAR Jurkats when incubated with B721.221 cell lines from (C). E) Staining of senescence-associated β-galactosidase activity in growing and senescent IMR90 primary fibroblasts. F) Western blot for p16 expression in growing (G) and senescent (S) IMR90 fibroblasts as well as Doxycycline-dosed HLA-B*35:01-expressing B721.221 cells and corresponding FITC-A intensity of scFab CAR Jurkat when incubated with the dosed B721.221 cells.

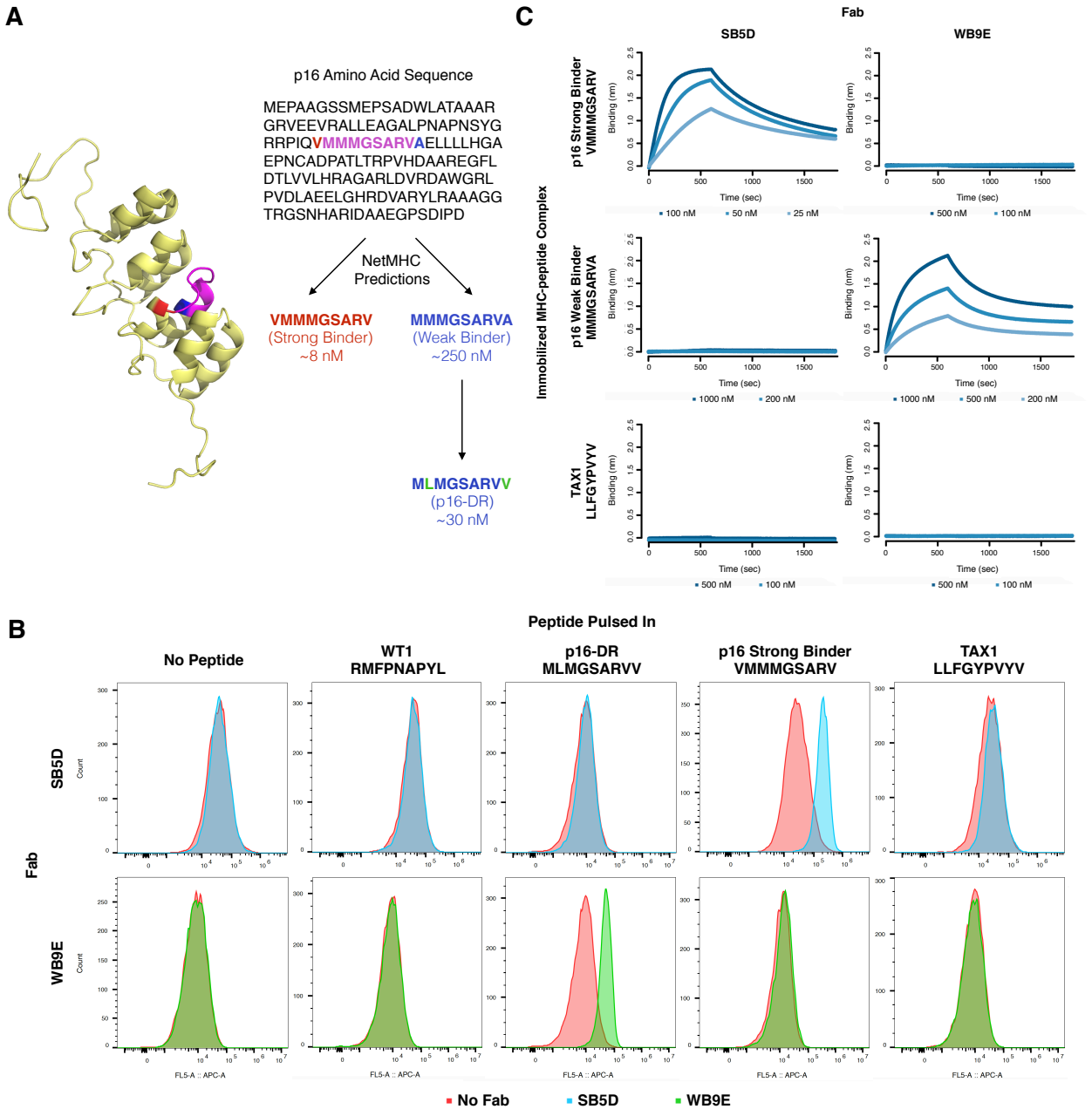

Figure 2.7: Engineering antibodies against predicted HLA-A*02:01 p16 MHC-peptide complexes. A) Application of NetMHC 4.0 predicted HLA-A*02:01-binding peptide sequences and affinities from p16 and engineering of tighter binding p16-DR peptide with predicted affinity (PDB: 1A5E). B) Flow cytometry analysis of Fabs using T2 lymphoblasts that lack endogenous MHC-peptide loading and allow loading with exogenously pulsed-in peptides. C) Octet analysis of Fabs against predicted HLA-A*02:01 p16 MHC-peptide complexes shows highly selective binding. SD5D binds the p16 strong binder MHC-peptide complex with a $k_{on} \approx$ 6.98E4 (1/Ms) and a $k_{off} \approx$ 9.27E-4 (1/s). WBE9 binds the p16 weak binder MHC-peptide complex with a $k_{on} \approx$ 7.71E3 (1/Ms) and a $k_{off} \approx$ 7.44E-4 (1/s).

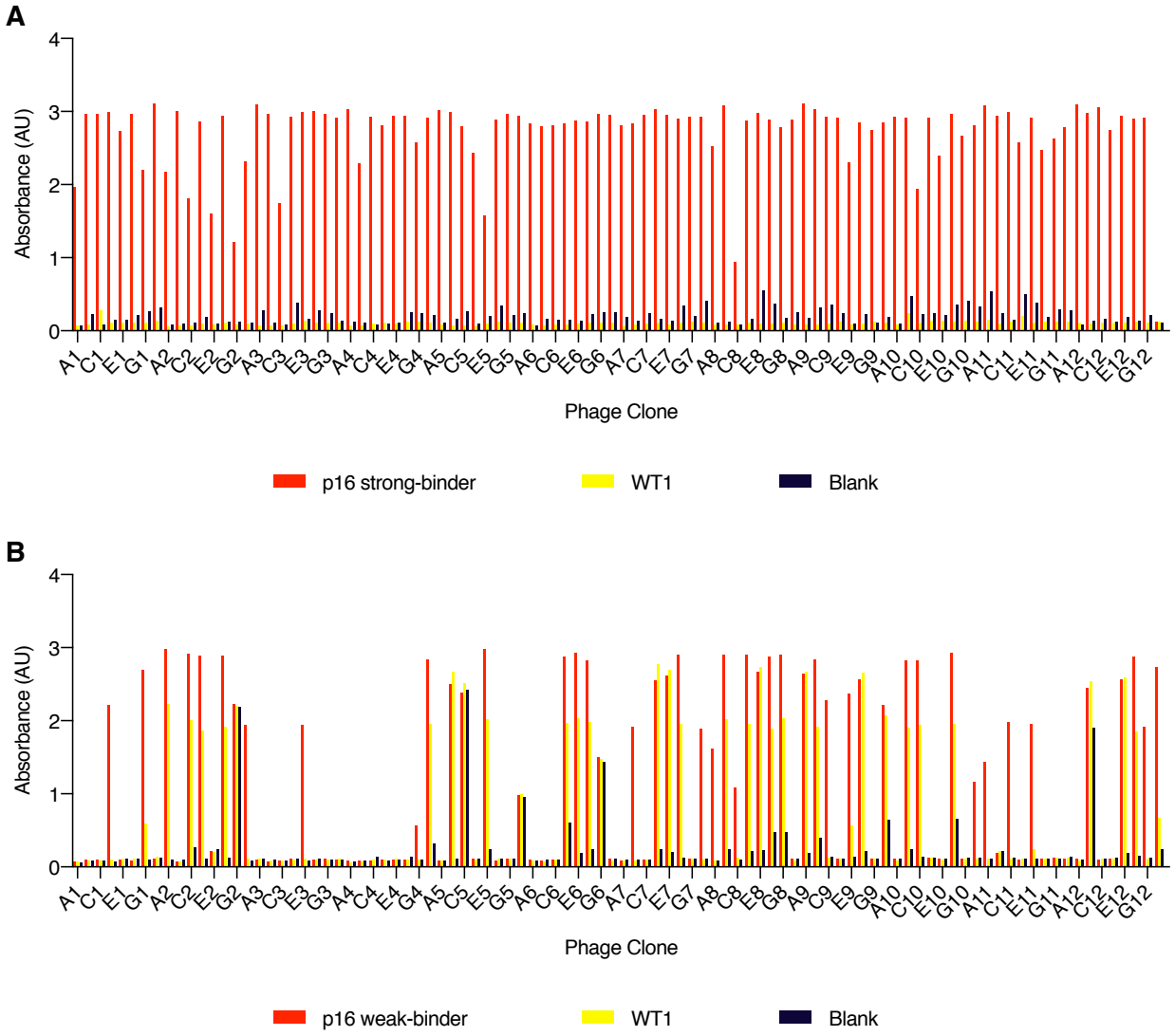

Figure 2.8: Single colony ELISA screening of Fab-phage clones against HLA-A*02:01 p16 MHC-peptide Complexes. A) Full ELISA screening Fab-phage clones against p16 strong-binding MHC-peptide complex. B) Full ELISA screening Fab-phage clones against p16 weak-binding MHC-peptide complex.

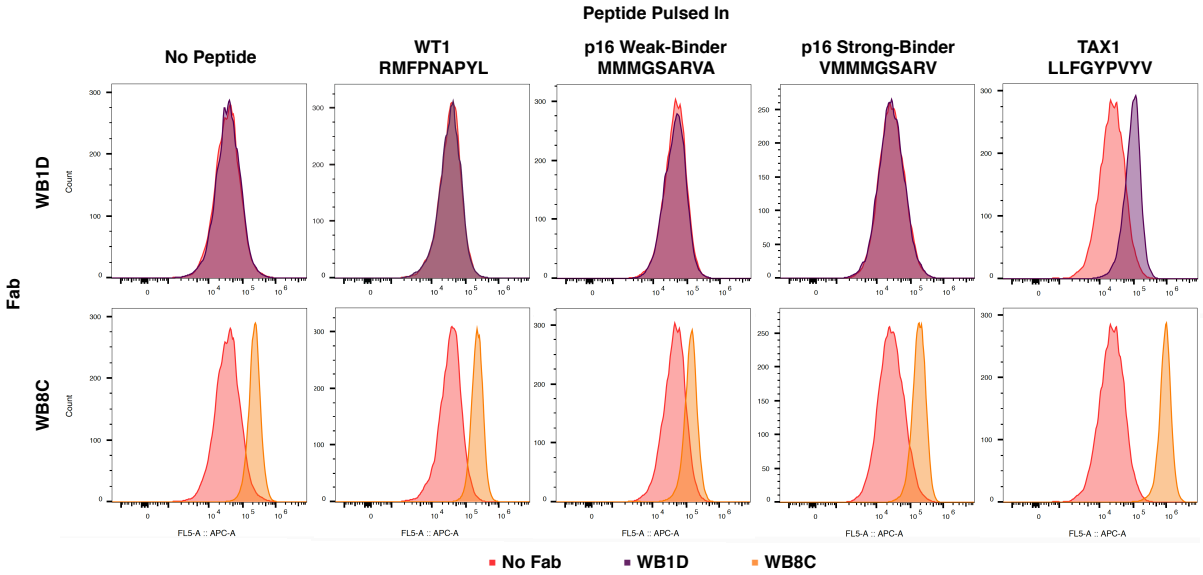

Figure 2.9: Flow cytometry on T2 lymphoblasts of Fabs identified via ELISA to be specific for p16 weak-binding MHC-peptide complex.

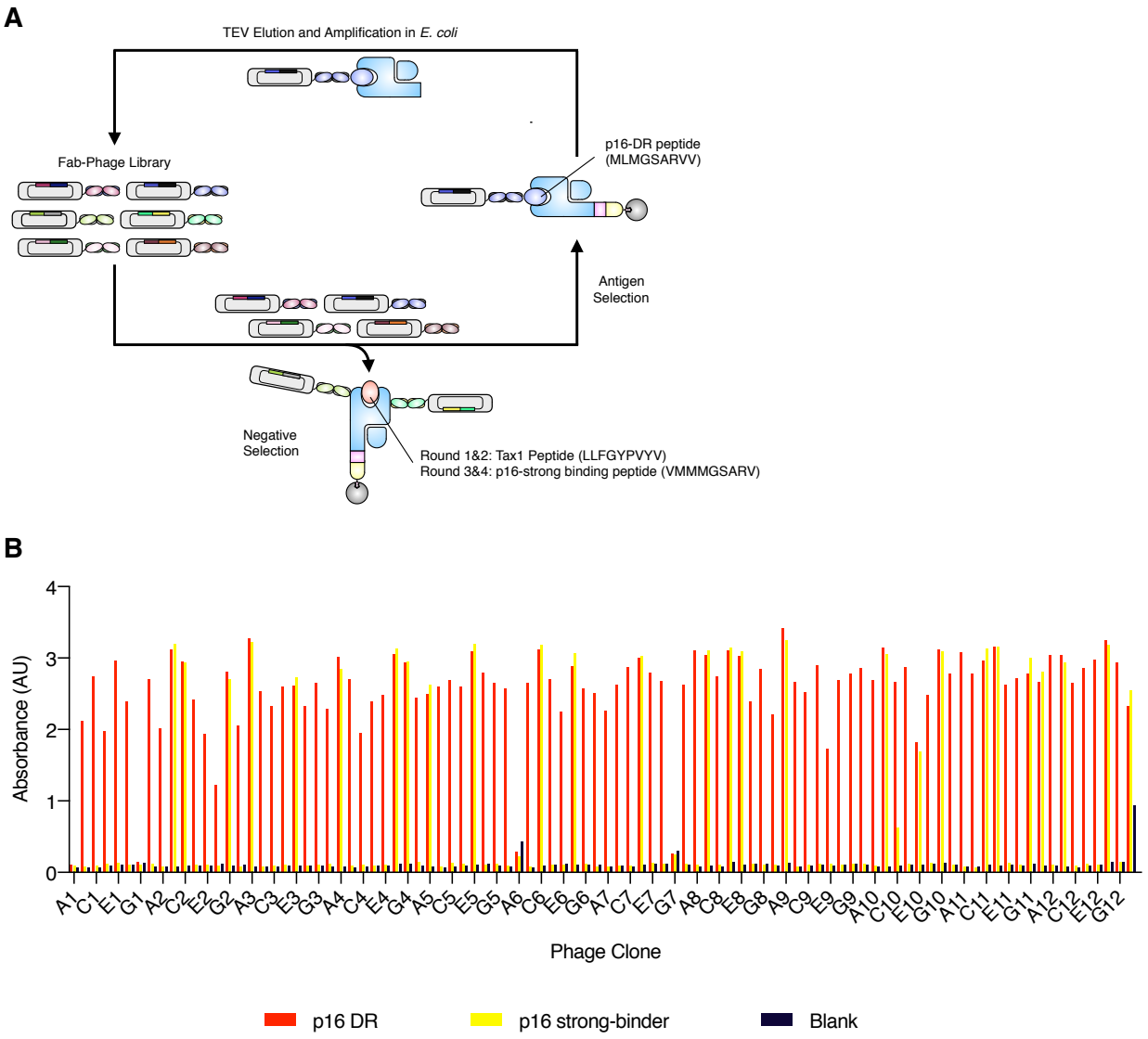

Figure 2.10: Fab-phage display selection for antibodies against p16-DR MHC-peptide complex. A) Selection strategy of p16-DR MHC-peptide complex. B) Full ELISA screen of Fab-phage clones against HLA-A*02:01 MHC-peptide complexes.

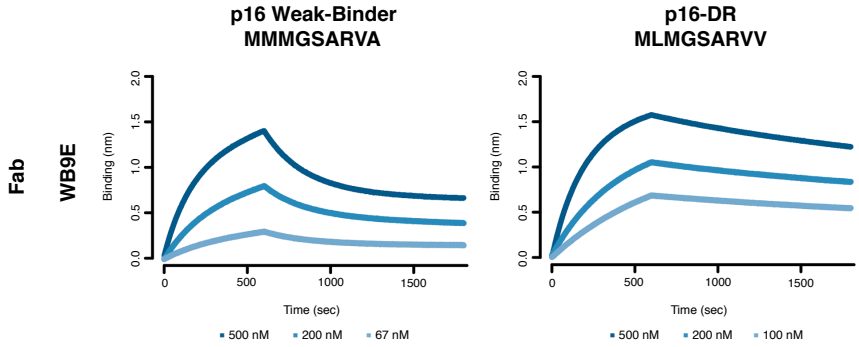

Figure 2.11: Octet binding of WB9E with p16 weak-binding and p16-DR MHC-peptide complex. WBE9 binds the p16 weak binder MHC-peptide complex with a $k_{on} \approx$ 7.71E3 (1/Ms) and a $k_{off} \approx$ 7.44E-4 (1/s). WBE9 binds the p16-DR MHC-peptide complex with a $k_{on} \approx$ 9.69E3 (1/Ms) and a $k_{off} \approx$ 2.07E-4 (1/s).

Chapter 3

Secreted HLA Fc-Fusion Profiles Immunopeptidome in Hypoxic PDAC and Cellular Senescence

Abstract

Human leukocyte antigens (HLA) present peptides from intracellular proteins on the surface of cells in MHC-peptide complexes. These complexes provide a biological window into the cell and peptides derived from disease-associated antigens can serve as biomarkers and therapeutic targets. Thus, proper identification of peptides and the corresponding presenting HLA allele in disease phenotypes is important for the design and execution of therapeutic strategies. Yet, current mass spectrometry methods for profiling the immunopeptidome limit progress as they typically require large sample input that are inherently complex, preventing study of several disease phenotypes and lowering confidence of peptide identification. Here, we describe a novel secreted HLA (sHLA) Fc-fusion construct that can capture HLA-associated peptides and allows for simple purification of peptides of a single HLA allele in different cell models. We used our sHLA immunopeptidomics method to profile the immunopeptidome of hypoxic PDAC and senescent cell lines to identify MHC-peptide complexes that could serve as potential biomarkers for these diseases. Bispecific T cell engagers (BiTEs) targeting the identified IF44L peptide demonstrated enrichment in senescence, indicating our method can identify peptides presented on the surface of diseased cells. Overall, this method was used to profile the immunopeptidome of seven cell lines, across two different HLA alleles, and identified >30000 unique HLA-associated peptides with ~9300 not previously deposited in the Immune Epitope Database. As this method can streamline the time between cell culture to sample injection from days to hours, we believe this method will be useful in the study of the immunopeptidome as therapeutic interest in MHC-peptide complexes as therapeutic targets increases in cancer and beyond.

Introduction

Class I major histocompatibility complexes (MHCs) present peptides derived from intracellular proteins at the surface of cells. With a primary role in immunosurveillance, these MHC-peptide complexes act as antigens for TCR-recognition to elicit immune responses if the complex contains a peptide derived from an immunogenic peptide, such as from a viral protein or containing a point mutation. Yet, peptides from endogenously expressed proteins can bind and be presented. This peptide pool, collectively known as the immunopeptidome, can reflect the proteome of a cell in a given phenotype and hence identifying such peptides are important for therapeutic targeting. Indeed, over the course of the past decade, antibodies targeting MHC-peptide complexes have expanded past neoantigens with successful targeting of disease-associated MHC-peptide complexes such as WT1 and PMEL[65,67,80,81,110].

Given the therapeutic promise of MHC-peptides as biomarkers for disease, there is increasing interest in profiling the immunopeptidome of various disease phenotypes. To date, the most common and practical way to identify these peptides is through mass spectrometry analysis. Yet, challenges remain with current immunopeptidomic methods, including large sample input (up to 10 billion cells), contamination, cell adherence, and importantly, pull down of all class I MHC-peptide complexes regardless of allele (up to six per cell)[111–113]. Additionally, current methods of sample preparation typically span 2-3 days in length, preventing high-throughput analysis. As HLA-associated peptides are inherently difficult to analyze and ID due to similarity in size and amino acid composition, multi-allelic peptide samples can compound decreasing confidence as to peptide origin and sequence when analyzed[111,113].

To circumvent these challenges, others have utilized engineered cell lines to express single HLA constructs. Generation of membrane bound mono-allelic HLA cell lines, such as

C1R and B721.221, have had great success in identifying tens of thousands of HLA-associated peptides to inform prediction algorithms[76,113,114]. While this method produces peptide samples displayed by a specific HLA, this method is restricted to cell lines that are initially HLA-null, thereby restricting the breadth of biological contexts that can be surveyed. Additionally, these cell lines have been reported to have low, but residual, endogenous HLA expression thereby contaminating the samples[113]. Others have developed soluble HLA constructs lacking the transmembrane domain, allowing the HLA to be loaded and subsequently secreted into the milieu to be pulled down[60,115]. While this method retains allele specificity and can be expanded to different cell types, it remains unoptimized and typically relies on bioreactors for cell culture[76]. Additionally, these soluble HLA methods still require copious amounts of material (25-10 mg) as it demands several purification and fractionation steps[60,115]. Hence, current mono-allelic approaches are not amendable to the study the immunopeptidome of cells under different phenotypes to identify disease-associated MHC-peptide complexes.

Here we describe a streamline method of immunopeptidomics that was used to profile the immunopeptidome of hypoxia and senescence using a secreted HLA Fc-fusion construct. This method provides temporal, mono-allelic analysis of the immunopeptidome in a matter of hours, not days, without requiring cell lysis and peptide fractionation. Using samples ranging from 12-130 million cells, we identified >30000 peptides ranging from ~600 to 10000 peptides per sample depending on cell line. We performed an antibody phage display campaign on a peptide confidently identified from senescent samples and used a BiTE to show enriched presentation on the surface of senescent cells. We believe this method will be useful in profiling the immunopeptidome of disease states and will be instrumental in target discovery of MHC-peptide complexes.

Results

sHLA Fc-fusion Captures HLA-associated Peptides in B721.221 cells

Fc-fusion proteins have served as structural scaffolds in the expression and solubilization of the extracellular domain of membrane proteins[116,117]. As HLA proteins lacking the transmembrane domain have been shown to be properly folded and loaded with peptide cargo[60,115], we hypothesized that a HLA Fc-fusion (henceforth referred to as sHLA) could be loaded and secreted similarly (**Figure 3.1**). With mono-allelic B721.221 cell lines providing a standard in the field by providing datasets for peptide processing and binding prediction, we sought to determine if our HLA Fc-fusion could capture HLA-associated peptides in this bonafide cell model. We engineered two B721.221 cells, each transduced to express a unique sHLA under doxycycline induction (**Figure 3.1**). After 52 hours with or without doxycycline treatment, media was collected and sHLA proteins were pulled down using magnetic Protein A beads and analyzed by western blot (**Figures 3.2A & 3.2B**). Cells treated with doxycycline demonstrated expression and secretion of each sHLA, indicating that this construct is processed as expected.

Using these monoallelic sHLA B721.221 cells lines, we performed immunopeptidomics by pulling out sHLA proteins and purifying peptides through acid elution and standard desalting procedures (**Figure 3.1**). Data were analyzed using a stringent 1% FDR, and m/z spectra demonstrated clean +1 and +2 charge populations (data not shown). Identified peptides aligned with expected peptide length (**Figures 3.2C & 3.2D**) and anchor residues (**Figures 3.2E &3.2F**) for each HLA allele. When compared to 9-mer peptides identified from membrane bound MHC-peptide complexes from the same cell line and a published set of 100,000 random 9mer peptides, peptides identified our sHLA method resembled the NetMHC affinity prediction profiles of those pulled out from full length, membrane bound MHC-peptide complexes (**Figures 3.2G &**

3.2H)[76,114]. Additionally, our sHLA method identified similar numbers of peptide ID's as those previously reported. Thus, our sHLA protein can capture HLA-associated peptides in a similar manner as membrane bound MHC-peptide complexes confirming our sHLA method works as expected.

sHLA Fc-fusion Profiles Immunopeptidome in Hypoxic PDAC

Hypoxia, where cell growth conditions drop to below 3% O_2, is a prominent feature in most solid tumors. When available oxygen to cancer cells becomes unsustainable, hypoxic pathways are activated and can manifest in extracellular remodeling, increased angiogenesis, and ultimately metastasis. As such, cancers such as pancreatic ductal adenocarcinoma (PDAC) that are commonly hypoxic tend to have lower survival rates. Hence, identifying markers of hypoxia is of great interest to the cancer field[118]. Yet, the immunopeptidome of the hypoxic cancers, specifically PDAC, has remained relatively understudied.

We chose three different PDAC cell lines used in the study of hypoxia: MiaPaCa-2, KP4, and Capan-1. MiaPaCa-2 and KP4 cells were transduced with our sHLA-B*35:01construct and Capan-1 cells were transduced with the sHLA-A*02:01 construct. Cells were grown either 5 days under 20% O_2 (normoxia) or 1% O_2 (hypoxia), with Doxycycline-treatment beginning after 3 days (**Figure 3.3A**). Across normoxic and hypoxic samples, we identified 7023 unique peptides in MiaPaCa-2's, 3112 unique peptides in KP4's, and 14257 unique peptides in Capan-1 (**Figure 3.3B**). Impressively, normoxic Capan-1 peptide counts ranged from ~8200-10000 HLA-A*02:01-associated peptides from ~130 million cells, demonstrating the potential depth this method can profile the immunopeptidome of a single allele. Of the peptides identified exclusively in hypoxia within each cell line, 99 in MiaPaCa-2's, 61 in KP4's, 135 in Capan-1's, were found with high confidence, appearing in at least 3 out of 4 hypoxic samples. Excitingly,

from these high confidence peptides found within hypoxic samples, we identified peptides from several biomarkers of hypoxia, such as KAD4 (HLA-A*02:01: NLDFNPPHV)[119], DYH11 (HLA-A*02:01: VLFEDAMQHV)[120], and SPAG4 (HLA-A*02:01: SLGKFTFDV)[121]. Interestingly, there were peptides confidently found exclusively in hypoxic samples, such as HLA-B*35:01-associated LPQGPLGTSF derived from TXNIP, despite peptides from the same protein identified in normoxic samples. This suggests that differential processing of peptides may be involved and exclusive to the hypoxic phenotype. More work will be required to dissect the underlying pathways that are over-represented in the immunopeptidome of hypoxia and could serve as therapeutic targets for treating solid tumors.

sHLA Fc-fusion Profiles Immunopeptidome in Cellular Senescence

Senescent cells, or those that have undergone permanent cell-cycle arrest due to compromised integrity or insult, have been shown to drive a host of age-related diseases. Recent senolytic strategies demonstrate a clear benefit of senescent cell removal, including increasing median healthy lifespan by upwards of 30%[54]. Hence, identifying novel markers of senescence is of great interest to the anti-aging field. Yet, little is known regarding the immunopeptidome of senescent cells, likely due to the fragility of cells and difficulty culturing such a large volume of non-proliferative cells for classic methods. Using our sHLA immunopeptidomics method, we sought to identify HLA-associated peptides in senescence.

We chose three different cell lines commonly used in the study of cellular senescence: MCF7 (breast cancer), PC3 (prostate cancer), and A549 (lung cancer). MCF7 cells were transduced with our sHLA-B*35:01 construct while PC3 and A549 cells were transduced with the sHLA-A*02:01 construct. As chemotherapy drugs are frequently used to drive cancer cells into the non-proliferative state of senescence, we treated each cell line with 250 nM doxorubicin

(a topoisomerase II inhibitor) for 24 hours and then cultured for 9 days post-treatment to allow for the senescent phenotype to develop. In parallel, each cell line was treated with DMSO for 24 hours to generate a growing sample (**Figure 3.4A**). Senescence was confirmed by beta-galactosidase activity staining and p21 expression (**Figures 3.4B & 3.5**).

Across growing and senescent samples, we identified 5795 unique peptides in MCF7's, 11105 unique peptides in PC3's, and 3795 unique peptides in A549's (**Figure 3.4C**). Of the peptides identified exclusively in senescence within each cell line, 466 in MCF7's, 1021 in PC3's, 190 in A549's, were found with high confidence, appearing in at least 3 out of 4 samples. Excitingly, from these high confidence peptides exclusive to senescence, we identified peptides from several biomarkers of senescence, such as GDF15 (HLA-A*02:01: ALPEGLPEA)[11], PGH2 (HLA-A*02:01: SVPDPELIKTV)[122], and CCPG1: (HLA-A*02:01: SLQEELNKL)[123]. Remarkably, each MCF7 senescent sample averaged less than 17 million cells per sample with an average peptide ID count of ~3200. This highlights the potential of using this method with smaller cell samples without sacrificing peptide counts. Interestingly, we saw a universal shift across all cell lines where more peptides were identified in senescent samples than growing. As senescent cells have an active secretory phenotype, our sHLA construct may be advantageous and have improved trafficking in phenotypes and cells that already secrete proteins. While data analysis continues in order to understand how the profiled immunopeptidome reflects the biological context and pathways of the senescent phenotype, we demonstrate our sHLA method can capture and identify peptides in senescent cells.

Antibodies Targeting IF44L MHC-peptide Complex Show Increased Presentation in Senescent Cells

We sought to confirm that peptides identified using our sHLA construct have enriched presentation in our disease phenotypes and could serve as potential therapeutic targets. Our immunopeptidomics analysis revealed the HLA-A*02:01-associated peptide, FMLGNYINL, derived from the interferon-induced protein IF44L showed to be specific to senescent PC3 cells both on a peptide and protein level. As antibodies have proven to be useful tools in specifically recognizing and targeting naturally presented MHC-peptide complexes, we pursued a phage display campaign to select for antibodies against the IF44L MHC-peptide complex.

Using a Fab-phage library, we first performed a negative clearance using an immobilized MHC-peptide complex containing a peptide derived from the viral protein TAX1, thereby removing any Fab-phage that bound elsewhere on the complex other than the peptide epitope. Taking the remaining phage, we performed a positive selection against immobilized IF44L MHC-peptide complex and eluted any bound phage with TEV protease cleavage (**Figure 3.6A**). After multiple rounds of selection, individual phage clones were screened via ELISA with one Fab (henceforth referred to as IFB2) demonstrating specific binding to the IF44L MHC peptide complex and not the TAX1 MHC-peptide complex (**Figure 3.6B).** Octet analysis revealed IFB2 bound to the IF44L MHC-peptide complex with an affinity of ~34 nM while exhibiting no binding to the TAX1 MHC-peptide complex (**Figures 3.6C & 3.6D**), highlighting IFB2 specificity. IFB2 bound to T2 lymphoblasts exogenously loaded with the IF44L peptide, demonstrating Fab ability to recognize the IF44L MHC-peptide complex on the surface of cells (**Figure 3.6E**). Therefore, we generated a high affinity, selective antibody that could be used to probe the surface of senescent cells for the IF44L MHC-peptide complex.

Historically, HLA-associated peptides have been suggested to be presented at extremely low copy numbers, with many quantitative analysis reporting well under 100 copies per cell –

often times only reaching single digit levels[78,79]. We converted our Fabs into bispecific T cell engagers (BiTEs) with the ability to activate T cells in the proximity to cells presenting IF44L MHC-peptide complexes (**Figure 3.6F**). T cell activation is highly sensitive and requires very few copies of antigen per cell to elicit a response, providing a suitable model to probe the surface of senescent cells. Using an NFAT-GFP Jurkats, in which GFP expression is a proxy for T cell activation, we were able to survey the surface of target cells for IF44L MHC-peptide presentation. When incubated with IFB2 BiTEs and T2 lymphoblasts loaded with peptide, Jurkats showed significantly greater activation in the presence of cells displaying IF44L MHC-peptide complexes than those displaying TAX1 (**Figure 3.6G**). Hence, the IFB2 BiTE successfully recognizes and activates T cells as expected. When incubated with IFB2 BiTE and growing or senescent MCF7 cells, Jurkats showed >2 fold GFP signal with senescent cells over growing (**Figure 3.6H**). These data show the IF44L peptide identified using the sHLA construct is indeed enriched on the surface of senescent cells, highlighting the potential of this method to easily identify potential targets in the immunopeptidome of disease models and opens the door for potential therapeutics.

Discussion

MHC-peptide complexes are becoming increasingly attractive as therapeutic targets as they can provide extracellular access to disease-associated antigens. Hence, identifying HLA-associated peptides and for specific HLA-alleles is important for therapeutic development and design. Yet, common immunopeptidomics methods require lysis of large samples and use pan-HLA pulldowns to purify mixed peptides across multiple alleles. Mono-alleleic HLA samples have been engineered, but are limited by cell line restriction, culturing conditions, and large sample sizes. Here, we describe a fast, simple, method utilizing a secreted HLA Fc-fusion construct

which can be used to purify allele-restricted HLA-associated peptides. Our method was able to profile the immunopeptidome of hypoxic PDAC and cellular senescence and identified several peptides to be disease-exclusive. Furthermore, Jurkats co-cultured with senescent cells and BiTEs targeting the IF44L peptide had increased activation over growing cells, indicating our sHLA method can identify MHC-peptide complexes enriched in disease phenotypes.

As immunopeptidomics becomes more mainstream and accessible, simpler and more rapid methods will be necessary. We believe this method, which takes mere hours as opposed to days to complete, will be useful in the profiling of several disease models such as viral or bacterial transfection, chemical perturbation, or oncogenic transformation. Additionally, one could also co-culture different cells and only profile the immunopeptidome of a single allele in a single cell line, something that is currently unattainable with today's methods. Lastly, this method can be used to generate datasets that can inform peptide binding and generation prediction algorithms that will be important as more HLA alleles are uncovered and characterized.

While this method shows improvement over current techniques, there are a number of limitations. Given that this requires lentiviral transduction to generate stable cell lines, primary cell lines or those excised directly from patients may not be amenable. Additionally, due to variability in sHLA expression under different phenotypes, we do not believe this method could be used for absolute or relative quantification of HLA-associated peptides. Thus, this method is useful strictly for profiling and identification purposes. Interestingly, we also suspect that sHLA's of a particular allele will not express in cells that endogenously express that HLA allele. For example, HLA-A*02:01 sHLA constructs did not appear to express in IMR90 fibroblasts and Panc-1 cells (data not shown). While more work is necessary to outline the requirements for

suitable cell lines, this may hinder the use of common alleles such as HLA-A*02:01 in the study of phenotypes with limited cell models.

In conclusion, this sHLA method can pull out HLA-associated peptides in an allele-restricted, disease-specific manner. As antibody-based therapeutics are developed and reactive TCR's are identified against specific MHC-peptide complexes, this powerful tool will be useful in target discovery and peptide triage. We believe this information of disease-associated peptides or neoantigens may drastically accelerate personalized medicine and reshape how we assess the potential of certain antigens.

Methods

Cloning

sHLA Fc-fusion was cloned into the lentiviral vector pLVX-TetOne-Puro. AviTag HLA-A*02:01 in the expression vector pMBio and β_2M in the expression vector pIN-III ompA2 were generous gifts from Dr. Ton Schumacher (Netherlands Cancer Institute). To generate our selection construct, we subcloned a TEV protease cleavage site in between HLA-A*02:01 and the AviTag. Fabs were subcloned from the phagemid into the expression vector pBL347. The light chain of the BiTE was cloned from the Fab plasmid into a pFUSE (InvivoGen) vector with the OKT3 anti-human CD3 scFv. The heavy chain of the BiTE was cloned from the Fab plasmid into the same vector but lacking the Fc domain. All constructs were sequence verified by Sanger sequencing.

Cell culture

B721.221 cells were a generous gift from Dr. Lewis Lanier (UCSF). Capan-1 pancreatic cancer cells were from Wells lab frozen stocks. KP4 and MiaPaCa-2 pancreatic cells were generous

gifts from Dr. Rushika Perera (UCSF). A549 lung cancer cells were a gift from Dr. Oren Rosenberg (UCSF). PC3 prostate cancer cells and MCF7 breast cancer cells were purchased from the UCSF Cell Culture Facility. B721.221, A549, PC3, and MCF7 cells were all grown in RPMI+10% Tetracycline-negative FBS+1% Pen/Strep. Capan-1, KP4, and MiaPaCa-2 cells were all grown in IMDM+10% Tetracycline-negative FBS+1% Pen/Strep. Cell lines transduced with the sHLA Fc-fusion were cultured in media with 2 μg/mL puromycin. sHLA Fc-fusion cell lines were cultured in respective media without FBS and with Doxycycline for sample collection. The NFAT-GFP reporter Jurkat cells used were a generous gift from Dr. Arthur Weiss (UCSF). Jurkats were cultured in RPMI+10% FBS+1% Pen/Strep+2 mg/mL G418. All cells were grown at 37°C, 5% O_2 unless otherwise stated.

To generate normoxic Capan-1, KP4, and MiaPaCa-2 cells, cells were grown for 3 days in IMDM+10% Tetracycline-negative FBS+1% Pen/Strep at 37°C, 5% O_2 before beginning Doxycycline treatment. Hypoxic cells were grown in a hypoxic chamber in IMDM+10% Tetracycline-negative FBS+1% Pen/Strep at 37°C, 1% O_2 prior to Doxycycline treatment. Hypoxic cells were only removed from the chamber to replaced media for the appropriate condition and exchange was conducted as quickly as possible to avoid the onset of the normoxic phenotype.

A549, MCF7, and PC3 cells were seeded one day prior to treatment. Cells were incubated in media containing either 250 nM Doxorubicin (Sigma-Aldrich) or the equivalent volume of DMSO for 24 hours. Growing samples were treated with Doxycycline immediately after DMSO treatment. For the senescent samples, media was replaced and then subsequently replaced every other day for 8 days post-doxorubicin treatment before Doxycycline treatment. Cells were seeded separately for western blot analysis and β-galactosidase activity staining. β-

galactosidase activity staining was performed using a Senescence β-Galactosidase Staining Kit (Cell Signaling) following the manufacturer's protocol.

Lentivirus and cell line generation

HEK293T cells were cultured in DMEM+10% FBS+1% Pen/Strep. Cells were seeded $5x10^5$ per well of a 6-well plate a day prior to transfection. Plasmids at the designated concentrations (1.35 μg pCMV delta8.91, 0.165 μg pMD2-G, 1.5 μg sHLA plasmid) were added to OptiMEM media with 9 μL FuGENE HD Transfection Reagent (Promega) at a 3:1 FuGENE:DNA ratio, incubated for 30 minutes, and subsequently transfected into HEK293T cells. The supernatant was harvested and cleared by passing through a 0.45-μm filter 72 hours post transfection. Cleared supernatant was added to target cells (~1 million cells) with 8 μg/mL polybrene and centrifuged at 1000 x g at 33°C for 3 hours. 24 hours post-transduction, media was replaced with appropriate fresh media. After an additional 24 hours, drug selection for stable cell lines was initiated by the addition of 2 μg/mL puromycin and expanded.

To expand successfully transduced B721.221 cells, live cells were isolated using SepMate™-50 (IVD) tubes and Lymphoprep™ (Stemcell Technologies). For isolation, cell cultures were centrifuged at 300 x g for 5 minutes and resuspended in 5 mL of cell culture media. 15mL Lymphoprep™ was added to each SepMate™-50 (IVD) tube, and the 5 mL cell suspension was subsequently added. Tubes were centrifuged at 400 x g for 10 minutes, and then supernatant was quickly decanted into 30 mL cell media and the SepMate™-50 (IVD) tube was discarded. The cell culture was spun at 300 x g for 5 minutes and supernatant was removed. Pellets were resuspended in cell media containing appropriate drug and expanded. A total of 2 isolations occurred for each cell line.

Mass Spectrometry Sample Preparation

Cell phenotypes were induced as described. Cells were cultured in media with 2 μg/mL Doxycycline for 24 hours, and then subsequently cultured in serum-free media with 2 μg/mL Doxycycline for 28 hours prior to media collection. For each 50 mL of media sample, 100 μL of Pierce™ Protein A Magnetic beads (Thermo Scientific) were washed twice with PBS prior to use. Beads were added to media was filtered with 0.45-μm filters and rotated for 1 hour at 4°C. Samples were spun at 500 x g for 5 minutes and media removed. Beads were washed strenuously with 10 mM Tris pH 8.0 made with Optima™ LC/MS water (Thermo Scientific). After washing, protein/peptides were eluted by incubating beads with 10% acetic acid for 10 minutes at room temperature. Beads were washed twice with 10% acetic acid, and washes and elution were pooled together. Samples were dried in a Genevac prior to desalting.

Dried down samples were resuspended in 75 μL of 1% TFA and vortexed vigorously. Samples were centrifuged at 21,000 x g for 5 minutes at RT to remove any remaining precipitate. Sample was placed in a magnetic rack, after which the supernatant was removed gently from the tube and placed in a prepared Pierce C18 column as per manufacturer's instruction. Shortly, each column was washed with 200 μL of 70% acetonitrile in water and spun down at 1500xg until dry. The columns were further washed with 200 μL of 50% acetonitrile in water and spun still dryness. Following the pre-wash steps, each column was further washed twice with 200 μL of 5% acetonitrile/0.5% TFA in water and spun till dryness. The sample was then loaded onto the column and spun till dryness. Each sample was reloaded onto the column to maximize peptide yield. Samples were then washed with 2x 200 μL of 5% acetonitrile/0.5% TFA in water, 200 μL of 5% acetonitrile/1% FA in water, and eluted in 2x 50 μL of 70% acetonitrile in water. Samples were dried to completion.

Mass Spectrometry

Liquid chromatography and mass spectrometry was performed as previously described[124]. Briefly, each sample was brought up in 6.5 µL of 2% acetonitrile/0.1% formic acid in water, vortexed vigorously, and spun down at maximum speed to remove any precipitate. The sample was transferred and 6 µL of the peptide supernatant was separated using a nanoElute UHPLC system (Bruker) with a pre-packed 25 cm x 75 µm Aurora Series UHPLC column + CaptiveSpray insert (CSI) column (120 A pore size, IonOpticks, AUR2-25075C18A-CSI) and analyzed on a timsTOF Pro (Bruker) mass spectrometer. Peptides were separated using a linear gradient of 7-30% (Solvent A: 2% acetonitrile, 0.1% formic acid, solvent B: acetonitrile, 0.1% formic acid) over 60min at 400 nL/min. Data-dependent acquisition was performed with parallel accumulation-serial fragmentation (PASEF) and trapped ion mobility spectrometry (TIMS) enabled with 10 PASEF scans per top N acquisition cycles. The TIMS analyzer was operated at a fixed duty cycles close to 100%using equal accumulation and ramp times of 100 ms each. Singly charged precursors below 800m/z were excluded by their position in the m/z-ion mobility plane, and precursors that reached a target value of 20,000 arbitrary units were dynamically excluded for 0.4 min. The quadrupole isolation width was set to 2 m/z for m/z < 700 and 3 m/z for m/z > 700 and a mass scan range of 100-1800 m/z. TIMS elution voltages were calibrated linearly to obtain the reduced ion mobility coefficients (1/K0) using three Agilent ESI-L Tuning Mix ions (m/z 622, 922, and 1,222).

Data Analysis

Briefly, for general database searching, peptides for each individual dataset were searched using PEAKS Online X version 1.5 against the entire Swiss-prot Human Proteome (Swiss-prot).

Enzyme specificity was set to Unspecific. Peptide length was specified between 8-12 amino acids. No fixed modifications were set, while acetylation (N-term) and methionine oxidation were set as variable modifications. The precursor mass error tolerance was set to 20 PPM and the fragment mass error tolerance was set to 0.03Da. Data was filtered at 1% for both protein and peptide FDR. All mass spectrometry database searching was based off of four biological replicates. Biological replicates underwent preparation, washing, and downstream LC-MS/MS preparation separately.

Western Blot

sHLA Fc-fusion samples from B721.221 cells were generated and purified as described. Beads were washed three times with PBS and protein was eluted with 0.1 M acetic acid. For growing and senescent samples, cells were washed twice on plate with PBS prior to lysis. Lysis buffer contained 1x RIPA (EMD Millipore), 1% protease inhibitor cocktail (Sigma-Aldrich), and 1 mM EDTA. Cells were lysed for 20 minutes on ice prior to sonication (1 minute, 20% amp, 1 second on/off pulse). Cells were spun at 16000 x g at 4°C for 5 minutes, and lysate protein concentration was determined using a Pierce™ BCA Protein Assay (Thermo Scientific).

Samples were run on a Bolt 4-12% Bis-Tris gel (Invitrogen), and transferred to a PVDF membrane (Thermo Scientific) using an Iblot™ (Thermo Scientific). Membranes were blocked in Odyssey® Blocking Buffer (TBS) (LiCOR) prior to staining. Membranes were stained with primary anti-FLAG (Cell Signaling, 14793S), anti-human HLA-A (Thermo Scientific, PA5-29911), anti-human HLA-B (Proteintech, 17260), anti-human p21 (Abcam, ab109520), and anti-human α-tubulin (Sigma-Aldrich, T6199) antibodies in blocking buffer for 1 hour at room temperature or overnight at 4°C. Secondary staining was performed using goat anti-rabbit IRDye® 800CW and goat anti-rabbit IRDye® 680RD antibodies (LiCOR Biosciences) in

blocking buffer for 1 hour at room temperature. Membranes were washed with three 5 minute washes of TBST between each staining step. Membranes were imaged using an Odyssey® CLx (LiCOR Biosciences).

Protein Expression and Purification

MHC-peptide complexes were expressed and refolded as previously described[109]. Peptides were purchased from ELIM Biopharmaceuticals, Inc. All peptides were >98% purity. MHC-peptide complexes were refolded at 10°C for 3 days and SEC-purified on a HiLoad 16/600 Superdex 75 pg column equilibrated in 10 mM Tris pH 8. After purification, MHC-peptide complexes were biotinylated using a BirA reaction kit (Avidity) per manufacturer's instructions in the presence of excess peptide and β_2M at 25°C for 4 hours. After biotinylation, MHC-peptide complexes were purified again via SEC to remove excess biotin. Proper folding was assessed by SDS-PAGE. Biotinylation was assessed by pre-incubating MHC-peptide complexes with NeutrAvidin and subsequently assessed by SDS-PAGE.

Fabs were expressed in E. coli C43 (DE3) Pro+ as previously described using an optimized autoinduction medium and purified by protein A affinity chromatography[37]. Fabs were subsequently buffer exchanged into PBS pH 7.4 and stored in 10% glycerol at -80°C and assessed by SDS-PAGE.

BiTEs were expressed and purified from Expi293F-BirA cells using transient transfection (Expifectamine, Thermo Scientific). Enhancers were added 20 hrs after transfection. Cells were incubated for 5 days at 37ºC and 8% CO_2. Media was then harvested by centrifugation at 4,000xg for 20 min. BiTEs were purified by protein A affinity chromatography and buffer exchanged into PBS pH 7.4, then stored in 10% glycerol at -80°C and assessed by SDS-PAGE.

Fab-phage selection

Phage selections were run as previously described[37]. Selections were performed on a KingFischer™ System (Thermo Scientific). Biotinylated antigens were immobilized using streptavidin-coated magnetic beads (Promega). In each round, phage was first cleared by incubation with beads loaded with MHC-peptide complexes loaded with TAX1 peptide. Unbound phage was next incubated with beads loaded with IF44L MHC-peptide complex. Beads were washed and bound phage was eluted with 50 μg/mL of TEV protease. Four rounds of selection were performed with decreasing amounts of IF44L MHC-peptide complex. Selections were performed in PBS+0.02% Tween-20+0.2% bovine serum albumin (PBSTB). Individual phage clones from the fourth round of selections were analyzed by ELISA.

Phage ELISA

For each phage clone, four different conditions were tested – Direct: IF44L MHC-peptide complex, Competition: IF44L MHC-peptide complex with an equal concentration of IF44L MHC-peptide complex in solution, Negative selection: TAX1 MHC-peptide complex, and Control: PBSTB. 384-well Nunc Maxisorp flat-bottom clear plates (Thermo Fisher Scientific) were coated with 0.5 μg/mL of NeutrAvidin in PBS overnight at 4°C and subsequently blocked with PBSTB. Plates were washed 3x with PBS containing 0.05% Tween-20 (PBST) and were washed similarly between each of the steps. 20 nM biotinylated IF44L MHC-peptide complex or TAX1 MHC-peptide complex was diluted in PBSTB and immobilized on the NeutrAvidin-coated wells for 30 minutes at room temperature, then blocked with PBSTB +10 μM biotin for 10 minutes. For the competition samples, phage supernatant was diluted 1:5 into PBSTB with 20 nM IF44L MHC-peptide complex 30 minutes prior to addition to the plate. For the direct samples, phage supernatant was diluted 1:5 in PBSTB. Competition and direct samples were

added to the plate for 30 minutes at room temperature. Bound phage was detected by incubation with anti-M13-horseradish peroxidase conjugate (Sino Biologics, 1:5000) for 30 minutes, followed by the addition of TMB substrate (VWR International). The reaction was quenched with the addition of 1 M phosphoric acid and the absorbance at 450 nm was measured using a Tecan M200 Pro spectrophotometer. Clones with high binding to IF44L MHC-peptide complex and low binding to PBSTB/TAX1 MHC-peptide complex were carried forward. Clones were further filtered using the competition ELISA where appropriate.

Bio-layer Interferometry

BLI measurements were made using an Octet RED384 (ForteBio) instrument. MHC-peptide complex was immobilized on a streptavidin biosensor and loaded for 200 seconds. After blocking with 10 μM biotin, purified binders in solution were used as the analyte. PBSTB was used for all buffers. Data were analyzed using the ForteBio Octet analysis software and kinetic parameters were determined using a 1:1 monovalent binding model.

Flow Cytometry of T2 Lymphoblasts

The day prior to Fab staining, T2 lymphoblasts were cultured in RPMI serum-free media containing 50 μg/mL peptide of interest at a concentration of 1 million cells/mL. Cells were spun down at 125 x g for 7 minutes and washed 1x in PBS pH 7.4+3% BSA. Each sample was resuspended in 10 μg/mL Fab for 30 minutes, and then washed 3x in PBS pH 7.4+3% BSA. Each sample was then stained with Protein A, Alexa Fluor® 647 conjugate (Life Technologies) for 30 minutes, and then washed 3x in PBS pH 7.4+3% BSA. Samples were resuspended in sterile PBS pH 7.4 and analyzed on a CytoFLEX (Beckman Coulter). Data were processed using FlowJo.

BiTE Assays

T2 lymphoblasts and NFAT-GFP Jurkats were seeded at 1:1 ratio ($5x10^4$:$5x10^4$) in a 96-well round bottom plate containing 50 μg/mL peptide of interest and 100 pM BiTE for 24 hours with n=3 technical replicates per condition. Cells where the percentage of GFP+ cells is gated so ~97% of Jurkat cells with no BiTE are classified as GFP negative. SKMEL5 cells were analyzed on the LSRII, T2 on the CytoFLEX. Growing and senescent MCF7 cells were prepared as described. Cells were lifted using 0.05% Trypsin-EDTA, and seeded with Jurkat NFAT-GFP cells in a 5:1 (MCF7:Jurkat, $2.5x10^5$:$5x10^4$) for 24 hours. All samples were analyzed on the CytoFlex and analyzed on FlowJo.

Figures and Tables

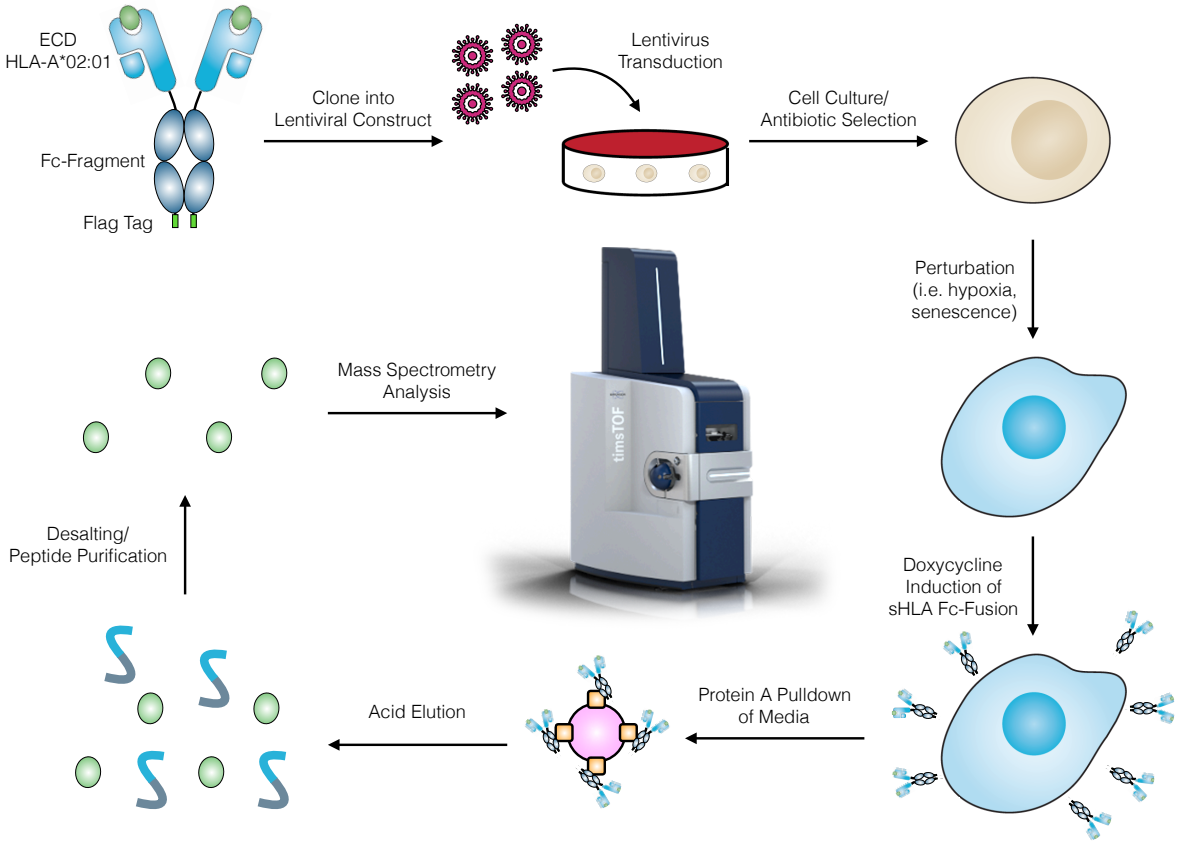

Figure 3.1: Workflow for sHLA cell line generation and subsequent immunopeptidomics.

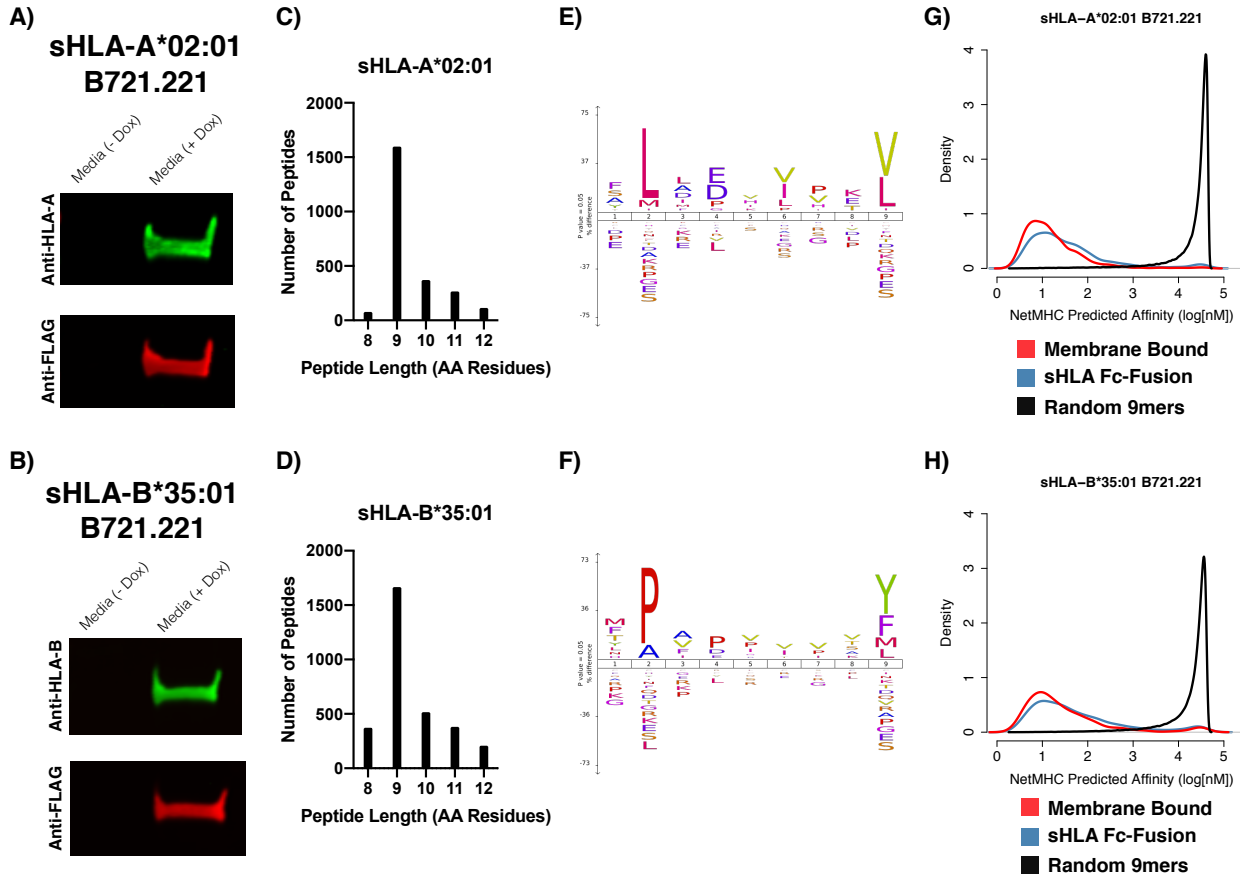

Figure 3.2: Secreted HLA Fc-fusions capture HLA-associated peptides in B721.221 cells. A & B) Western blot of eluted sHLA Fc-fusion protein captured from Doxycycline-treated or –free media of sHLA monoallelic B721.221 cell lines. C &D) Quantification of peptide length from each sHLA B721.221 immunopeptidomics dataset. E & F) ICE logos of 9mer peptides from each sHLA B721.221 immunopeptidomics dataset. G &H) NetMHC predicted affinities of our 9mer peptides from sHLA B721.221 immunopeptidomics dataset compared to published 9mers identified from membrane bound monoallelic B721.221 cells and a published list of 100,000 9mer peptides.

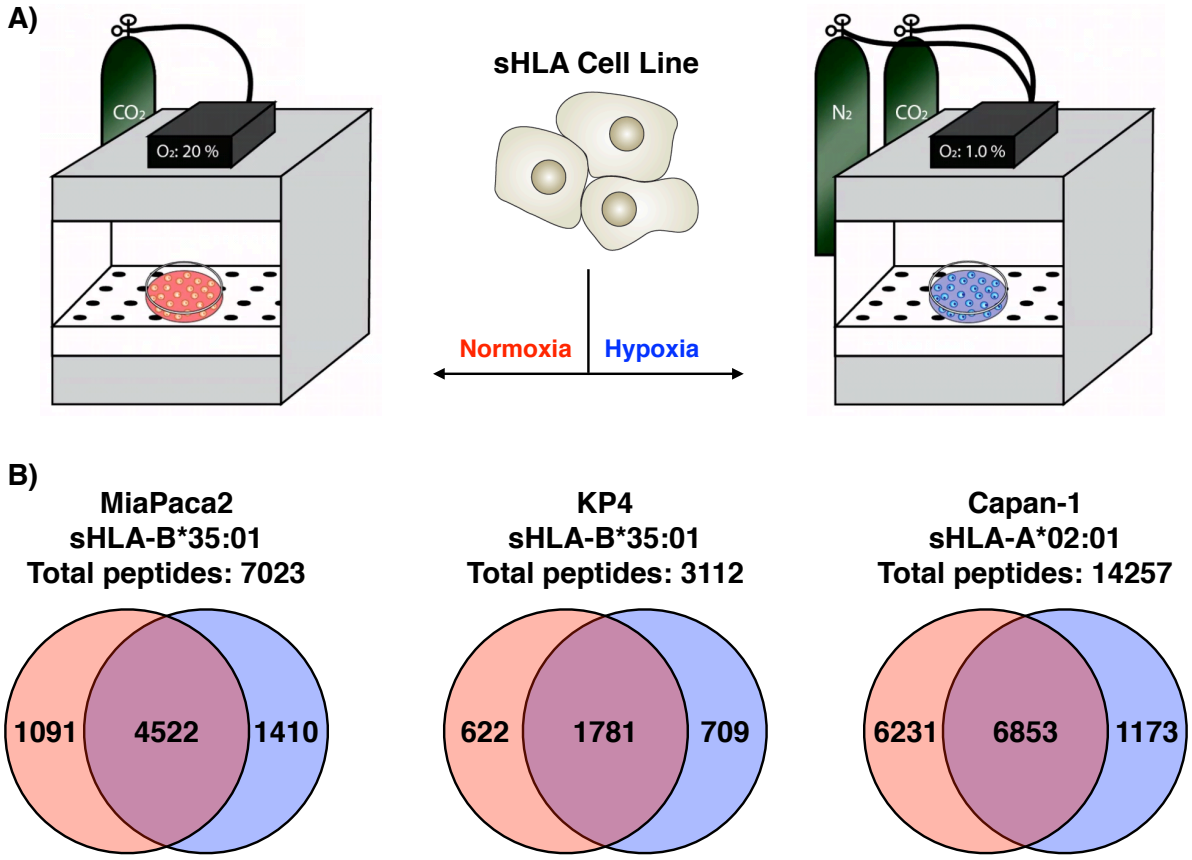

Figure 3.3: Immunopeptidomics of hypoxic PDAC cells using sHLA Fc-fusions. A) Strategy for generating normoxic and hypoxic cells for immunopeptidomics. B) Number of peptides identified in normoxic and hypoxic samples for each cell line.

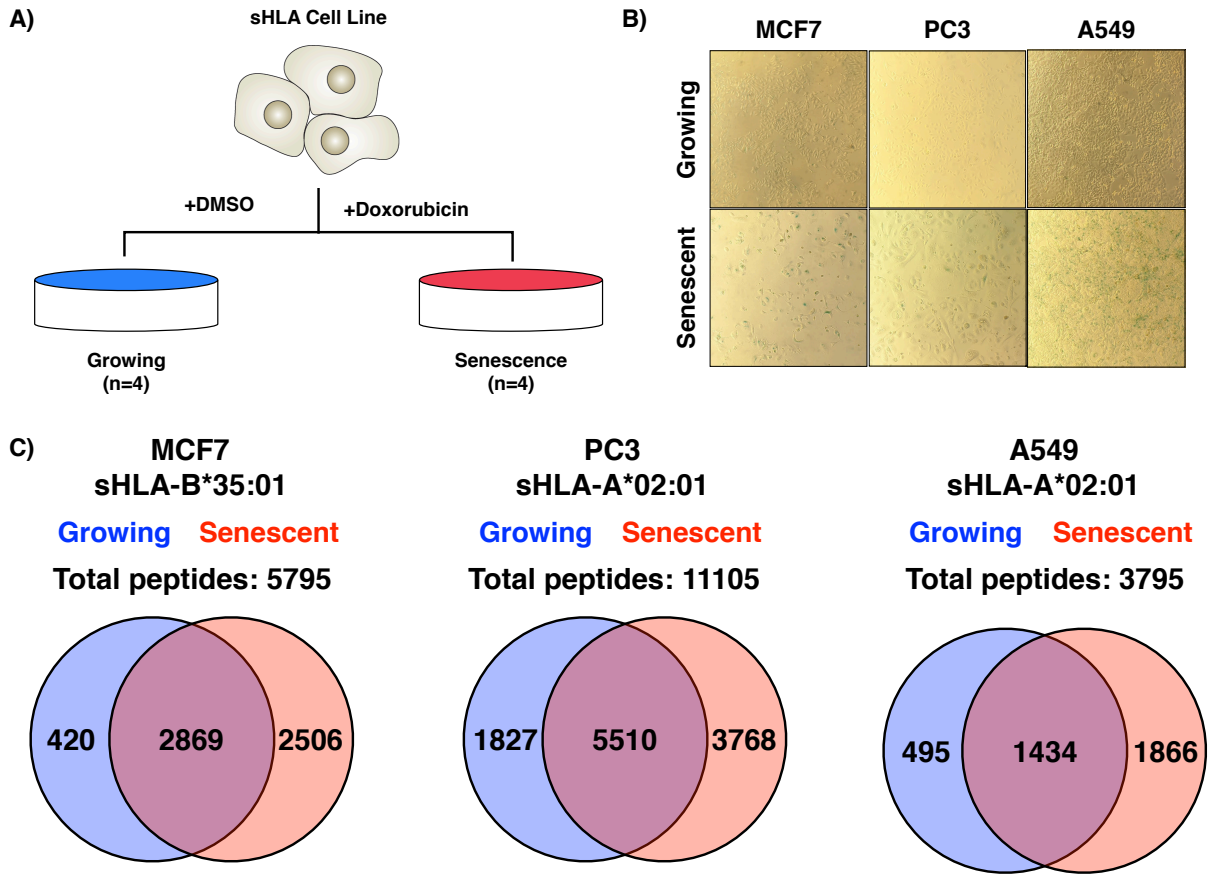

Figure 3.4: Immunopeptidomics of senescent cells using sHLA Fc-fusions. A) Strategy for generating growing and senescent cells for immunopeptidomics. Each cell line was treated for 24 hours with respective reagent. Growing cells were Doxycycline-treated immediately after DMSO removal while senescent cells were cultured for 9 days prior to doxycycline-treatment. B) β-galactosidase activity staining of growing and senescent cell lines. C) Number of peptides identified in growing and senescent samples for each cell line.

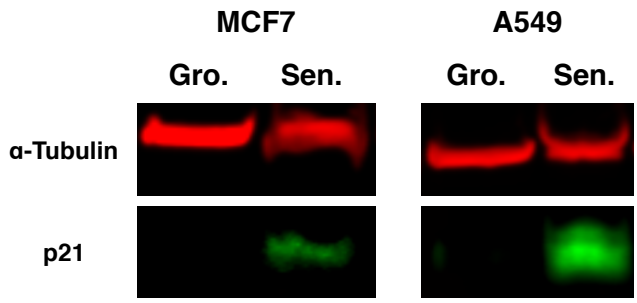

Figure 3.5: Western blot of growing and senescent cell lines for the expression of the senescence-associated marker p21. PC3 cells did not have detectable levels of p21.

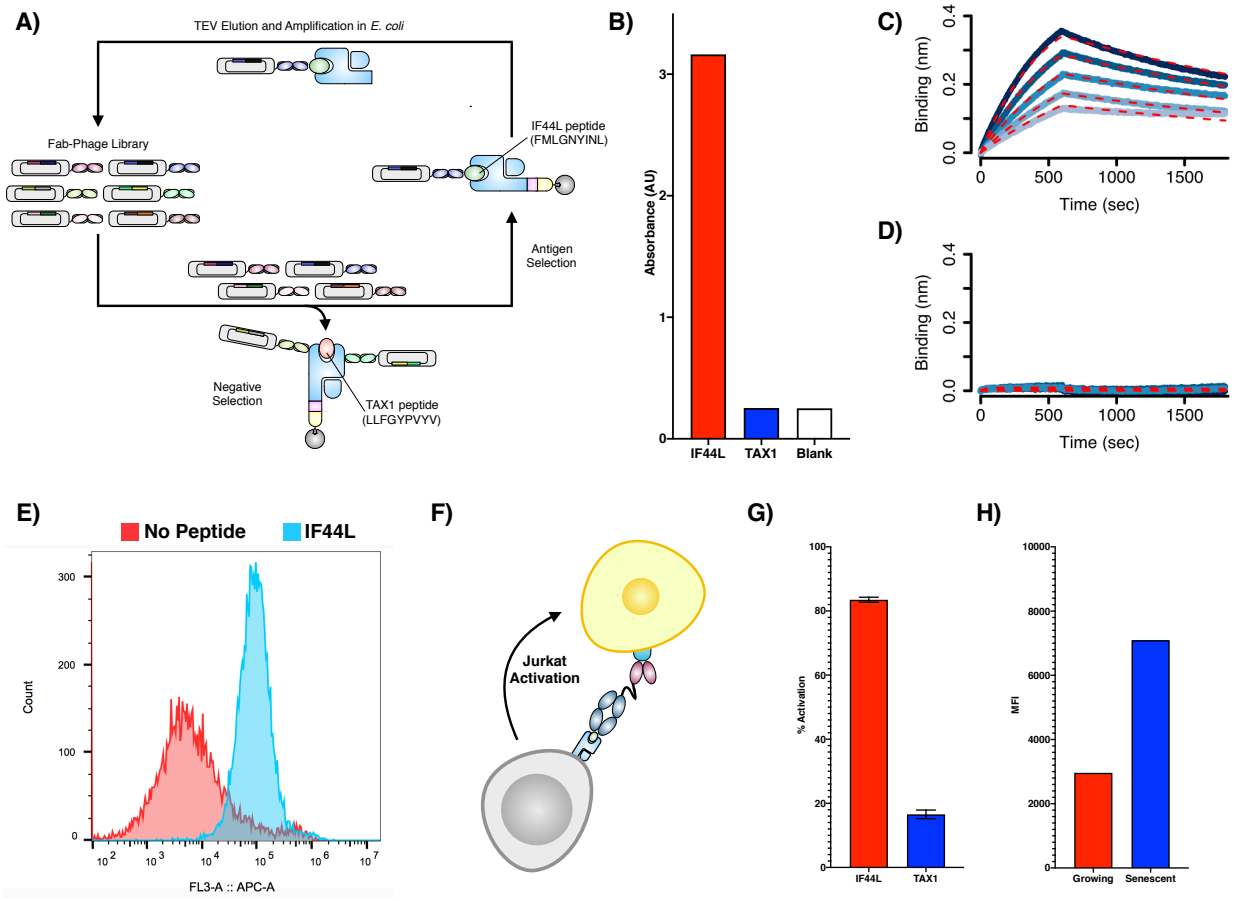

Figure 3.6: Antibodies targeting IF44L MHC-peptide complex show increased presentation in senescent cells. A) Differential phage display selection strategy to select for IF44L MHC-peptide complexes. B) ELISA results of the Fab-phage clone IFB2. C) Octet analysis of IFB2 Fab against the IF44L MHC-peptide complex. Concentrations in descending order are 200 nM, 150 nM, 100 nM, 75 nM, and 50 nM. D) Octet analysis of IFB2 Fab against the TAX1 MHC-peptide complex. Concentrations in descending order are 200 nM, 150 nM, and 100 nM. E) Flow cytometry analysis of IFB2 Fab using T2 lymphoblasts loaded with no peptide or the IF44L peptide. F) Schematic of IFB2 BiTE assays, where one arm binds to the IF44L MHC-peptide complex on target cells and the other binds CD3 on NFAT-GFP Jurkats, thereby inducing Jurkat activation. G) Percent activation of NFAT-GFP Jurkats incubated with 100 pM IFB2 BiTE and T2 lymphoblasts loaded with either IF44L or TAX1 peptide. H) Median FITC-A of NFAT-GFP Jurkats incubated with 100 pM IFB2 BiTE and either growing or senescent MCF7 breast cancer cells.

Chapter 4

MEK inhibition enhances presentation of targetable MHC-I tumor antigens in mutant melanomas

Abstract

Combining multiple therapeutic strategies in NRAS/BRAF mutant melanoma – namely MEK/BRAF kinase inhibitors, immune checkpoint inhibitors, and targeted immunotherapies – may offer an improved survival benefit by overcoming limitations associated with any individual therapy. Still, optimal combination, order, and timing of administration remain under investigation. Here, we measure how MEK inhibition alters anti-tumor immunity by utilizing quantitative immunopeptidomics to profile changes the peptide MHC (pMHC) repertoire. These data reveal a collection of tumor antigens whose presentation levels are selectively augmented following therapy, including several epitopes present at over 1000 copies-per-cell. We leveraged the tunable abundance of MEKi-modulated antigens by targeting 4 epitopes with pMHC-specific T cell engagers and antibody drug conjugates, enhancing cell killing in tumor cells following MEK inhibition. These results highlight drug treatment as a means to enhance immunotherapy efficacy by targeting specific up-regulated pMHCs and provide a methodological framework for identifying, quantifying, and therapeutically targeting additional epitopes of interest.

Introduction

In recent years, cancer treatment paradigms have increasingly incorporated information regarding a patient's genetic profile to identify appropriate therapeutic modalities, otherwise known as "precision medicine." Targeted therapies against aberrant activation of mitogen activated protein kinase (MAPK) signaling pathway, including BRAF and MEK inhibitors (BRAFi, MEKi), have transformed the standard of care for BRAF and NRAS mutant melanoma patients - representing ~50% and ~20% of melanomas, respectively[125,126]. Unfortunately, despite these targeted therapies showing some initial efficacy in extending progression free survival (PFS), either alone (MEKi, NRAS) or in combination (BRAF), a majority of patients acquire

resistance and experience disease progression with one year[127–133]. Immune checkpoint inhibitors (ICIs), which target cell surface receptors controlling the activation or inhibition of an immune response, have shown remarkable clinical success in melanoma[134,135]. However, only a subset of patients respond; those who do frequently experience immune related adverse events (irAEs) and many develop resistance[136,137].

It has been proposed that combining MAPK inhibitors and ICIs may increase efficacy, in part due to increasing evidence that MEK/BRAF inhibitors can sensitize tumors to immunotherapy through up-regulation of class I major histocompatibility molecules (MHCs), as well as increase immune cell infiltration, T cell activation, antigen recognition, and more[138–141]. NRAS mutant melanoma trials have suggested that MEKi/ICI treatment may enhance PFS[131,142]. Additionally, several clinical trials evaluating a triple combination of MEKi, BRAFi, and ICIs have shown enhanced efficacy in BRAF-mutant melanoma, though at the expense of increased toxicity[143,144]. Therefore, despite promising initial results, there remains much to learn about how exposure to kinase inhibitors alters the immune system, and how these alterations can be leveraged with ICIs and/or targeted immunotherapies[145] . Measuring how the antigen repertoire, referred to as the "immunopeptidome," presented by class I MHCs changes in response to therapy is central to understanding the relationship between drug treatment and immune response, as recent reports highlight the potential for dynamic repertoire shifts in the identify and abundance of peptide MHCs (pMHCs) following perturbation[146–148]. To better understand how to optimally combine therapies in BRAF/NRAS melanoma and identify antigens as therapeutic targets, a precise, molecular understanding of relative and absolute quantitative changes in pMHC presentation following treatment is required.

To this end, we used quantitative immunopeptidomics to measure the relative changes in presentation of pMHC repertoires in response to MEKi *in vitro*. This analysis showed increased expression of both putative and well-characterized tumor associated antigens (TAA) following MEKi treatment. Copies-per-cell estimations of 18 MEKi-modulated TAAs enabled the selection of four TAAs with high MEKi-induced expression as targets for pMHC-specific antibody-based 4 therapies, which show enhanced ability to mediate T cell cytotoxicity with higher antigen expression levels[81,149–151]. The pMHC-Abs were used to generate antibody-drug conjugates and T-cell engagers, which reveal a strong relationship between epitope density, therapeutic modality, and cytotoxicity, and highlight MEKi as a means to enhance efficacy by increasing target antigen expression. Our work provides the methodological framework to discover and exploit drug-induced pMHC complexes for new immunotherapies.

Results

MEK inhibition increases MHC-I expression in melanoma cell lines

To evaluate how MEK inhibition alters pMHC expression in NRAS and BRAF mutant melanomas, we selected 2 NRAS and 4 BRAF mutant cell lines (V600E) which exhibited a range of sensitivities to binimetinib (**Figure 4.1A**). We measured class-I MHC (MHC-I) surface expression with flow cytometry and found 72 hours of treatment resulted in a maximal increase in expression over a DMSO treated control without requiring cell passaging (**Figure 4.1B**).

Hence, we selected 72 hours as the timepoint for all subsequent experiments. All cell lines showed elevated surface MHC-I expression following low (100 nM) or high-dose (1 μM) binimetinib treatment at 72 hours, with high-dose treatment generally resulting in a larger increase (**Figures 4.2A & 4.1C**). Primary melanocytes treated with binimetinib did not show a strong change in surface HLA expression, similar to previously reported results in trametinib

treated PBMCs[140], suggesting this effect is specific to oncogenic cell phenotypes (**Figure 4.1D**).

We next investigated how the pMHC repertoires presented on these six cell lines were altered quantitatively in response to MEKi treatment. We employed our previously described framework for multiplexed, quantitative profiling of pMHC repertoires utilizing isobaric labeling (TMT) and heavy isotope-labeled peptide MHCs (hipMHC) standards for accurate relative quantitation of endogenous pMHCs. In triplicate, cells were treated with DMSO or binimetinib (100 nM NRAS mutant cells, 100 nM/1 μM BRAF mutant cells) for 72 hours (**Figure 4.2B**). Cells were lysed, and three hipMHC standards were spiked into the lysate mixture prior to immunoprecipitation. Isolated endogenous and isotopically labeled peptides were subsequently labeled with TMT, combined, and analyzed by LC-MS/MS for quantitative immunopeptidomic profiling.

In total, these analyses identified 15,450 unique MHC peptides derived from 6,292 unique proteins (**Figure 4.3A**). Peptides matched expected class I length distributions (**Figure 4.3B**), and a majority were predicted to be binders of each cell line's HLA allelic profile (**Figure 4.3C**). Notably, nearly 80% of peptides were only identified in a single cell line, despite several cell lines having some allelic overlap. (**Figure 4.3D**). While highly abundant proteins like vimentin and beta-actin were the source of 198 and 47 unique pMHCs across analyses, most source proteins (60%) produced just 1 or 2 MHC peptides, highlighting the uniqueness of the immunopeptidome despite similarities in cell type, disease phenotype, and HLA alleles across cell lines (**Figure 4.3E**).

Quantitative immunopeptidomics showed a median increase in pMHC expression levels following binimetinib treatment in most conditions, with similar average changes observed across peptides predicted to bind to HLA-A, HLA-B, and HLA-C (**Figure 4.3F**). However, in

contrast to surface staining, measuring the average change in HLA expression, MS analysis showcased a wide distribution in presentation levels across peptides (**Figure 4.2C**). For example, while the average fold change in HLA levels in A375 cells treated with 1 μM binimetinib was 2.45-fold, some peptides increased 16-fold or more in presentation while others decreased 4-fold. In SKMEL2 cells, several peptides changed 3 to 4-fold in presentation despite no change in surface HLA expression. These data illustrate the highly dynamic nature of the immunopeptidome, where individual pMHCs experience significant changes in presentation often not captured by surface staining alone.

Tumor associated antigens are selectively enriched in presentation with MEK inhibition

We investigated which peptides increased significantly relative to the median change in presentation to determine if any pMHCs were selectively enriched following MEK inhibition. We observed that two peptides in the SKMEL5 (low MEKi) analysis, derived from known TAAs (dopachrome tautomerase (DCT or "TRYP2") and premelanosome protein (PMEL or "gp100"), had some of the highest changes in presentation, increasing 2.8 and 5.3-fold, respectively (**Figure 4.2D**). These peptides were also two of the most abundant pMHCs in the analysis, ranking in the 99th percentile of precursor ion abundance (**Figure 4.2E**). To determine whether enriched presentation of DCT and PMEL peptides was indicative of increased expression of TAA-derived peptides broadly, we performed a non-parametric test to measure TAA enrichment significance in response to MEK inhibitor treatment. For this analysis, we compiled a custom tumor associated antigen library derived from the literature in mass spectrometry analyses and immunogenicity assays as well as online databases (**Table 4.1**)[152] This list comprised over 1000 unique pMHC sequences, and was biased towards North America/Europe high frequency alleles (i.e. HLA-A*02:01)[153]. Therefore, we utilized the peptide's source proteins to generate a protein-

based TAA library rather than the peptide sequence itself (**Table 4.2**). We rank-ordered peptide source proteins by fold change in presentation with MEKi; in cases where multiple peptides were derived from the same source protein, the maximal/minimal fold change was selected to assess positive/negative enrichment.

In both SKMEL5 and SKMEL28 cells, TAAs were significantly positively enriched following low-dose MEKi (**Figure 4.2F**). Beyond DCT, and PMEL, enriched TAAs included melanoma differentiation antigens from the MAGE family, MLANA (MART-1), and TYR, among others, which are well characterized antigens with demonstrated immunogenic potential (**Figure 4.4A**)[64,154]. Many of these TAAs also show a dose dependent increase in presentation, with peptides derived from TRYP1, DCT, and PMEL increasing over 10-fold with high binimetinib treatment in SKMEL5 cells (**Figure 4.2G**). Furthermore, this dose-dependent response occurs regardless of whether mean HLA expression increases proportionally (Figure 1H), and even sub-cytotoxic doses of MEKi (10 nM) resulted in an increase in TAA presentation despite no change in average MHC surface expression (**Figure 4.4B**).

This effect was not exclusive to binimetinib, as trametinib-treated SKMEL5 cells showed similar TAA enrichment (**Figure 4.4C**). Peptides rank-ordered by precursor ion abundance also reached significance, suggesting TAAs are both some of the most abundant peptides presented and change the most in presentation with MEK inhibition (**Figure 4.4D**). We applied the enrichment analysis framework to all cell lines and binimetinib treatment doses and discovered binimetinib significantly enriched ($p<0.05$) TAA presentation in all cases, suggesting a mechanistic basis for this response (**Figure 4.2I**).

It has been reported that ERK is a negative regulator for IFN-γ/STAT1 signaling, and that inhibition of ERK can drive an interferon regulatory factor response, increasing transcription of

interferon response genes such as *HLA-A/B/C* and *B2M*[155–158]. We investigated whether IFN-γ stimulation also enriched TAA presentation using previously published results for four cell lines[148], and found no global TAA enrichment in IPC298, SKMEL2, and SKMEL28 cells, with SKMEL5 being the only exception (**Figure 4.2I**). While IFN-γ stimulation increases pMHC expression to a greater extent than MEK inhibition, melanoma differentiation tumor antigens like TRYP1, DCT, and PMEL still showed a larger change in expression with MEK inhibition, suggesting MEK inhibition drives a distinct peptide repertoire from IFN-γ stimulation (**Figures 4.5A & 4.5B**). CDK4/6 inhibitor treatment, such as palbociclib, has also been shown to increase antigen presentation[148,159]. We again performed the TAA enrichment analysis using previously reported data[160], and found that in just a few cell line/treatment combinations there was significant enrichment. Taken together, we find MEK inhibitors robustly drive upregulation of TAAs, district from other perturbations known to alter pMHC expression levels.

Absolute quantification of treatment-modulated tumor associated antigens

MEK inhibitor-modulated TAAs present an attractive class of epitopes for targeted immunotherapy, as these antigens have high abundance relative to other epitopes and their expression can be further augmented in response to therapy. We hypothesized MEKi may enhance the anti-tumor immune response for immunotherapies targeted against MEKi-modulated antigens, though determining the appropriate immunotherapeutic strategy for each antigen requires knowledge of epitope abundance, as antibody-drug conjugates require higher epitope abundances than T-cell engager therapies[149,150].

To this end, we performed absolute quantification experiments to estimate copies-per cell abundance of 18 HLA-A*02:01 epitope targets that increase in presentation following 100 nM MEKi. We utilized a previously developed assay, "SureQuant Iso-MHC[152]," where a series of

three peptide isotopologues with 1, 2, or 3 stable isotopically labeled (SIL) amino acids (1-3H) per target were loaded into MHC molecules (hipMHCs) and titrated into cell lysates across a 100-fold linear range as an embedded standard curve (**Figure 4.6A**). A fourth isotopologue with 4 SIL-amino acids was added exogenously at a high concentration prior to analysis to leverage internal-standard triggered parallel reaction monitoring data acquisition (IS-PRM, "SureQuant"), guiding the sensitive and selective targeting of endogenous peptides and isotopologue peptide standards to measure peptide concentration within the sample, thereby enabling copies-per-cell measurements from a defined number of cells. We estimated copies-per-cell for our 18 TAA panel in A375 and RPMI-7951 cells treated with DMSO, low, or high dose MEKi for 72 hours, and extended our previous analysis of SKMEL5 cells by measuring the target panel in SKMEL5 cells with high dose MEKi treatment and compared the data to DMSO and low dose measurements[152].

All 18 peptides were quantifiable across high MEKi treated SKMEL5 cells, as expected since the panel was developed using discovery data in SKMEL5 cells. While we would not expect to detect the entire panel across A375 and RPMI-7951 cell lines (for example, A375 are PMEL-), 13 and 11 peptides were quantifiable within A375 and RPMI-7951 cells, respectively, an increase over the 7 and 8 peptides identified in the multiplexed discovery analyses (**Figures 4.6B & 4.7**). The 3 RPMI-7951 peptides detected by SureQuant that were not detected in the discovery analysis had an average of 42-179 copies per cell, whereas most of the peptides detected using both methods had greater than 400 copies per cell, demonstrating the sensitivity of the SureQuant Iso-MHC method in detecting and quantifying epitopes of lower abundance.

Peptides showed a wide range in presentation levels within and across cell lines and treatment conditions, spanning under 10 copies-per-cell (ex. GVYDGEEHSV-MAGEB2 in

A375s 9 and RPMI-7951 cells with DMSO) to over 100,000 copies-per-cell (RLLGTEFQV - SLC45A2 in SKMEL5 cells with binimetinib treatment) (**Figure 4.6B**). In most cases, expression increased following MEK inhibitor treatment, though some changes were larger than those measured in the multiplexed DDA analyses, likely a consequence of ratio compression (**Figure 4.7**)[160,161]. For example, the AMLGTHTMEV-PMEL peptide showed a ~2-fold change with 100 nM MEKi treatment in the DDA SKMEL5 analysis, but a ~6.5-fold change in the LF-target analyses, suggesting fold-changes in presentation measured by multiplexed-DDA analyses may be underestimated for the most dynamically changing peptides in response to binimetinib.

Generating pMHC-specific antibodies against MEKi-modulated TAAs

Antibody-based immunotherapies have shown the increasing promise of pMHC's as therapeutic targets, both in the context of melanoma and cancer as a whole[64,65,67,78,81]. MEKi-induction of shared TAAs described here may present a therapeutic opportunity to use pMHC-targeted antibodies in combination with MEKi. We selected four HLA-A*02:01 associated TAAs with high epitope abundance in SKMEL5 cells as antigens for antibody generation. These peptides (derived from SLC45A2, PMEL, DCT, and PRUNE2) exhibited a range of basal and MEKi-induced presentation levels – three of which were also identified in at least one other cell line (**Figure 4.6C**). To identify pMHC-specific antibodies, we performed a phage display campaign first clearing 2 Fab-phage libraries with an immobilized pMHC containing a decoy peptide (GILGFVFTL from influenza, "Flu peptide"). Remaining phage were incubated with pMHC's of interest and bound phage were eluted via TEV protease and subsequently propagated to enrich for selective binders (**Figure 4.8A**). After iterative rounds of selection, ELISA screening of individual clones identified 15 unique Fabs that showed specificity and predicted high affinity (<20 nM) across our 4 pMHC targets (Figure S10). Flow cytometry using T2 lymphoblasts – an

HLA-A*02:01+ cell line null for TAP which allows for exogenous peptide loading – revealed 1 Fab per pMHC that specifically recognized the pMHC on the surface of cells in a peptide dependent manner (**Figure 4.9**). Upon conversion to IgG's, these antibodies demonstrated exquisite selectivity in recognizing only peptide-specific target cells (**Figures 4.8B & 4.10**), each with subnanomolar affinity (**Figure 4.8C**).

SKMEL5 cells treated with DMSO or high dose MEKi for 72 hours displayed an increase in median fluorescence intensity in MEKi treated cell compared to DMSO when stained with fluorophore-conjugated pMHC-specific IgG's, in line with our immunopeptidomic analysis. (**Figure 4.8D**). Due to the superior tumor-specific expression profiles in skin as well poor biophysical properties of the antibody targeting the PRUNE2 pMHC (data not shown), we selected SLC45A2, DCT, and PMEL-specific antibodies to evaluate for efficacy in vitro.

Therapeutic modality, antibody properties, and epitope expression influence efficacy of pMHC-specific antibody-based therapies

Previously reported data have demonstrated that ADCs targeting pMHCs require a high epitope density for efficacy, as only cells with expression levels above ~40,000 copies/cell showed an effect on viability greater than 20%[150]. While peptide-pulsing to exogenously load high levels of the target peptide or an overexpression system is frequently used to achieve high epitope densities for pMHC-specific ADCs[150,151], here we hypothesized the high endogenous expression of the SLC45A2 "RLLGTEFQV" epitope in SKMEL5 cells may be effectively targeted by an ADC. To that end, we conjugated Monomethyl auristatin F (MMAF), a tubulin polymerization inhibitor, to the anti-SLC45A2 pMHC IgG (**Figure 4.11A**) and evaluated viability in SKMEL5 & RPMI-7951 (low epitope density) cells 10 pre-treated with DMSO or 1 μM MEKi for 72 hours to augment pMHC presentation of the target epitope. In SKMEL5 cells, MEKi

pretreatment resulted in a superior therapeutic window following 72 hours of ADC treatment, with a 40% reduction in viability achieved with MEKi compared to 28% with DMSO at 30 nM ADC (**Figures 4.11B & 4.12A**). In contrast, RPMI-7951 cells showed just an 18% reduction in viability in both conditions, confirming that high epitope density is required for anti-pMHC ADC efficacy.

Comparing SLC45A2 transcript expression across 57 BRAF/NRAS melanoma cell lines revealed SKMEL5's expression is in the upper quartile of abundances, whereas RPMI-7951 is in the lower quartile (**Figure 4.11C**). Furthermore, RLLGTEFQV concentration across SKMEL5 & RPMI-7951 relative to the previously reported concentration in 10 melanoma tumors[152], shows that just 1 tumor had a RLLGTEFQV concentration above 100 fmol (~10,000 copies per cell in SKMEL5 cells) (**Figure 4.11D**). These data suggest that although a subset of melanoma patients with high surface presentation the target epitope may benefit from an ADC approach, another strategy with a lower threshold for presentation may be more efficacious for patients with lower surface expression. As the PMEL and DCT epitopes showed lower surface presentation levels than SLC45A2 in SKMEL5 cells as well, we hypothesized bispecific T cell engagers (BiTEs) may be more efficacious against these sparse epitopes, particularly in combination with MEKi[80,149].

To this end, we generated BiTEs by fusing the PMEL, DCT, and SLC45A2 Fabs to the anti-CD3 single-chain variable fragment OKT3 (scFv, **Figure 4.11E**) BiTE construct showed selective T-cell activation in a NFAT-GFP Jurkat reporter cell line when incubated with T2 lymphoblasts loaded with target peptide in comparison to the decoy Flu peptide (**Figures 4.11F & 4.12B**). We next tested Jurkat activation in SKMEL5 cells, and saw that cells pre-treated with

1 μM MEKi for 72 hours showed superior activation across all 3 BiTES, suggesting higher target expression leads to a higher proportion of activated effector cells (**Figures 4.11G & 4.12C**).

To assess cytotoxicity, we cocultured SKMEL5, RPMI-7951, or A375 cells pre-treated with DMSO or 1 μM MEKi for 72 hours with primary human T cells isolated from healthy donor blood (effector to target ratio 2:1) in the presence of increasing concentrations of BiTE for 48 hours. While RPMI-7951 cells were not responsive to the SLC45A2-ADC, the SLC45A2-BiTE did yield a cytotoxic response, with MEKi pre-treated cells showing increased cell death with an IC50 of 0.5 nM with MEKi compared to 1.8 nM with DMSO (**Figures 4.11H & 4.12D**). By comparison, SKMEL5 cells showed a similar response regardless of MEKi treatment, likely due to the already high presentation levels at baseline (**Figure 4.12E**). SKMEL5 cells showed a similar cytotoxic response to the DCT-BiTE regardless of treatment condition, possibly because both DMSO and MEKi-treated cells presented the target epitope at levels had above 1000 copies/cell (**Figure 4.11I**). For A375 cells, the DCT-BiTE showed a superior reduction in cell viability with MEKi-pretreatment, where expression levels increased from 20 to 1346 copies/cell. The PMEL-BiTE exhibited a similar trend in SKMEL5 cells, where a concentration of just 0.1 nM PMEL-BiTE was required to reduce SKMEL5 viability by 50% in MEKi pre-treated cells, in contrast to 6.2 nM required in DMSO-treated cells (**Figure 4.11J**). While the efficacy of each BiTE varies between cell lines and targeted epitope, these data suggest that epitopes presented above ~1000 copies/cell are most effectively targeted by BiTEs, and that MEKi treatment can be used to augment presentation levels for increased efficacy in cases where endogenous expression of the target epitope is low.

In cases where MEKi treatment may not be a viable strategy to augment presentation of target antigens (ex. therapeutic resistance, non BRAF/NRAS mutant melanoma), utilizing a

combination of BiTES that target patient epitopes may enhance cytotoxicity. Furthermore, two pMHC-specific antibodies can be combined to generate tri-specific T-cell engager molecules 11 (TriTEs), which may increase cytotoxic response and/or lower the concentration of therapy required for efficacy. Accordingly, we generated a TriTE against SLC45A2 and PMEL (**Figure 4.11K**) and observed enhanced Jurkat activation when T2 lymphoblasts were pulsed with both peptides at BiTE concentrations below 1 nM (**Figure 4.12F**). In SKMEL5 cells (DMSO) cocultured with human T cells and the SLC45A2/PMEL TriTE, we observed a greater cytotoxic response than DMSO-treated cells incubated with the PMEL or SLC45A2 BiTEs alone (**Figures 4.11H & 4.12E**), reducing the IC50 to 0.7 nM (**Figure 4.11L**). Overall, we demonstrate T-cell engagers against TAA pMHC's can induce cytotoxicity in melanoma and in several cases, MEKi-treated melanoma lines can enhance this cytotoxic effect, thus potentially providing a therapeutic strategy for eliminating melanoma.

Discussion

The emergence of drug resistance and/or toxicities to small molecule targeted therapies and checkpoint immunotherapies remain a significant barrier to achieving complete remission in BRAF or NRAS mutant melanoma. While the advantages of combining MEK inhibition with ICI have been well documented, combination therapy trials evaluating dosing schedules and drug combinations are still being evaluated for efficacy. To better understand how to optimally combine MEKi with immunotherapy, here we perform a comprehensive analysis characterizing pMHC repertoire response to MEK inhibition using relative and absolute quantitative immunopeptidomics. We identify significantly enriched TAA presentation as a common mechanism to MAPK pathway inhibition in vitro & in vivo in NRAS-mutant and BRAF-mutant melanomas. While elevated surface HLA presentation in response to MEKi has been previously

reported, our data reveal that many of the enriched TAAs increased well beyond average changes in HLA surface expression, in some cases more than 10-fold.

Elevated TAA presentation was observed across varying levels of sensitivities to MEKi, including at sub-cytotoxic doses, and was common to NRAS-mutant and BRAF-mutant lines, suggesting that this response may be shared across many melanoma patients. A multi-omics analysis highlighted changes in cellular plasticity following MEKi as a likely mechanism for the up-regulation of certain TAAs.

One of the primary criticisms of utilizing shared tumor associated/tissue differentiation antigens (as opposed to tumor-specific antigens, i.e. "neoantigens") as a therapeutic target for TCR-based therapies is that their low expression in non-tumor tissue can lead to off-target toxicity, likely attributed to the high sensitivity of T cells[162–164]. We hypothesized these antigens with high basal or MEKi-induced expression could be intelligently leveraged using antibody-based therapies, which require higher thresholds of antigen presentation for efficacy than TCR-focused approaches, limiting off target toxicity in low-expressing, non-target tissue.

Here, four pMHC-specific antibodies were generated and incorporated into ADC and BiTE formats. Using these reagents, we demonstrated enhanced cell killing following MEKi treatment with either therapeutic modality. Cytotoxicity is observed using just the endogenous or MEKi-augmented antigen presentation levels, in contrast to engineered or overexpression cellular system, which may be less likely to represent physiologically relevant epitope densities[151].

Importantly, this work connects targeted immunotherapy response to epitope abundance measurements made using embedded hipMHC multipoint calibrants for accurate quantitative estimations. This is distinct from studies employing exogenous peptide standards for absolute

quantification, which underestimate copy-per-cell estimations due to significant losses occurring during sample processing, leading to inaccurate conclusions regarding the sensitivity profile of a given pMHC-targeted modality[81,165]. Here, we confirm that high (>4e4 copies-per-cell) surface expression is required for ADC efficacy, potentially due to low turnover rates of pMHCs. In contrast, BiTES were effective at lower epitope densities, where the greatest difference in cytotoxic response was observed when cells had fewer than ~1000 copies-per-cell. BiTES showed similar efficacy against targets present at 1000 copies-per-cell or higher, though future studies exploring more pMHCs may further elucidate the relationship between antibody affinity and epitope density.

In this study we primarily tested the cytotoxicity of a single pMHC-specific BiTE on tumor cells, BiTEs could be used in combination to enhance efficacy, or engineered as TriTEs against different epitopes for a single TAA or two different TAAs, offering a multitude of "off the shelf" targeted immunotherapy opportunities to target highly abundant, shared TAAs. Peptide MHC specific antibodies and MEKi-induced expression could also be utilized for other antibody-based therapeutic strategies such as to initiate antibody-mediated cellular cytotoxicity (ADCC)[65], Fabs conjugated to immunotoxins[64], or engineered as pMHC-specific chimeric antigen receptor T-cells[166], where higher expression may also enhance efficacy and/or improve the therapeutic window. Furthermore, though the focus of the therapeutic modalities generated in this study was limited to HLA-A2:01, the same strategy could be employed for other high frequency alleles using MEKi-modulated TAAs identified within this study.

Though resistance to MEKi is inevitable for many melanoma patients, utilizing MEKi to boost TAA antigen presentation prior to or concurrently with ICI and antigen-specific immunotherapies like those described within this study or others (ex. vaccines, cell therapy) may

improve therapeutic response. Beyond melanoma, a variety of different therapeutic modalities across cancer types have also been demonstrated to enhance HLA presentation[159,167,168]. Employing quantitative immunopeptidomics in these settings may unlock additional treatment-modulated tumor antigens and provide critical insights as to how to appropriately leverage them for optimal therapeutic potential.

Methods

Cell Lines

SKMEL5, SKMEL28, A375, RPMI-7951, and T2 cell lines were obtained from ATCC [ATCC HTB-70, ATCC HTB-72, CRL1619, HTB-66, and CRL-1992 respectively] and maintained in DMEM medium (Corning). IPC298 and SKMEL2 cells were provided by Array Biopharma and maintained in RPMI 1640 (Gibco) and MEM-α (Gibco) mediums, respectively. Primary epidermal melanocytes (normal, human, adult) were obtained from ATCC (PCS-200-013) and maintained in dermal cell basal medium (ATCC PCS-200-030) supplemented with adult melanocyte growth kit (ATCC PCD-200-042). NFAT-GFP Jurkat cells were a generous gift from Dr. Arthur Weiss (UCSF) and were maintained in RPMI1640 + 2 mg/mL Geneticin (Gibco). All medium was supplemented with 10% FBS (Gibco) and 1% penicillin/streptomycin (p/s, Gibco) except for primary melanocytes (p/s only). Cells were routinely tested for mycoplasma contamination, and maintained in 37 °C, 5% CO2. All experiments were performed on passages 4-10.

Peptide synthesis

Heavy leucine-containing peptides for hipMHC quantification correction (ALNEQIARL+7, SLPEEIGHL+7, and SVVESVKFL+7 were synthesized at the MIT-Koch Institute Swanson

Biotechnology Center in Biopolymers and Proteomics Facility using standard Fmoc chemistry using an Intavis model MultiPep peptide synthesizer with HATU activation and 5 μmol chemistry cycles as previously described[160]. Standard Fmoc amino acids were procured from NovaBiochem and Fmoc-Leu (13C6, 15N) was obtained from Cambridge Isotope Laboratories. Light peptides for pMHC-antibody generation (PMEL, DCT, PRUNE2, SLC45A2) were synthesized on a Gyros-Protein Technologies Tribute with UV feedback at a 100 micromole scale using standard Fmoc chemistry and HATU/NMM activation chemistry. Both light and heavy leucine-containing peptides were purified on a Gilson GX-271 preparative HPLC system by reverse phase, and quality assured with MS on a Bruker MicroFlex MALDI-TOF and by RP-HPLC on an Agilent model 1100 HPLC. Isotopologue peptides for SureQuant-IsoMHC analyses were synthesized using HeavyPeptide AQUA Custom Synthesis Service (Thermo Scientific) and were purified to >97% and validated with amino acid analysis as previously described[152].

Cloning

Fabs were subcloned from the Fab-phagemid into an E. coli expression vector pBL347. The heavy chain of the IgG was cloned from the Fab plasmid into a pFUSE (InvivoGen) vector with a human IgG1 Fc domain. The light chain of the IgG was cloned from the Fab plasmid into the same vector but lacking the Fc domain. The light chain of the BiTE was cloned from the Fab plasmid into a pFUSE (InvivoGen) vector with an anti-CD3 scFv (OKT3). The heavy chain of the BiTE was cloned into the same vector lacking the OKT3. SCD3-arm of the TriTE was converted into a scFab and cloned into a pFUSE (InvivoGen) vector with the KIH strategy "knob" human Fc domain[169]. MLA2-arm of the TriTE was converted into a scFab and cloned into a pFUSE (InvivoGen) vector with the KIH strategy "hole" human Fc domain followed by OKT3. All constructs were sequence verified by Sanger sequencing.

Protein expression and purification

MHC-peptide complexes for selection were expressed and refolded as previously described[109]. Briefly, MHC-peptide complexes were refolded at 10°C for 3 days and SEC-purified on a HiLoad 16/600 Superdex 75 pg column equilibrated in 10 mM Tris pH 8. After purification, MHC-peptide complexes were biotinylated using a BirA reaction kit (Avidity) per manufacturer's instructions in the presence of excess peptide and β2M at 25°C for 4 hours. After biotinylation, MHC-peptide complexes were purified again via SEC to remove excess biotin. Proper folding was assessed by SDS-PAGE. Biotinylation was assessed by pre-incubating MHC-peptide complexes with NeutrAvidin and subsequently assessed by SDS-PAGE.

Fabs were expressed in E. coli C43 (DE3) Pro+ as previously described using an optimized autoinduction medium and purified by protein A affinity chromatography[37]. IgGs, BiTEs, and TriTEs were expressed in Expi293 BirA cells using transient transfection (Expifectamine, Thermo Scientific). After transfection for 3–5 d, media was harvested, IgGs and TriTEs purified by Ni-NTA affinity chromatography and BiTEs were purified using protein A affinity chromatography. All proteins were buffer exchanged into PBS pH 7.4 and stored in 10% glycerol at -80°C and assessed by SDS-PAGE.

All proteins were then buffer exchanged into phosphate-buffered saline (PBS) containing 20% glycerol, concentrated, and flash frozen for storage. All other proteins were buffer exchanged into PBS by spin concentration and stored in aliquots at −80°C. The purity and integrity of all proteins were assessed by SDS-PAGE. Fabs were subsequently buffer exchanged into PBS pH 7.4 and stored in 10% glycerol at -80°C and assessed by SDS-PAGE.

Fab-phage selection

Phage selections were run as previously described[37]. Selections were performed on a KingFischerTM System (Thermo Scientific). Biotinylated antigens were immobilized using streptavidin-coated magnetic beads (Promega). In each round, phage was first cleared by incubation with beads loaded with MHC-peptide complexes loaded with FLU peptide. Unbound phage was next incubated with beads loaded with MHC-peptide complex of interest. Beads were washed and bound phage was eluted with 50 μg/mL of TEV protease. Four rounds of selection were performed with decreasing amounts of MHC-peptide complex of interest. Selections were performed in PBS+0.02% Tween-20+0.2% bovine serum albumin (PBSTB). Individual phage clones from the fourth round of selections were analyzed by ELISA.

Phage ELISA

For each phage clone, four different conditions were tested – Direct: MHC-peptide complex of interest, Competition: MHC-peptide complex of interest with an equal concentration of MHC-peptide complex in solution, Negative selection: FLU MHC-peptide complex, and Control: PBSTB. 384-well Nunc Maxisorp flat-bottom clear plates (Thermo Fisher Scientific) were coated with 0.5 μg/mL of NeutrAvidin in PBS overnight at 4°C and subsequently blocked with PBSTB. Plates were washed 3x with PBS containing 0.05% Tween-20 (PBST) and were washed similarly between each of the steps. 20 nM biotinylated MHC-peptide complex was diluted in PBSTB and immobilized on the NeutrAvidin-coated wells for 30 minutes at room temperature, then blocked with PBSTB + 10 μM biotin for 10 minutes. For the competition samples, phage supernatant was diluted 1:5 into PBSTB with 20 nM MHC-peptide complex of interest for 30 minutes prior to addition to the plate. For the direct samples, phage supernatant was diluted 1:5 in PBSTB. Competition and direct samples were added to the plate for 30 minutes at room

temperature. Bound phage was detected by incubation with anti-M13-horseradish peroxidase conjugate (Sino Biologics, 1:5000) for 30 minutes, followed by the addition of TMB substrate (VWR International). The reaction was quenched with the addition of 1 M phosphoric acid and the absorbance at 450 nm was measured using a Tecan M200 Pro spectrophotometer. Clones with high binding to MHC-peptide complex of interest, low binding to PBSTB/FLU MHC-peptide complex, and a competition ratio (Competition AU/Direct AU) ≥0.5 were carried forward.

Bio-layer Interferometry

BLI measurements were made using an Octet RED384 (ForteBio) instrument. MHC-peptide complex was immobilized on an streptavidin biosensor and loaded for 200 seconds. After blocking with 10 μM biotin, purified binders in solution were used as the analyte. PBSTB was used for all buffers. Data were analyzed using the ForteBio Octet analysis software and kinetic parameters were determined using a 1:1 monovalent binding model.

IgG NHS-Fluorophore Conjugation

Purified IgG's were buffer exchanged into PBS pH 8.3. Concentrated IgG to ~11 mg/mL (with the exception of P2B1 which was only 2 mg/mL), and added 20 mM NHS-AF488 (Fluoroprobes) at either a 10:1 or 5:1 (Dye:IgG) ratio. Conjugation reactions were incubated at room temperature for 1 hour, and then quench by adding equivalent volume of 1 M glycine pH 8.4 as dye. Reactions were further incubated for 1 hour and then buffer exchanged into PBS pH 7.4 until all excess dye was removed. IgG and dye concentration was determined by UV.

ADC conjugation

Purified IgG was buffer exchanged into PBS pH 7.4 and concentrated to 35μM. 20x 100 mM

piperidine-derived oxaziridine molecule (Elledge et al., 2020) was added to PBS pH 7.4, and subsequently added to IgG for a final IgG concentration of 35μM. Labeling was conducted at room temperature for 2 hours, and buffer exchanged with PBS pH 7.4 to remove unconjugated oxaziridine. 5% v/v 5 mM DBCO-PEG4-Glu-vc-PAB-MMAF (Levena Biopharma) was added to oxaziridine-labeled IgG and incubated overnight at room temperature. IgG was buffer exchanged into PBS pH 7.4 to remove unconjugated MMAF. Conjugation efficiency was assessed by intact protein mass spectrometry using a Xevo G2-XS Mass Spectrometer (Waters).

Flow cytometry

Surface HLA expression in melanoma cells

Cells were seeded and treated with DMSO or binimetinib in 10 cm plates, then lifted with 0.05% Trypsin-EDTA and 10^6 cells/mL were spun at 300 g for 3 minutes, washed with ice cold flow buffer [1X PBS supplemented with 3% bovine serum albumin (BSA)] and incubated with fluorophore-conjugated antibody at 0.5 μg mL^{-1} in flow buffer for 30 minutes on ice. After incubation, cells were washed again, and resuspended in flow buffer plus 5 μL of propidium iodide (PI) staining solution (10 μg mL^{-1}, Invitrogen) per sample. Analyses were performed on an LSRII (BD Biosciences) and all flow cytometry data was analyzed using FlowJo (version 10.7.2). Antibody: Alexa Fluor 488 HLA-A, B, C, clone W6/32 [Biolegend, cat # 311413]. The gating strategy previously described[160].

pMHC-Fab and pMHC-antibody staining

T2 lymphoblasts: the day prior to Fab staining, T2 lymphoblasts were cultured in RPMI serum-free media containing 50 μg/mL peptide of interest at a concentration of 1e6 cells/mL. Cells were collected by centrifugation and washed 1X in flow buffer. Each sample was resuspended in 10 μg/mL Fab for 30 minutes, and then washed 3x in flow buffer. Each sample was then stained

with an anti-human Fab goat mAb Alexa Fluor 647 conjugate (Jackson ImmunoResearch) for 30 minutes, and then washed 3x in flow buffer. Samples were resuspended in 200 μL sterile PBS pH 7.4 and analyzed on a CytoFLEX (Beckman Coulter). For pMHC-antibody staining (full length IgG), T2 cells were incubated with the peptide of interest overnight, harvested, and stained with either primary pMHC specific IgG antibodies or a human IgG isotype control (Abcam, ab20619) at 10 μg/mL for 20 minutes on ice. Cells were then washed with flow buffer 1X and incubated with protein A-488 secondary antibody conjugate (Invitrogen, P11047) for 20 minutes (1:1000 dilution). Cells were washed again with flow buffer and resuspended in PI staining solution prior to analysis on the LSRII.

SKMEL5 cells: SKMEL5 cells were pre-treated with DMSO or 1 μM binimetinib for 72 hours in 10cm plates and were subsequently harvested (106 cells/mL), washed, and stained with fluorophore-conjugated pMHC-antibodies at 2 μg/mL, and analyzed using the LSRII.

Jurkat NFAT-GFP activation

SKMEL5 cells were treated in 10 cm plates with DMSO or 1 μM binimetinib for 72 hours, after which cells were seeded in a 24 well plate at a ratio of 250,000 SKMEL5 cells to 50,000 Jurkat NFAT-GFP cells (5:1) in Jurkat culture medium with n=3 technical replicates per condition and incubated with a pMHC-specific or anti-GFP (control) BiTE for 24 hours. T2 cells were seeded at 1:1 ratio (5e4 cells to 5e4 cells) in a 96-well round bottom plate. Cells were washed 2x with flow buffer and resuspended in PI staining solution. Cells were gated where the percentage of GFP positive cells were gated so ~97% of Jurkat cells with no BiTE were classified as GFP negative. SKMEL5 cells were analyzed on the LSRII, T2 on the CytoFLEX.

Cell viability assays

Binimetinib dose response

Half-maximal inhibitory concentrations (IC50) of binimetinib (Selleckchem, MEK162) were determined for each cell line using CellTiter-Glo (CTG) luminescent cell viability assay (Promega). Cells were seeded at density of 10,000 (SKMEL2, SKMEL28, IPC298) or 5,000 (SKMEL5, A375, RPMI-7951) cells/well in a 96 well plate and allowed to adhere overnight. Cells were then treated with binimetinib or DMSO as a vehicle control in fresh medium for 72h and assayed. All viability data was acquired using a Tecan plate reader Infinite 200 with Tecan icontrol version 1.7.1.12. IC50 values were calculated using a 4-parameter logistic curve in Prism 9.0.0.

Antibody-drug conjugate cell killing assays

SKMEL5 or A375 cells were pre-treated for 72 hours with DMSO or 1 μM binimetinib in 10 cm plates, and subsequently seeded at a density of 5,000 cells/well in a 96 plate. Cells were incubated antibody-drug conjugate with n=4 technical replicates per treatment condition for an additional 72 hours and similarly assayed with CTG.

T-cell/target cell co-incubation cell killing assays

Deidentified buffy coats from healthy human donors were obtained from Massachusetts General Hospital. Peripheral blood mononuclear cells (PBMCs) were isolated by density-based centrifugation using Ficoll (GE Healthcare). CD8+ T cells were isolated from PBMCs using a CD8+ T cell negative selection kit (Stemcell). T cells were mixed with Human T-activator CD3/CD28 DynaBeads (Thermo Scientific) in a 1:1 ratio and maintained in R10 + IL-2 [RPMI 1640 (Thermo Scientific) supplemented with 10% heat-inactivated FBS (Thermo Scientific), 1% HEPES (Corning), 1% Lglutamine (Thermo Scientific), 1% Pen/Strep (Corning) and 50 IU/mL of IL-2 (R&D Systems)] for 7 days prior to use in cell killing assays. DynaBeads were removed by magnetic separation prior to coincubation of primary T cells with target cells. Target cells

were treated with DMSO or 1 μM MEKi for 72 hours and were subsequently seeded in a 96-well plate with primary T-cells in R10 + IL-2 at an effector to target ratio of 2:1 and incubated with BiTEs for 48 hours with n=3 technical replicates per condition. Cells were assayed with CTG, and percent cytotoxicity was calculated by subtracting the average luminescence signal of the T-cell only condition and normalizing to the no BiTE condition. ((X-[T-cell only]) / ([average-no-BiTE] – [T-cell only])) x 100.

UV-mediated peptide exchange for hipMHCs

UV-mediated peptide exchange was performed using recombinant, biotinylated Flex-T HLA-A*02:01 monomers (BioLegend), using a modified version of the commercial protocol. Briefly, 2-4 μL of 500 μM peptide stock, 2 μL of Flex-T monomer, and 32 μL of 1X PBS were combined in a 96-well U-bottom plate. On ice, plates were illuminated with ultraviolet light (365 nm) for 30 minutes, followed by a 30-minute incubation at 37 °C protected from light. Concentration of stable complexes following peptide exchange was quantified using the Flex-T HLA class I ELISA assay (Biolegend) per manufacturer's instructions for HLA-A*02:01. ELISA results were acquired using a Tecan plate reader Infinite 200 with Tecan icontrol version 1.7.1.12.

Peptide MHC isolation

Cultured cells were seeded in 10 cm plates, allowed to adhere overnight, and treated for 72h with binimetinib or DMSO vehicle control. At the time of harvest, cells were washed with 1X PBS, and lifted using 0.05% Trypsin-EDTA (Gibco). Cells were pelleted at 500 g for 5 minutes, washed twice more in 1X PBS, and pelleted again. Cells were resuspended in 1 mL lysis buffer [20 nM Tris-HCl pH 8.0, 150 mM NaCl, 0.2 mM PMSO, 1% CHAPS, and 1X HALT Protease/Phosphatase Inhibitor Cocktail (Thermo Scientific)], followed by brief sonication (3 x

10 second microtip sonicator pulses) to disrupt cell membranes. Lysate was cleared by centrifugation at 5000 g for 5 minutes and quantified using bicinchoninic acid protein assay kit (Pierce). For in vitro analyses, $1x10^7$ cells were used for each condition. Frozen CLX tumor samples were homogenized in lysis buffer, cleared by centrifugation, and quantified using BCA as described in the in vitro analyses. For each sample, 7 mg of lysate was used. For absolute quantification analyses, ~5 mg of lysate was used.

Peptide MHCs were isolated by immunoprecipitation (IP) and size exclusion filtration, as previously described[160]. Briefly, 0.5 mg of pan-specific anti-human MHC Class I (HLAA, HLA-B, HLA-C) antibody (clone W6/32, Bio X Cell [cat # BE0079]) was bound to 20 µL FastFlow Protein A Sepharose bead slurry (GE Healthcare) for 3 hours rotating at 4°C. Beads were washed 2x with IP buffer (20 nM Tris-HCl pH 8.0, 150 mM NaCl) prior to lysate and hipMHC addition (in vitro analyses), and incubated rotating overnight at 4°C to isolate pMHCs. For TMT-labeled DDA analyses, 30 fmol of the following hipMHC standards were added prior to IP for quantification correction: $ALNEQIARL_7$, $SLPEEIGHL_7$, and $SVVESVKFL_7$. For absolute quantification analyses, 1, 10, or 100 fmol of 1-3H Iso18 hipMHCs standards were added to each immunoprecipitation. Beads were washed with 1X Tris buffered saline (TBS) and water, and pMHCs were eluted in 10% formic acid for 20 minutes at room temperature
(RT). Peptides were isolated from antibody and MHC molecules using a passivated 10K molecule weight cutoff filter (PALL Life Science), lyophilized, and stored at -80°C.

pMHC labeling with Tandem Mass Tags and SP3 cleanup

For labeled analyses, 100 µg of pre-aliquoted Tandem Mass Tag (TMT) 6-plex, 10-plex, or TMTpro was resuspended in 30 µL anhydrous acetonitrile, and lyophilized peptides were resuspended in 100 µL 150 mM triethylammonium bicarbonate, 50% ethanol. Both were gently

vortexed, centrifuged at 13,400 g for 1 minute, and combined. TMT/peptide mixtures were incubated on a shaker for 1 hour at RT, followed by 15 minutes of vacuum centrifugation. After combining labeled samples, we washed tubes 2x with 25% acetonitrile (MeCN) in 0.1% acetic acid (AcOH) and added it to the labeled mixture, which was subsequently centrifuged to dryness.

Sample cleanup was performed using single-pot solid-phase-enhanced sample preparation (SP3) as previously described[170]. Briefly, a 1:1 mix of hydrophobic/hydrophilic Sera-mag carboxylate-modified speed beads (GE Healthcare) was prepared at a final bead concentration of 10 μg μL^{-1}. Labeled samples were resuspended in 30 μL of 100 mM ammonium bicarbonate (pH 7-8) and added to 500 μg of bead mix with 1 mL MeCN. Peptides were allowed to bind for 10 minutes at RT, washed 2x with MeCN, and eluted with 2% DMSO, for 1 minute of sonication in a bath sonicator. TMT-labeled peptides were transferred to a fresh microcentrifuge tube and centrifuged to dryness. Peptides were resuspended in 0.1% formic acid, 5% MeCN and analyzed by MS.

HF-X LC-MS/MS data acquisition

Chromatography

Peptides were resuspended in 0.1% acetic acid and loaded on a precolumn packed inhouse (100 μm ID Å~ 10 cm packed with 10 μm C18 beads (YMC gel, ODS-A, 12 nm, S-10 μm, AA12S11)). The precolumn was then washed with 0.1% acetic acid and connected in series to an analytical capillary column with an integrated electrospray tip (~1 μm orifice) with 5μM C18 beads, prepared in house ((50 μm ID Å~ 12 cm with 5 μm C18 beads (YMC gel, ODS-AQ, 12 nm, S-5 μm, AQ12S05)).

Labeled pMHC analyses

Peptides were eluted using a 130-minute gradient with 10-45% buffer B (70% Acetonitrile, 0.2M

acetic acid) from 5-100 minutes and 45-55% buffer B from 100-120 minutes at a flow rate of 0.2 mL/min for a flow split of approximately 10,000:1. Peptides were analyzed using a Thermo Q Exactive HF-X Hybrid Quadrupole-Orbitrap mass spectrometer, and data were acquired using Thermo Fisher Scientific Xcalibur version 2.9.0.2923. Standard mass spectrometry parameters were as follows: spray voltage, 2.5 kV; no sheath or auxiliary gas flow; heated capillary temperature, 250 °C.

The HF-X was operated in data-dependent acquisition (DDA) mode for LF and TMT analyses. LF: Full-scan mass spectrometry spectra (mass/charge ratio (m/z), 350 to 2,000; resolution, 60,000) were detected in the Orbitrap analyzer after accumulation of ions at 3e6 target value with a maximum IT of 50 ms. For every full scan, the top 20 most intense ions were isolated (isolation width of 0.4 m/z) and fragmented (collision energy (CE): 28%) by higher energy collisional dissociation (HCD) with a maximum injection time of 350 ms, AGC target 1e5, and 30,000 resolution. Charge states < 2 and > 4 were excluded, and dynamic exclusion was set to 45 seconds. TMT: Full-scan mass spectrometry spectra (mass/charge ratio (m/z), 400 to 2,000; resolution, 60,000) were detected in the Orbitrap analyzer after accumulation of ions at $3e^6$ target value with a maximum IT of 50 ms. For every full scan, the 20 most intense ions were isolated (isolation width of 0.4 m/z) and fragmented (collision energy (CE): 31%) by higher energy collisional dissociation (HCD) with a maximum injection time of 350 ms, AGC target 1e5, and 30,000 resolution. Charge states < 2 and > 4 were excluded, and dynamic exclusion was set to 60 seconds.

Exploris 480 LC-MS/MS data acquisition

pMHC samples were analyzed using an Orbitrap Exploris 480 mass spectrometer (Thermo Scientific) coupled with an UltiMate 3000 RSLC Nano LC system (Dionex), Nanospray Flex ion

source (Thermo Scientific), and column oven heater (Sonation). Samples were resuspended in 0.1% formic acid and directly loaded onto a 10-15 cm analytical capillary chromatography column with an integrated electrospray tip (~1 μm orifice), prepared and packed in house (50 μm ID 1.9 μM C18 beads, ReproSil-Pur). Unless otherwise defined, standard mass spectrometry parameters were as follows: spray voltage, 2.0 kV; no sheath or auxiliary gas flow; heated capillary temperature, 275°C.

Labeled DDA pMHC analyses

pMHC elutions were injected in 15-25% fractions for improved coverage of the immunopeptidome. TMT-6/10 chromatography: Peptides were eluted using a gradient with 8-25% buffer B for 50 minutes, 25-35% for 25 minutes, 35-55% for 5 minutes, 55-100% for 2 minutes, hold for 1 minutes, and 100% to 3% for 2 minutes. TMT-Pro chromatography: Peptides were eluted using a gradient with 8-25% buffer B for 50 minutes, 25-45% for 30 minutes, 45-100% for 2 minutes, hold for 1 minutes, and 100% to 3% for 2 minutes. The Exploris was operated in data dependent acquisition (DDA) mode. Full scan mass spectra (350-1200 m/z, 60,000 resolution) were detected in the orbitrap analyzer after accumulation of 3e6 ions (normalized AGC target of 300%) or 25 ms. For every full scan, MS2 were collected during a 3 second cycle time. Ions were isolated (0.4 m/z isolation width) for a maximum of 150 ms or 75% AGC target and fragmented by HCD with 32% CE (TMT-6/10) or 30% (TMT-pro) at a resolution of 45,000. Charge states < 2 and > 4 were excluded, and precursors were excluded from selection for 30 seconds if fragmented n=2 times within 20 second window.

Isotopologue absolute quantification analyses

Survey analyses of 4H peptides: Peptides were eluted with 6-25% buffer B for 53 minutes, 25-45% for 12 minutes, 45-97% for 3 minutes, and 97% to 3% for 1 minute. The Exploris was

operated in data dependent acquisition (DDA) mode with an inclusion list2. Full scan mass spectra (300-1500 m/z, 120,000 resolution) were detected in the orbitrap analyzer after accumulation of 3e6 ions or 50 ms. For each full scan, up to 20 ions were subsequently isolated for targets on the inclusion with (+/- 5 ppm of targets m/z) with a minimum intensity threshold of 1e6. Ions were collected with a 10s maximum injection time, AGC target: 1000%, and fragmented by HCD with 30% nCE.

SureQuant-IsoMHC targeted analyses

Standard mass spectrometry parameters for SureQuant acquisition are as follows: spray voltage: 1.6kV, heated capillary temperature: 280°C. A custom SureQuant acquisition method was built using the Thermo Orbitrap Exploris Series 2.0 software. Full-scan mass spectra were collected with scan range: 350-1200 m/z, AGC target value: 3e6, maximum IT: 50 ms, resolution: 120,000. 4H peptides matching the m/z (+/- 3 ppm) and exceeding the defined intensity threshold (1% apex intensity from the survey analysis) were isolated (isolation width 1 m/z) and fragmented by HCD (nCE: 27%) with a scan range: 150-1700 m/z, maximum IT: 10 ms, AGC target: 1000%, resolution: 7,500. A product ion trigger filter next performs pseudo-spectral matching, where an MS2 scan of the 1H, 2H, 3H, and endogenous peptides are triggered at the defined mass offsets if the 4H trigger peptide contains $n \geq 5$ product ions from the defined list. Scan parameters are the same as the first MS2 scan but with 250 ms max IT, resolution 120,000. The inclusion list, ions for pseudo-spectral matching, and additional method paramters and details have been previously reported.

LC-MS/MS data analysis

All mass spectra were analyzed with Proteome Discoverer (PD, version 2.5) and searched using Mascot (version 2.4) against the human SwissProt database. MS/MS spectra were matched with

an initial mass tolerance of 10 ppm on precursor masses and 20 mmu for fragment ions. Data analyses were performed using Matlab version R2019b, and Microsoft Excel version 16.34.

pMHC analyses

No enzyme was used, static modifications included N-terminal and lysine TMT, and variable modifications included oxidized methionine for all analyses and phosphorylated serine, threonine, and tyrosine for cell treatment analyses. Treatment analyses were also searched against a previously published catalog of over 40,000 predicted antigenic mutations in cancer cell lines.15 Heavy leucine-containing peptides were searched for separately with heavy leucine (+7), c-terminal amidation, and methionine oxidation as dynamic modifications against a custom database of the synthetic peptide standards. All analyses were filtered with the following criteria: search engine rank =1, isolation interference ≤ 30%, and length between 8 and 15 amino acids. Label-free analyses were filtered with ion score ≥ 20, and labeled samples were filtered with ion score ≥ 15 and percolator q-value ≤ 0.05. Area under the curve (AUC) quantitation was performed using the minora feature detector in PD with match between runs enabled and filtered for ion score ≥ 20.

For TMT-labeled in vitro samples, ratios against a reference channel (usually TMT126) were calculated and the median of all ratios for correction hipMHCs was used to determine the final correction parameters. Only PSMs of heavy leucine-coded peptides with an average reporter ion intensity within 10-fold of the interquartile range of endogenous PSM reporter ion intensities were used for correction. To evaluate differences between conditions, the log2 transformed ratio of arithmetic mean intensity for drug- and DMSO-treated samples (n=3) was calculated. To determine if peptides were significantly increasing, an unpaired, 2-sided t-test was performed, and peptides with $p < 0.05$ were considered significantly increasing/decreasing. To evaluate

which peptides were significantly enriched above the mean, treated samples were mean centered by dividing the ion intensity of each peptide by the mean fold-change across all peptides, after which a student's 2-tailed t-test was performed on adjusted values. Peptides with a mean-adjusted p-value < 0.05 were considered significantly enriched. Mean centering was not performed on samples where the mean log2 fold change was between -0.07 and 0.07.

Isotopologue absolute quantification analyses

Peak areas of 6 preselected product ions for each peptide (endogenous and 1-3H isotopologues) were exported from Skyline ((version 20.2.1.28) and summed for all ions quantifiable across the endogenous and isotopologues as previously described.2 1-3H peptides were used to generate a calibration curve, from which endogenous pMHC concentrations were determined. Concentrations outside of the standard curve were extrapolated.

Figures and Tables

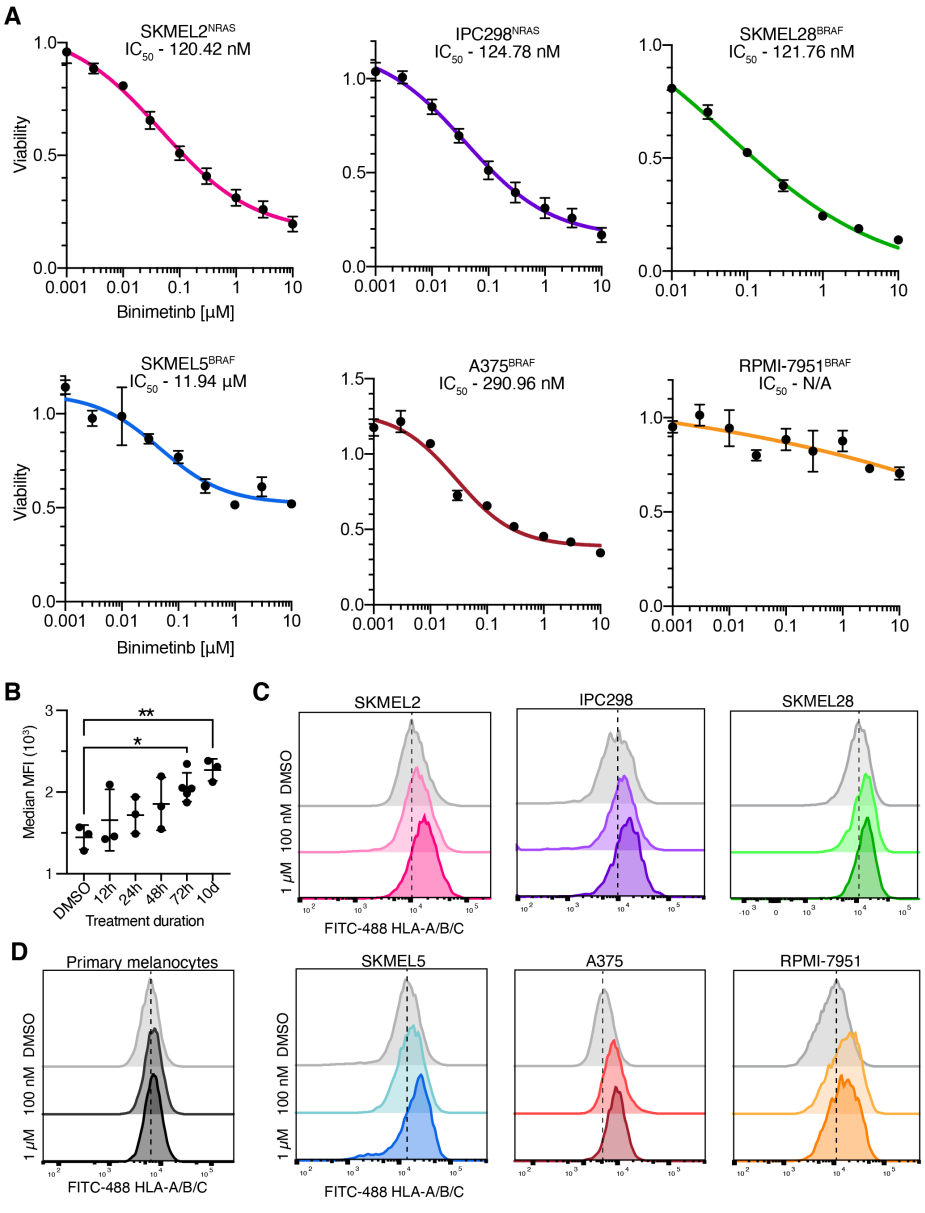

Figure 4.1: Phenotypic characterization of cellular response to binimetinib. A) Cell viability (fraction of DMSO control) at 72 hr after binimetinib treatment. Data are represented as mean values +/- SD for n=3 replicates. Lines represents a four-parameter nonlinear regression curve fit. B) Surface HLA expression of SKMEL5 cells treated with 100 nM binimetinib measured by flow cytometry. Data are represented as mean values +/- SD for n=3 replicates and significance between replicates (*p<0.05, **p<0.01) is calculated using a one way ANOVA test comparing each value to the DMSO control. C-D) Flow cytometry measurements of surface HLA expression in cells. Data are represented as % of maximum signal, and the distributions are representative of three independent experiments.

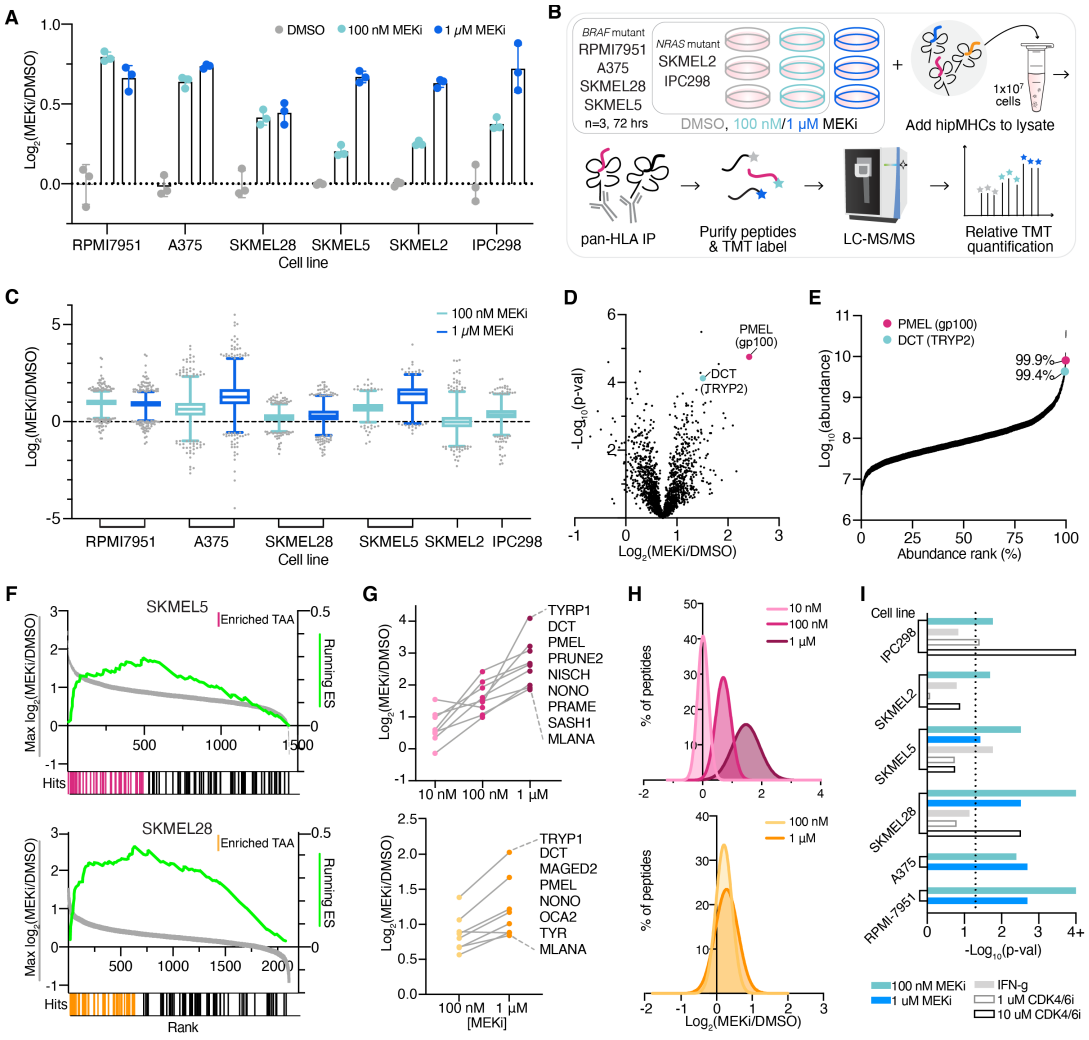

Figure 4.2: MEKi enriches TAA presentation on pMHCs. A) Fold change in median surface expression levels (over average DMSO control condition) of HLA-A/B/C in cell lines treated with vehicle control or binimetinib (MEKi) for 72 hr. Error bars represent standard deviation of n=3 biological replicates. B) Experimental setup for quantitative immunopeptidomics experiments. C) Relative changes in pMHC expression +/- MEKi. Data are represented as a box and whiskers plot, with whiskers displaying the 1-99 percentiles. D) Volcano plot of the average fold change in pMHC expression for SKMEL5 cells treated with 100 nM binimetinib for 72 hr (n=3 biological replicates for DMSO and MEKi treated cells) versus significance (mean-adjusted p value, unpaired two-sided t test). E) pMHCs ranked by precursor ion area abundance. F) TAA Enrichment plots of TAA enrichment in SKMEL5 +/- 100 nM MEKi (top, pink) and SKMEL28 +/- 100 nM MEKi (bottom, orange), displaying running enrichment scores (green, right y-axis), and fold change in pMHC presentation (left y-axis) versus rank (x-axis) for each peptide (gray). Hits denote TAA peptides, and colored hits represent enriched TAAs. SKMEL5 p = 0.001=4, SKMEL28 p = 0.001. G) Selected enriched TAA peptides in SKMEL5 (top) and SKMEL28 (bottom) analyses. H) Frequency distribution of pMHC fold change with MEK inhibition. SKMEL5 (top): 10 nM: μ=0.01, 100 nM: μ=0.70, 1 μM: μ=1.47. SKMEL28 (bottom): 100 nM: μ=0.21, 1μM: μ=0.28. I) Significance values for TAA pathway enrichment. Dotted line indicates and p<0.05 and values ≥4 (Log10 adjusted) represent p<0.0001.

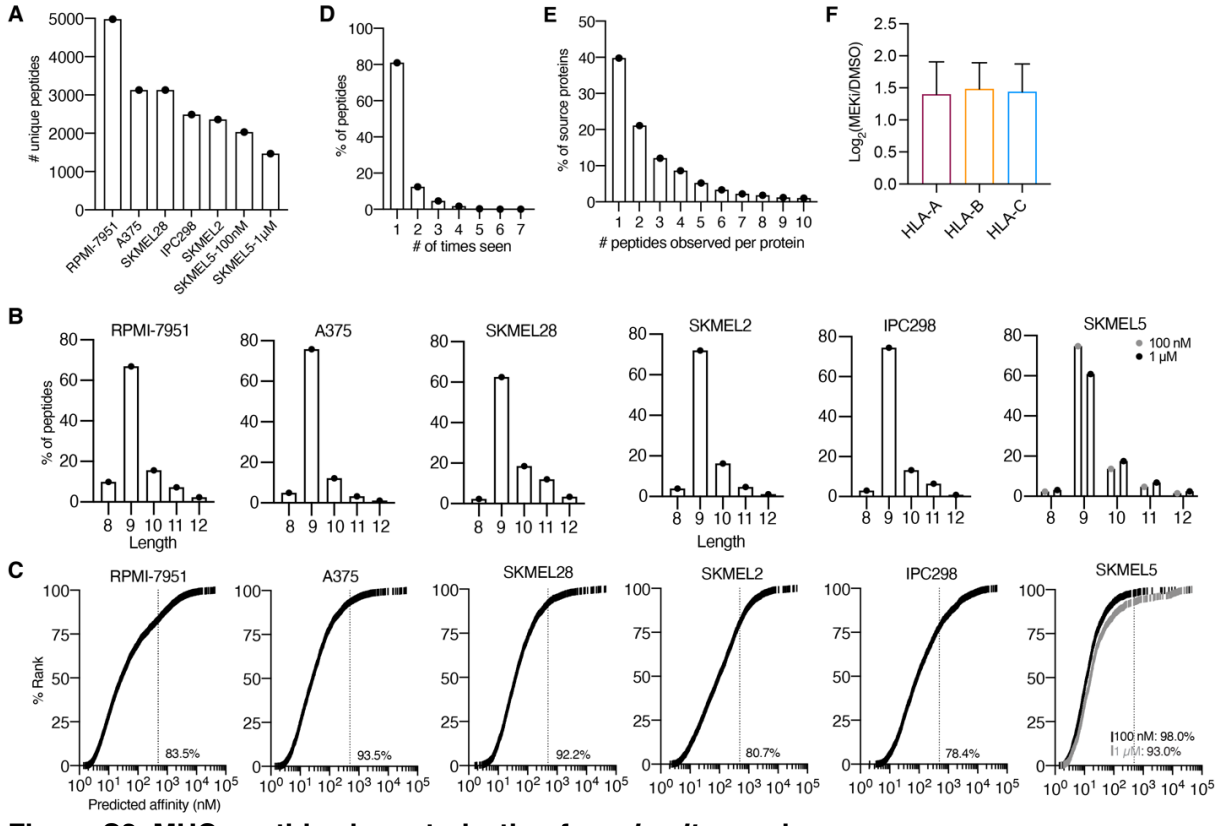

Figure 4.3: MHC peptide characterization from in vitro analyses. A) Number of unique peptides identified in each sample. B) Peptide length distribution for each cell line. C) Predicted binding affinity of 9-mer peptides, rank ordered. Dotted line represents threshold for binding at ≤500 nM. Percentage of peptides ≤500 nM are listed on each plot. D) Distribution of the number of times each peptide was seen across in vitro analyses. E) Distribution of the number of peptides observed per source protein. F) Average fold change in presentation for SKMEL5 9-mers +/- 1 uM MEKi segregated by highest predicted affinity to HLA-A/B/C. Error bars represent +/- stdev. Tukey's multiple comparisons test shows no significant difference between pairwise comparisons.

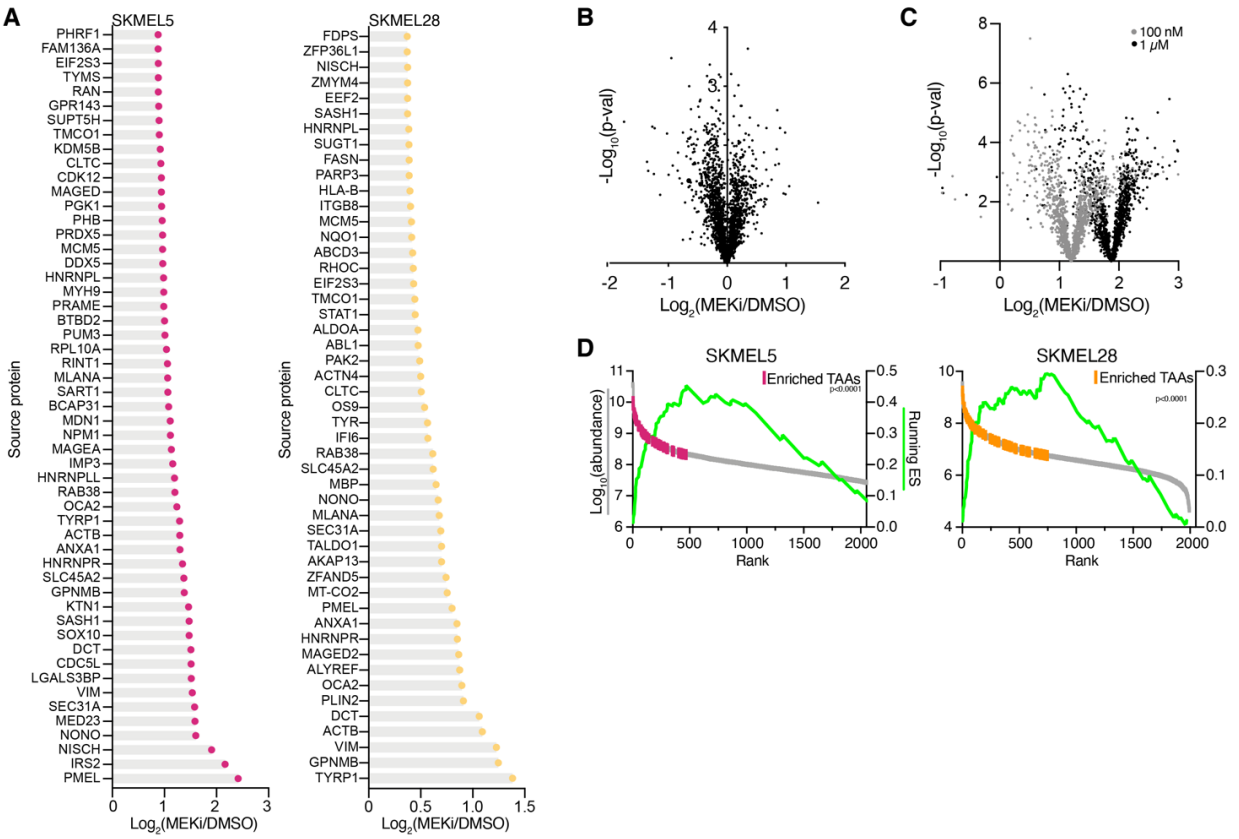

Figure 4.4: TAA pMHC enrichment following binimetinib treatment. A) Enriched TAA pMHC expression changes with 100 nM MEKi. B-C) Volcano plots of the average fold change in pMHC expression with 10 nM binimetinib treatment (B) and 100 nM and 1 μM trametinib treatment (C). Data shown are the mean of n=3 biological replicates per condition versus significance (mean-adjusted p value, unpaired two-sided t test). D) Enrichment plots with peptides rank ordered by precursor ion abundance. $p<0.0001$ for both SKMEL5 100 nM and SKMEL28 100 nM analyses.

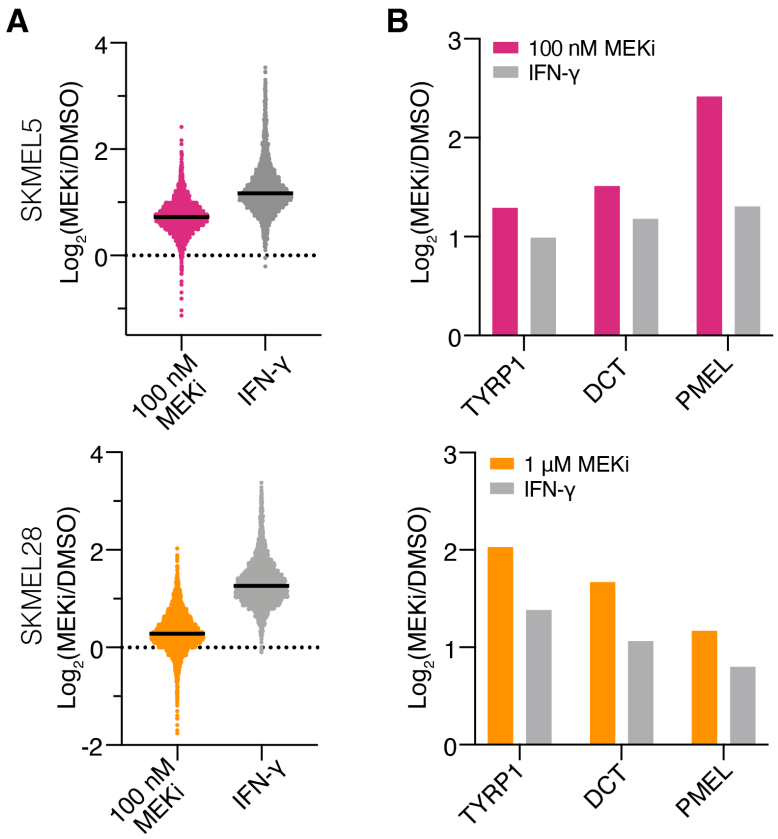

Figure 4.5: Comparison of pMHC repertoire response to MEKi versus and IFN-γ. A) Distribution of pMHC changes in expression with binimetinib (100 nM) or IFN-γ (10 ng/mL) for 72 hr. B) Changes in pMHC expression for selected TAA peptides.

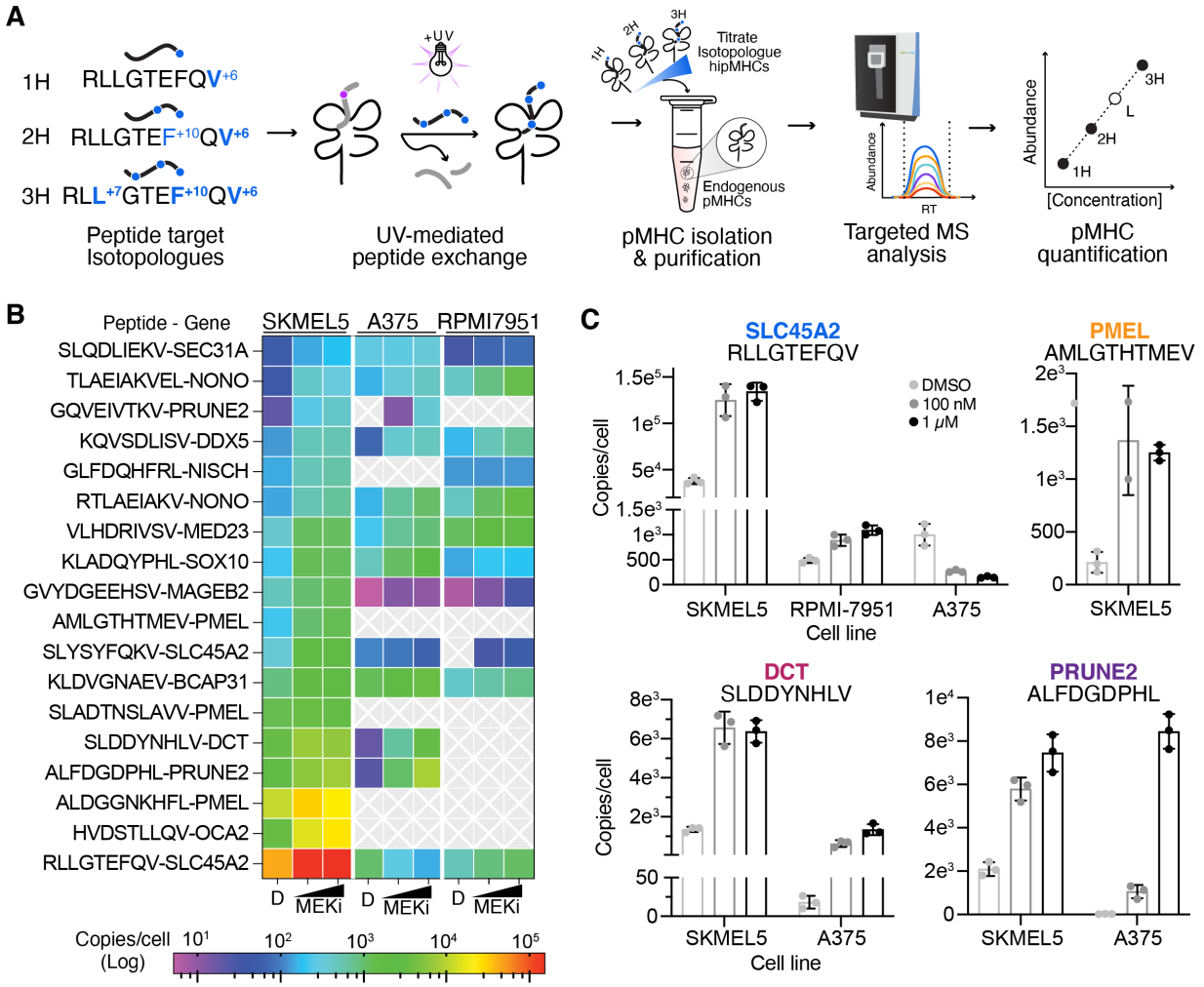

Figure 4.6: Absolute quantification of MEKi-inducible TAAs. A) Schematic of SureQuant isoMHC workflow for multipoint absolute quantification of 18 TAAs. B) Heatmap of copies/cell for each cell line treated with DMSO, 100 nM MEKi, or 1 μM MEK for n=3 biological replicates. C) Copies/cell for select epitopes across cell lines and treatment conditions.

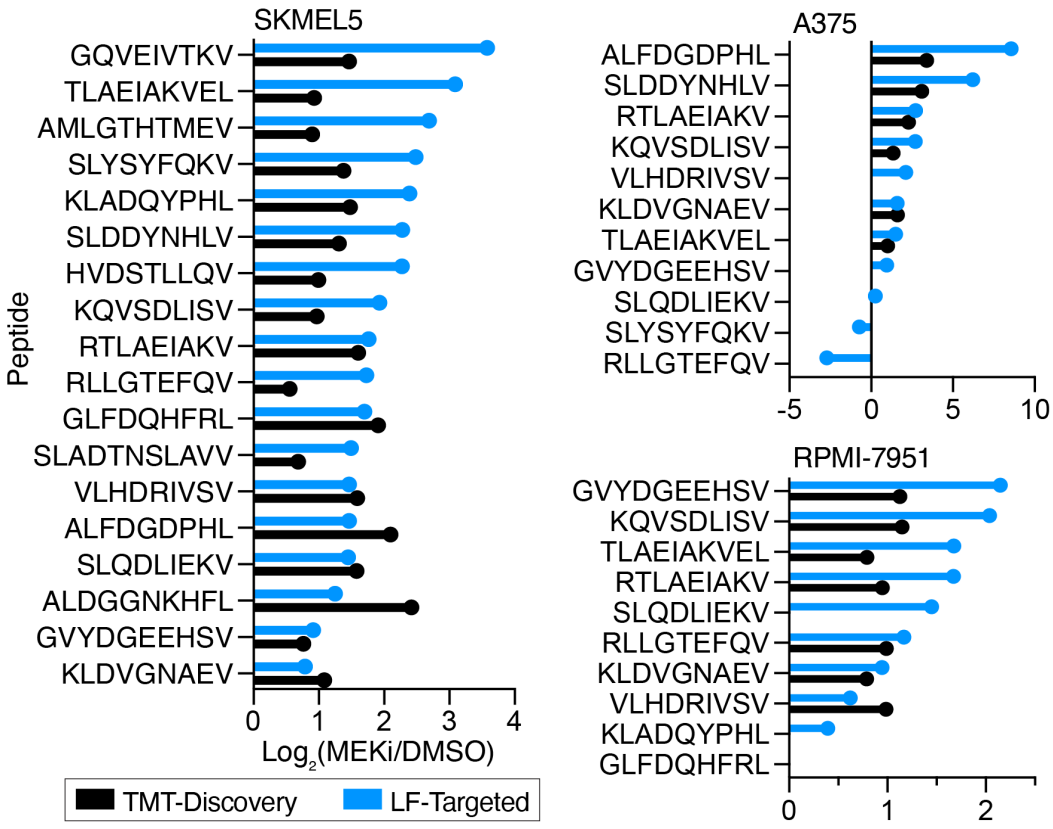

Figure 4.7: TAA presentation changes measured in discovery versus targeted analyses. Average fold change in presentation (1 μM MEKi) of Iso18 targets identified in multiplexed, TMT-labeled discovery analyses and label free targeted analyses (SureQuant-IsoMHC) for n=3 biological replicates per condition. Peptides without a TMT-Discovery datapoint were not identified by DDA, and only peptides measured in both DMSO and 1 μM MEKi conditions with SureQuant Iso-MHC are shown.

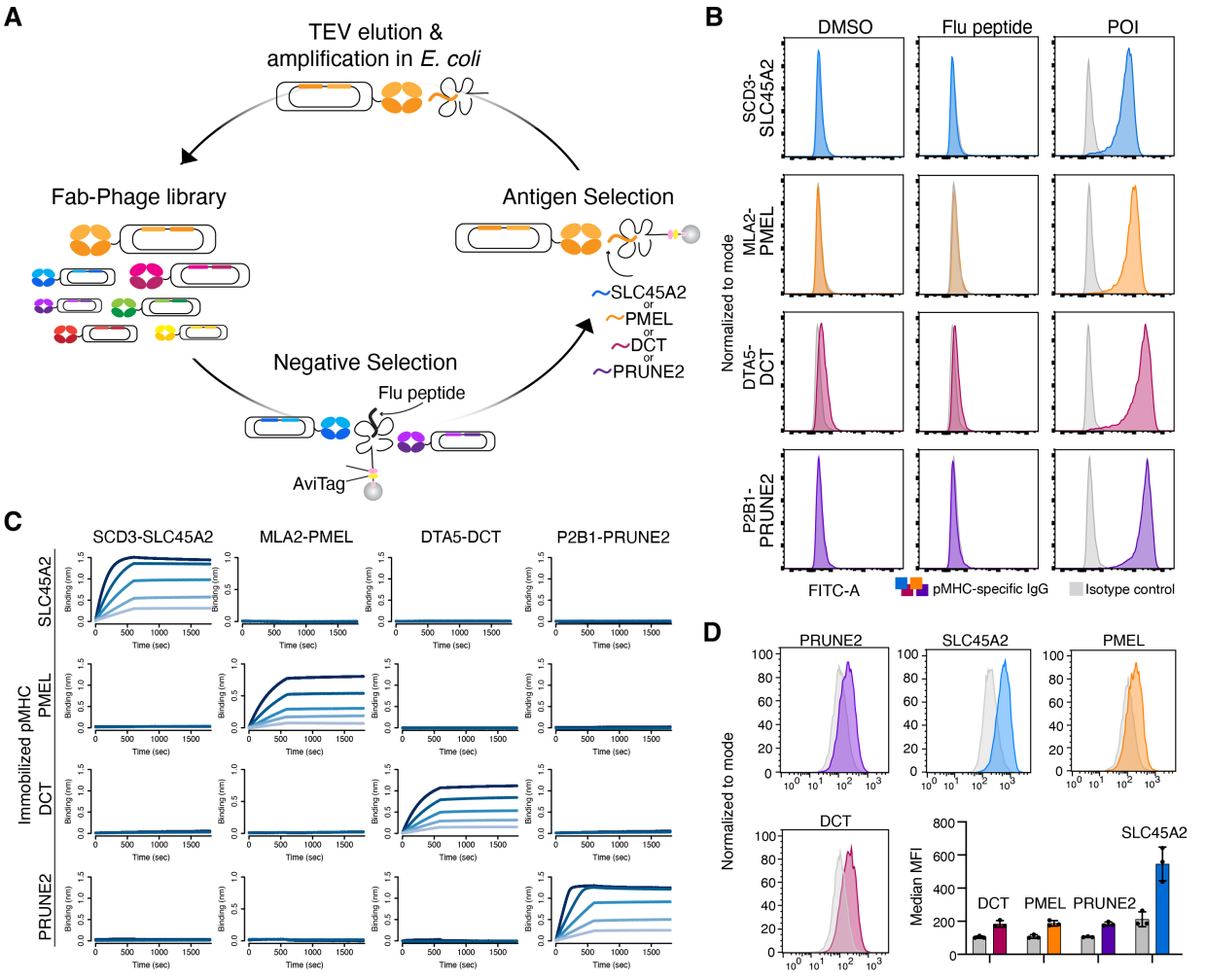

Figure 4.8: Generation of pMHC-specific antibodies. A) Schematic of phage display selection. B) Fluorescence intensity of T2 cells loaded with DMSO (negative control), a decoy FLU peptide, or peptide of interest (POI) stained with a pMHC-specific IgG (color) or an isotype control (grey). C) Bio-layer interferometry (BLI) analysis of IgG's (two-fold dilutions starting at 20 nM) against selected HLA-A*02:01 MHC-peptide complexes. D) Fluorescence intensity of SKMEL5 cells treated with DMSO or 1 μM MEKi for 72 hours stained with Alexa fluor 488-conjugated pMHC-specific antibodies. Data show a representative histogram and bar graph of median MFI where error bars show standard deviation for n=3 biological replicates per condition.

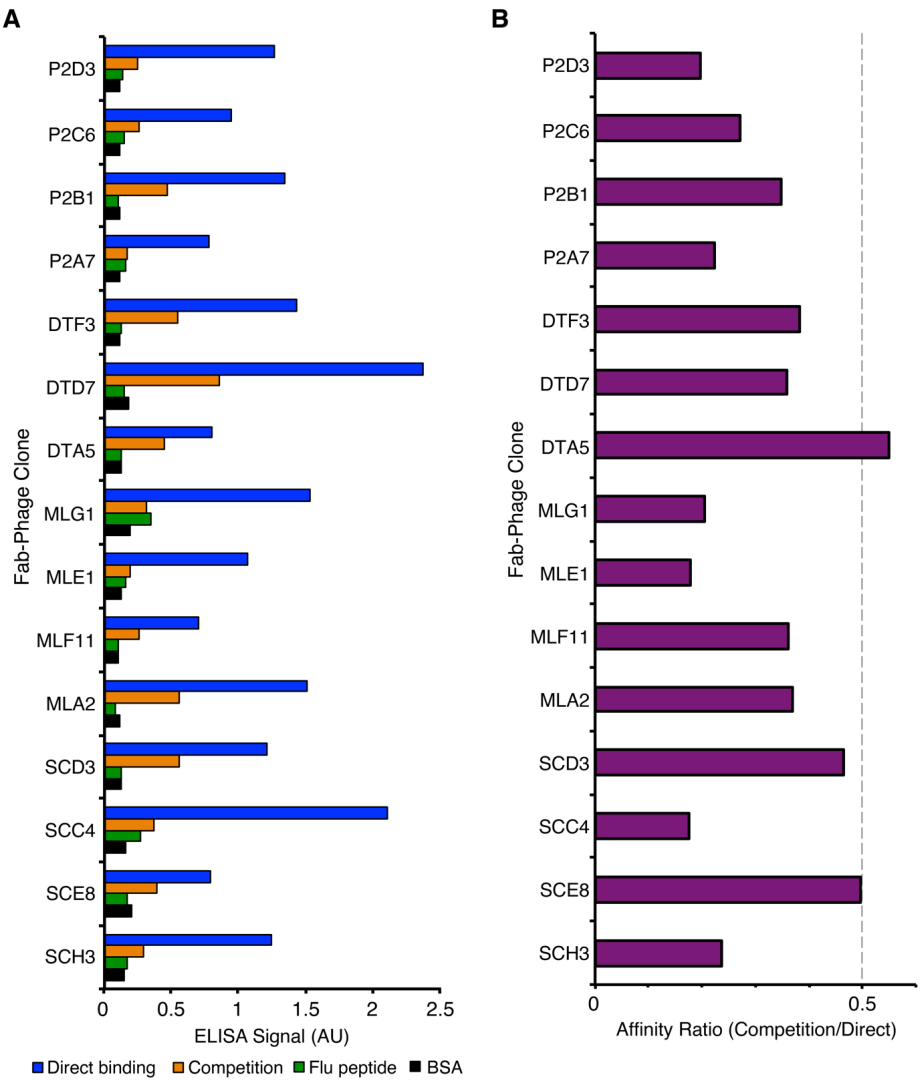

Figure 4.9: ELISA characterization of Fab-phage clones. A) Fab-phage ELISA screen of each MHC-peptide complex. Clones with signal above 0.5 AU and affinity ratios less than 0.5 were considered high affinity, with predicted relative affinities of <20 nM. B) Affinity ratios for all unique Fab-phage clones across all phage-display selections for MHC-peptide complexes.

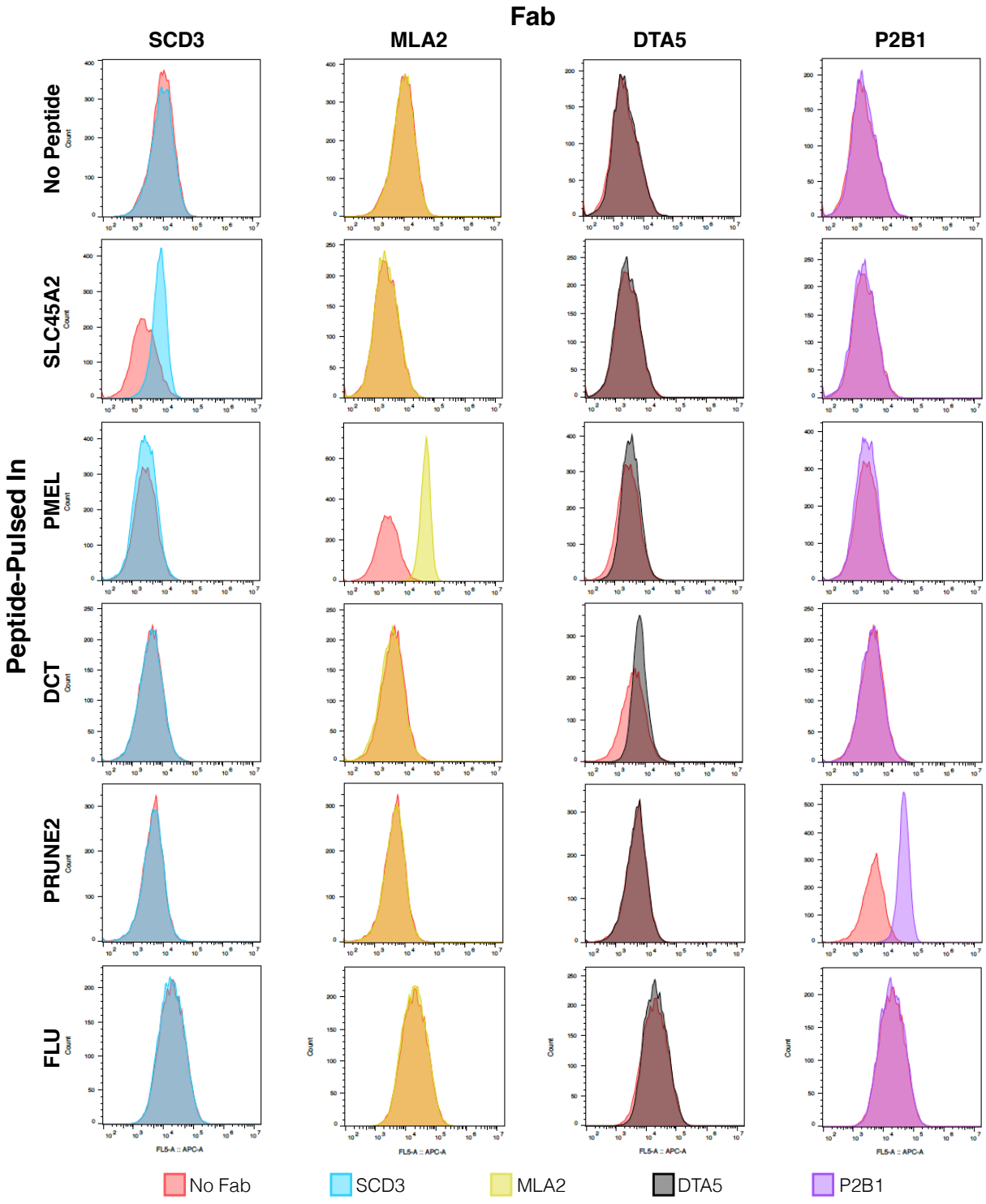

Figure 4.10: Peptide specificity of pMHC-specific Fabs. Fluorescence intensity of T2 cells loaded with no peptide (negative control), a decoy FLU peptide, or peptide of interest stained with a pMHC-specific Fab.

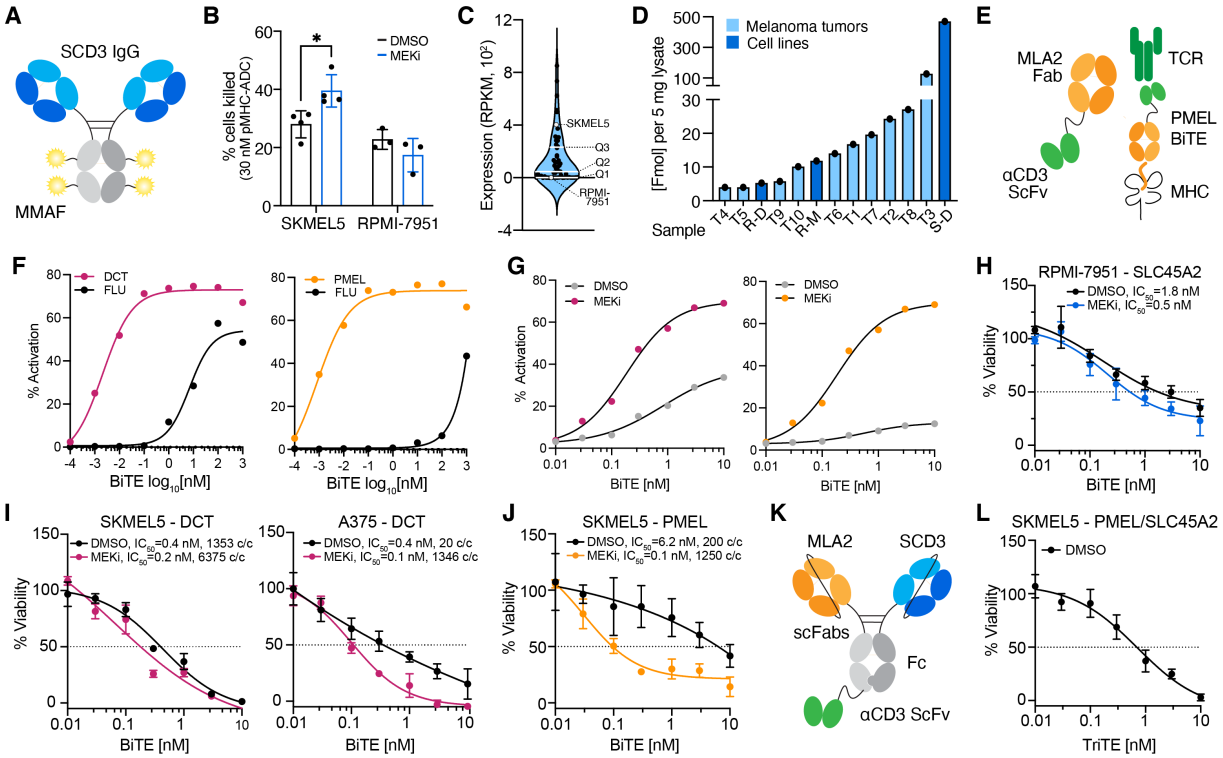

Figure 4.11: MEKi enhances cytotoxicity of pMHC-specific antibody-based therapies. A) Schematic of ADC targeting the SLC45A2 epitope. B) Percent of cells killed with SLC45A2-ADC relative to the DMSO control. Error bars represent +/- stdev for n=4 (SKMEL5) and n=3 (RPMI-7951) biological replicates. *adjusted p-value = 0.017, Sidak's multiple comparisons test. C) SLC45A2 transcript expression across n-57 BRAF/NRAS mutant melanoma cell lines. D) RLLGTEFQV pMHC concentration across cell lines and melanoma tumors (previously reported). S=SKMEL5, R=RPMI-7951, D=DMSO, M=1 μM MEKi. E) Schematic of PMEL-targeted BiTE. F-G) Percent of GFP+ Jurkat cells following incubation with peptide-pulsed T2 cells (F) or SKMEL5 cells (G) and PMEL-BiTE. Lines represent a 4PL nonlinear fit, and error bars show +/- SEM for n=3 biological replicates. H-J), L) Cell viability (percentage of untreated control) of target cells incubated with normal human T cells (effector:target 2:1) & a pMHC-specific BiTE/TriTE for 48 hours. K) Schematic of PMEL/SLC45A2-targeted TriTE.

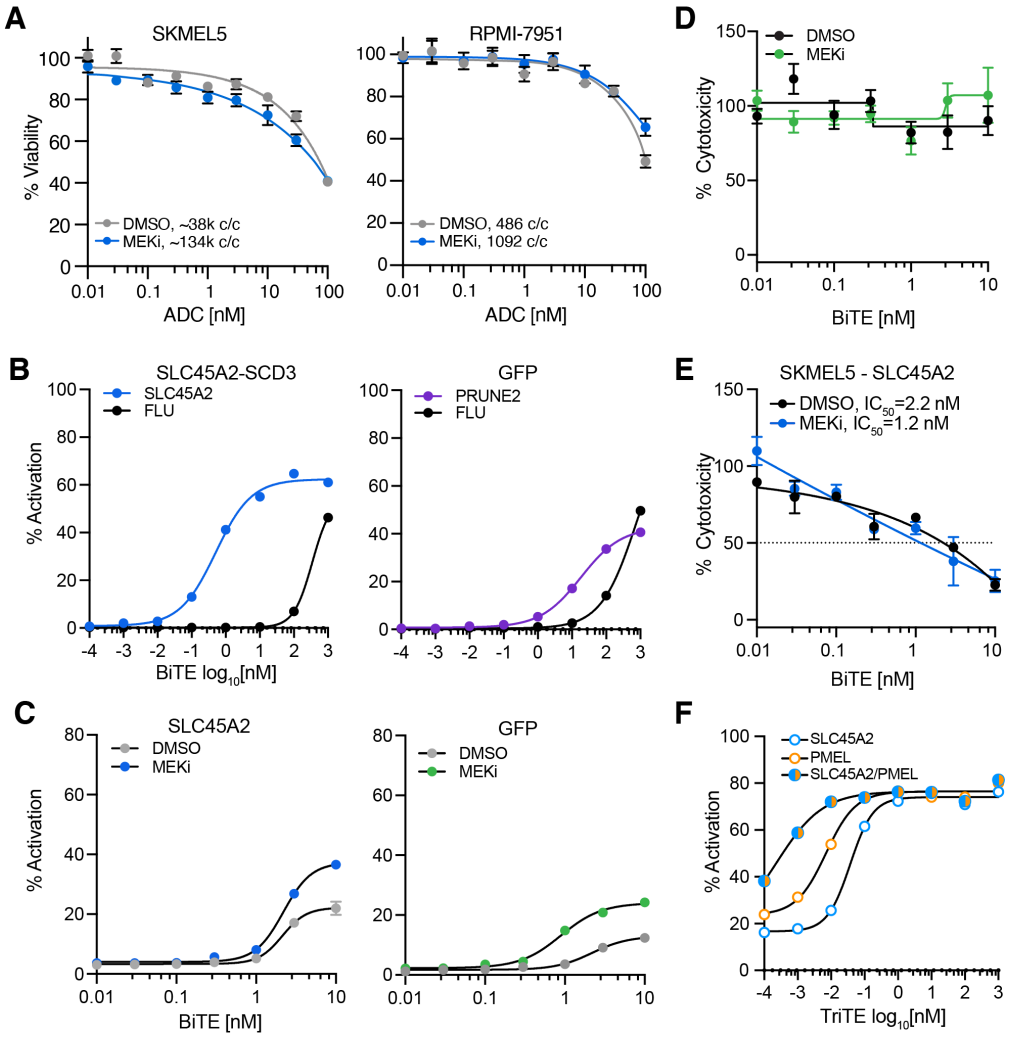

Figure 4.12: Characterization of pMHC-specific ADCs and BiTEs *in vitro*. A) Cell viability after 72 hr incubation with SLC45A2-ADC. Error bars represent +/- SD for n=4 biological replicates. Lines represent a four parameter logistic (4PL) nonlinear regression curve. c/c denotes average copies per cell. B-C) Percent of GFP+ Jurkat cells following incubation with peptide-pulsed T2 cells (B) or SKMEL5 cells (C) and a pMHC-specific BiTE or negative control BiTE (anti-GFP) for 24 hours. D) Cell viability (percentage of untreated control) of target cells incubated with normal human T cells (effector:target 2:1) & a negative control anti-GFP BiTE for 48 hours. E) Cell viability (percentage of untreated control) of target cells incubated with normal human T cells (effector:target 2:1) & a pMHC-specific BiTE or 48 hours. F) Percent GFP+ Jurkat cells following incubation with SKMEL5 (DMSO) cells and TriTEs for 24 hours.

Table 4.1 Tumor associated antigen peptide library for enrichment analyses.

AAAAAIFVI	ALIHHNTHL	AMLDLLKSV	AVFDGAQVTSK	DLTSFLLSL	ESDPIVAQY
AAANIIRTL	ALISKNPV	AMLERQFTV	AVLTKQLLH	DLWKETVFT	ESFSGSLGHL
AAFDGRHSQTL	ALKDSVQRA	AMLGTHTMEV	AVMALENNYEV	DNGAKSVVL	ESLFRAVITK
AAGIGILTV	ALKDVEERV	AMLGTHTMEVTV	AVQEFGLARFK	DPARYEFLW	ESVMINGKY
AARAVFLAL	ALLALTSAV	AMTKDNNLL	AVTNVRTSI	DPKDAEKAI	ETAGPQGPPHY
AAVEEGIVLGGG	ALLAVGATK	AMVGAVLTA	AVVDLQGGGHSY	DPSTDYYQEL	ETFTEGQKL
ACDGERPTL	ALLEIASCL	AMYDKGPFRSK	AVVGILLVV	DPYKATSAV	ETHLSSKRY
ACDPHSGHFV	ALLESSLRQA	ANADLEVKI	AVYGQKEIHRK	DQYPYLKSV	ETILTFHAF
AEEAAGIGIL	ALLKDTVYT	ANDPIFVVL	AWISKPPGV	DRASFIKNL	ETLGFLNHY
AEEAAGIGILT	ALLMPAGVPL	APAGRPSAS	AWLVAAAEI	DSDPDSFQDY	ETVELQISL
AEEHSIATL	ALLNIKVKL	APAGRPSASR	AYACNTSTL	DSFPMEIRQY	ETVSEQSNV
AEHIESRTL	ALLPSLSHC	APAGVREVM	AYDFLYNYL	DSFPMEIRQYL	EVAPDAKSF
AEINNIIKI	ALLPTALDAL	APDGAKVASL	AYGLDFYIL	DTEFPNFKY	EVAPPASGTR
AELESKTNTL	ALMDKSLHV	APLLRWVL	AYIDFEMKI	DVNGLRRVL	EVDPASNTY
AELLNIPFLY	ALMEQQHYV	APLQRSQSL	AYTKKAPQL	DVTSAPDNK	EVDPIGHLY
AELVHFLLL	ALMVRQARGL	APNTGRANQQM	AYVPQQAWI	DVWSFGILL	EVDPIGHLYIF
AEPINIQTW	ALNFPGSQK	APRGVRMAV	CHILLGNYC	DYIGPCKYI	EVDPIGHVY
AFLPWHRLF	ALPPPLMLL	APVIKARMM	CIAEQYHTV	DYKSAHKGF	EVFEGREDSVF
AFLRHAAL	ALPSFQIPV	AQAEHSITRV	CILGKLFTK	DYLQCVLQI	EVFPLAMNY
AGDGTTTATVLA	ALQDIGKNIYTI	AQCQETIRV	CITFQVWDV	DYLQYVLQI	EVFPLAMNYL
AGFKGEQGKGEP	ALQKAKQDL	AQDPHSLWV	CLAFPAPAKA	DYLRSVLEDF	EVFQNANFRSF
AGYLMELCC	ALRCASPWL	AQPDTAPLPV	CLGHNHKEV	DYPSLSATDI	EVHNLNQLLY
AHVDKCLEL	ALREEEEGV	AQYEHDLEVA	CLLSGTYIFA	DYSARWNEI	EVIGRGHFGCVY
AIDELKECF	ALSDHHIYL	ARGPESRLL	CLLWSFQTSA	EAAGIGILTV	EVIPYTPAM
AIIDPLIYA	ALSEDLLSI	ARGQPGVMG	CLVFLAPAKA	EADPTGHSY	EVIPYTPAMQR
AIISGDSPV	ALSVMGVYV	ARHRRSLRL	CLVFPAPAKA	EAFIQPITR	EVIPYTPAMQRY
AISANIADI	ALTAVAEEV	ARSVRTRRL	CLVFPAPAKAV	EEFGRAFSF	EVIQWLAKL
AIYDHINEGV	ALTDIDLQL	ARTDLEMQI	CMHLLLEAV	EEKLIVVLF	EVISCKLIKR
AIYDHVNEGV	ALTEHSLMGM	ASERGRLLY	CMLGDPVPT	EEYLQAFTY	EVISSRGTSM
AIYKQSQHM	ALTERSLMGM	ASFDKAKLK	CMTWNQMNL	EEYNSHQSL	EVITSSRTTI
AKYLMELTM	ALTPVVVTL	ASGPGGGAPR	CQWGRLWQL	EFKRIVQRI	EVKLSDYKGKYV
ALAGLSPV	ALVDAGVPM	ASLDSDPWV	CTACRWKKACQ	EFQKMRRDL	EVLDSLLVQY
ALAPAPAEV	ALVSIIKV	ASLIYRRRLMK	CTACRWKKACQR	EGDCAPEEK	EVLLRPGLHFR
ALARGAGTVPL	ALWGPDPAAA	ASSTLYLVF	CYMEAVAL	EILGALLSI	EVMSNMETF
ALASHLIEA	ALWGPDPAAAF	ASYLDKVRA	CYTWNQMNL	ELAEYLYNI	EVRGDVFPSY
ALAVLSVTL	ALWKEPGSNV	ATAGDGLIELRK	DAKNKLEGL	ELAGIGILTV	EVTFVPGLY
ALCQNGYHGT	ALWMRLLPL	ATAGIIGVNR	DALVLKTV	ELAPIGHNRMY	EVTSSGRTSI
ALCQNGYHGTI	ALWMRLLPLL	ATAQFKINK	DCLVFLAPA	ELFQDLSQL	EVVEKYEIY
ALCRWGLLL	ALWPWLLMA	ATATPCWTWLL	DEKQQHIVY	ELHLLQDEEV	EVVHKIIEL
ALDEKLLNI	ALWPWLLMA(T)	ATFSSSHRYHK	DELEIKAY	ELHLLQDKEV	EVVRIGHLY
ALDGGNKHFL	ALWPWLLMAT	ATGFKQSSK	DEVYQVTVY	ELSDSLGPV	EVYDGREHSA
ALDVYNGLL	ALYGDIDAV	ATIIDILTK	DFMIQGGDF	ELTLGEFLK	EYILSLEEL
ALEEANADL	ALYLVCGER	ATLPLLCAR	DIKAKMQAS	ELTLGEFLKL	EYLQLVFGI
ALENNYEVL	ALYSGVHKK	ATQIPSYKK	DLDVKKMPL	ELVRRILSR	EYLSLSDKI
ALFDIESKV	ALYVDSLFFL	ATSPPASVR	DLILELLDL	ELWKNPTAF	EYRGFTQDF
ALGDLFQSI	AMAPIKVRL	ATTNILEHY	DLKGFLSYL	EPLARLEL	EYSKECLKEF
ALGGHPLLGV	AMAQDPHSL	ATVGIMIGV	DLLSHAFFA	EQYEQILAF	EYSRRHPQL
ALIDCNPCTL	AMAQDPHSLWV	AVAANIVLTV	DLPAYVRNL	ERGFFYTPK	EYTAKIALL
ALIEVGPDHFC	AMARDPHSL	AVASLLKGR	DLPPPPPLL	ERLERQERL	EYYLQNAFL
ALIGGPPV	AMARDPHSLWV	AVCPWTWLR	DLSPGLPAA	ERSPVIQTL	FALQLHDPSGY

(Table 4.1 continued)

FATPMEAEL	FLPETEPPEM	FVGEFFTDV	GLWRHSPCA	HTMEVTVYHR	IMIHDLCLA
FATPMEAELAR	FLPETEPPEML	FVSGSGIAIA	GLYDGMEHL	HTRTPPIIHR	IMIHDLCLV
FAWERVRGL	FLPHFQALHV	FVSGSGIATA	GMVTTSTTL	HTYLEPGPVTAQ	IMIHDLCLVFL
FEITPPVVL	FLPRNIGNA	FVWLHYYSV	GMWESNANV	HVDSTLLQ	IMLCLIAAV
FGLATEKSR	FLQDVMNIL	FYTPKTRRE	GPFGAVNNV	HVDSTLLQV	IMNDMPIYM
FGLFPRLCPV	FLRAENETGNM	GADGVGKSA	GPFGPPMPLHV	HVYDGKFLAR	IMPGQEAGL
FIASNGVKLV	FLRNFSLML	GADGVGKSAL	GPRESRPPA	HYTNASDGL	IMPKAGLLI
FIDKFTPPV	FLRNFSLMV	GAFEHLPSL	GQHLHLETF	IALNFPGSQK	IPSDLERRIL
FIDNTDSVV	FLRNLVPRT	GAIAAIMQK	GRAPQVLVL	IARNLTQQL	IPSNPRYGM
FIDSYICQV	FLSSANEHL	GASGVGSGL	GSHLVEALY	ICLHHLPFWI	IQATVMIIV
FIFPASKVYL	FLSTLTIDGV	GCELKADKDY	GSPATWTTR	IESRTLAIA	IRRGVMLAV
FIFSILVLA	FLTGNQLAV	GDFGLATEK	GSSDVIIHR	IEVDGKQVEL	ISGGPRISY
FIIENLKAA	FLTKRGGQV	GEISEKAKL	GTAAIQAHY	IIGGGMAFT	ISKPPGVAL
FILPVLGAV	FLTKRGRQV	GERGFFYT	GTADVHFER	IIMFDVTSR	ISSVLAGASCPA
FINDEIFVEL	FLTKRSGQV	GEVDVEQHTL	GTATLRLVK	IISAVVGIL	ISTQQQATFLL
FIQVYEVERA	FLTKRSGQVCA	GFKQSSKAL	GTMDCTHPL	IITEVITRL	ITARPVLW
FKNIVTPRT	FLTKRSRQV	GIMAIELAEL	GTMDCTHSL	ILAKFLHWL	ITDFGLAKL
FLAELAYDL	FLTPKKLQCV	GIPPAPHGV	GTSSVIVSR	ILAKFLHWLe	ITDFGLARL
FLAKLNNTV	FLTPLRNFL	GIPPAPRGV	GTWESNANV	ILAVDGVLSV	ITDQVPFSV
FLALIICNA	FLTSGTQFSDA	GIVEQCCTSI	GTYEGLLRR	ILDEKPVII	ITKKVADLVGF
FLAPAKAVV	FLWGPRALA	GLAPPQHLIRV	GVALQTMKQ	ILDFGLAKL	ITQPGPLAPL
FLAPAKAVVYV	FLWGPRALV	GLASFKSFLK	GVFIQVYEV	ILDKKVEKV	ITQPGPLVPL
FLASESLIKQI	FLWGPRAYA	GLCEREDLL	GVLVGVALI	ILDKVLVHL	IVDCLTEMY
FLDEFMEGV	FLWSVFMLI	GLEALVPLAV	GVNPVVSYAV	ILDSSEEDK	IVDSLTEMY
FLDRFLSCM	FLWSVFWLI	GLEKIEKQL	GVRGRVEEI	ILDTAGREEY	IYMDGTADFSF
FLEGNEVGKTY	FLYDDNQRV	GLFDEYLEMV	GVYDGREHTV	ILFGISLREV	KAFLTQLDEL
FLFAVGFYL	FLYGALLLA	GLFGDIYLA	GYCASLFAIL	ILGALLSIL	KAFQDVLYV
FLFDGSPTY	FLYTLLREV	GLGLPKLYL	GYDQIMPKI	ILHNGAYSL	KAKQDLARL
FLFLLFFWL	FMHNRLQYSL	GLGNRWTSRT	GYDQIMPKK	ILIDWLVQV	KALRLSASALF
FLGMESCGI	FMNKFIYEI	GLGPVAAV	HAIPHYVTM	ILKDFSILL	KASEKIFYV
FLGYLILGV	FMTRKLWDL	GLIEKNIEL	HIAGSLAVV	ILLEAPTGLA	KAYGASKTFGK
FLHHLIAEIH	FMTSSWWGA	GLKAGVIAV	HLCGSHLVEA	ILLEAPTGLV	KCDICTDEY
FLIIWQNTM	FMTSSWWRA	GLLDKAVSNV	HLFGYSWYK	ILLRDAGLV	KCQEVLAWL
FLIVLSVAL	FMTSSWWRAPL	GLLDQVAAL	HLLTSPKPSL	ILLWAARYD	KEADPTGHSY
FLLDILGAT	FMVEDETVL	GLLETTVQKV	HLSTAFARV	ILMEHIHKL	KEAGNINTSL
FLLENAAYL	FMVELVEGA	GLLGQEGLVEI	HLSYHRLLPL	ILMEHIHKLK	KECVLHDDL
FLLENAAYLD	FPALRFVEV	GLLQVHHSCPL	HLSYHWLLPL	ILMEHIHKLKA	KECVLRDDL
FLLFIFKVA	FPSDSWCYF	GLMDVQIPT	HLVEALYLV	ILMHCQTTL	KEFEDDIINW
FLLGLIFLL	FPYGTTVTY	GLPAGAAAQA	HLWVKNMFL	ILNAMIAKI	KEFEDGIINW
FLLKAEVQKL	FQRQGQTAL	GLPGQEGLVEI	HLWVKNVFL	ILPLHGPEA	KEFKRIVQR
FLLKLTPLL	FRSGLDSYV	GLPPDVQRV	HLYQGCQVV	ILSAHVATA	KEFTVSGNILTI
FLLQMMQICL	FSIDSPDSL	GLPPDVQRVh	HMYHSLYLK	ILSLELMKL	KELEGILLL
FLLQMMQVCL	FSYMGPSQRPL	GLPPPPPLL	HPLVFHTNR	ILTVILGVL	KELPSLHVL
FLLSLFSLWL	FTHNEYKFYV	GLQHWVPEL	HPRQEQIAL	ILVLASTITI	KEPSEIVEL
FLMLVGGSTL	FTWAGKAVL	GLQLGVQAV	HPRYFNQLST	ILYENNVITV	KEWMPVTKL
FLMSSWWPNL	FTWAGQAVL	GLREDLLSL	HQILKGGSGTY	ILYENNVIV	KFHRVIKDF
FLNQTDETL	FTWEGLYNV	GLREREDLL	HRWCIPWQRL	IMAIELAEL	KFLDALISL
FLPATLTMV	FVEHDDESPGL	GLRRVLDEL	HSATGFKQSSK	IMDQVPFSV	KGSGKMKTE
FLPEFGISSA	FVEHDLYCTL	GLSPNLNRFL	HSSSHWLRLP	IMFDVTSRV	KIADPICTFI
FLPETEPPEI	FVFLRNFSL	GLSTILLYH	HSWITRSEA	IMIGVLVGV	KIDEKTAELK

(Table 4.1 continued)

KIFDEILVNA	KLQELNYNL	KTWDQVPFS	LLDGTATLRL	LLMPAGVPL	LMLGEFLKL
KIFGSLAFL	KLQQKEEQL	KTWDQVPFSV	LLDKAVSNVI	LLMPAGVPLT	LMLQNALTTM
KIFSEVTLK	KLQVFLIVL	KTWDQVPFSVSV	LLDRFLATV	LLMWITQCF	LMVLMLAAL
KILDAVVAQK	KLSEGDLLA	KTWGQYWQ	LLDTNYNLF	LLNAFTVTV	LMWAKIGPV
KINKNPKYK	KLSEQESLL	KTWGQYWQV	LLDTNYNLFY	LLNATIAEV	LNIDLLWSV
KIQEILTQV	KLTQINFNM	KVAELVHFL	LLDVAPLSL	LLNLPDKMFL	LNIYEKDDKL
KIQRNLRTL	KLVERLGAA	KVAELVRFL	LLDVPTAAV	LLNLPVWVL	LNLPDKMFL
KIWEELSVLE	KLVMSQANV	KVFGSLAFV	LLEAPTGLV	LLNQPDKMFL	LPAVVGLSPGEC
KIWEELSVLEV	KLVVVGAVGV	KVHPVIWSL	LLEEMFLTV	LLPENNVLSPV	LPGEVFAI
KIYSENLKL	KLYSENLKL	KVIDQQNGL	LLESAFPGGL	LLPPLLEHL	LPHAPGVQM
KIYSENLKLA	KLYSENLKLA	KVLEFLAKL	LLFETVMCDT	LLQAEAPRL	LPHNHTDL
KIYSENLTL	KLYSENLTL	KVLEHVVRV	LLFGLALIEV	LLQDSVDFSL	LPHSEITTL
KIYSENLTLA	KLYSENLTLA	KVLEYVIKV	LLFLLQMMQI	LLQEEEEEL	LPHSSSHWL
KLADQYPHL	KMAAFPETL	KVLHELFGMDI	LLFLLQMMQV	LLQEYNWEL	LPLLALLAL
KLAEAERVGLHK	KMAELVHFL	KVNIVPVIAK	LLFPYILPPKA	LLQGWVMYV	LPMEVEKNSTL
KLAKPLSSL	KMDAEHPEL	KVSAVTLAY	LLFSFAQAV	LLQLGYSGRL	LPPPPPLLDL
KLATAQFKI	KMFVKGAPDSV	KVVEFLAML	LLGATCMFV	LLQLYSGRL	LPQKKSNAL
KLCKVRKITV	KMFVKGAPESV	KYDCFLHPF	LLGCPVPLGV	LLQMMQICL	LPRWPPPQL
KLCPVQLWV	KMISAIPTL	KYIQESQAL	LLGDLFGV	LLQMMQVCL	LPSSADVEF
KLDETGNSL	KMLDHEYTT	KYLATASTM	LLGNCLPTV	LLQVHHSCPL	LQSRGYSSL
KLDETGNSLK	KMLKSFLKA	KYLKLSSSEL	LLGPGRPYR	LLRGYHQDAY	LRAGRSRRL
KLDETGNSLKV	KMNVFDTNL	KYVGIEREM	LLGPTVML	LLSAEVQQHL	LRRYLENGK
KLDVGNAEV	KMQASIEKA	LAALPHSCL	LLGRFELIGI	LLSAVLPSV	LSIGTGRAM
KLEGLEDAL	KMRRDLEEA	LAAQERRVPR	LLGRNSFEV	LLSDDDVVV	LSRLSNRLL
KLFGSLAFV	KMVELVHFL	LALWGPDPAA	LLHVHHSCPL	LLSDEDVAL	LTLGEFLK
KLFGVLRLK	KMYAFTLES	LAMPFATPM	LLIADNPQL	LLSDEDVALM	LTLGEFLKL
KLGDCIWTYL	KMYAFTLESV	LAPAKAVVYV	LLIDLTSFL	LLSDEDVALMV	LTLTTGEWAV
KLGDCIWTYLS	KNKRILMEH	LASEKVYTI	LLIDLTSFLL	LLSDEDVEL	LTYNDFINK
KLGDCIWTYPS	KPIVVLHGY	LATEKSRWS	LLIGATIQV	LLSDEDVELM	LTYVSFRNL
KLIETYFSK	KPQQKGLRL	LATEKSRWSG	LLIGATIQVT	LLSDEDVELMV	LVALLACLTV
KLIGDPNLEFV	KPRQSSPQL	LAVDGVLSV	LLIGATMQV	LLSETVMCDT	LVALLVCLTV
KLIKDGLIIRK	KPSGATEPI	LCGSHLVEAL	LLIGATMQVT	LLSGQPASA	LVCGERGFFY
KLKHYGPGWV	KPSPPYFGL	LDKVRALEE	LLIGGFAGL	LLSHGAVIEV	LVFGIELMEV
KLLDISELDMV	KQDFSVPQL	LEEKKGNYV	LLIKKLPRV	LLSILCIWV	LVFLAPAKAVV
KLLEYIEEI	KQDNSTYIMRV	LEEYNSHQSL	LLLDDLLVSI	LLSLFSLWL	LVHFLLLKY
KLLGPHVEGL	KQLPEEKQPLL	LEKQLIEL	LLLEAVPAV	LLSPLHCWA	LVLKRCLLH
KLLGPHVLGV	KQPAIMPGQSY	LGYGFVNYI	LLLELAGVTHV	LLSPLHCWAV	LVMAPRTVL
KLLMVLMLA	KQSSKALQR	LGYGFVNYV	LLLGIGILV	LLSSGAFSA	LVQENYLEY
KLLQIQLCA	KRIQEIIEQ	LHHAFVDSIF	LLLGPLGPL	LLTSRLRFI	LVVVGAVGV
KLLQIQLCAKV	KRTLKIPAM	LIAHNQVRQV	LLLGTIHAL	LLTTLSNRV	LWMRLLPLL
KLLQIQLRA	KSEMNVNMKY	LIFDLGGGT	LLLHCPSKTV	LLVALAIGCV	LYATVIHDI
KLLQIQLRAKV	KSLNYSGVK	LIFDLGGGTFD	LLLLDVAPL	LLVSEIDWL	LYAWEPSFL
KLLSSGAFSA	KSMNANTITK	LIYDSSLCDL	LLLLTVLTV	LLWWIAVGPV	LYLVCGERGF
KLMPPDRTAV	KTCPVQLWV	LIYRRRLMK	LLLPAEVQQHL	LLYKLADLI	LYSACFWWL
KLMSPKLYVW	KTIHLTLKV	LKLSGVVRL	LLLPALAGA	LMAGCIQEA	LYSDPADYF
KLNVPATFML	KTLGKLWRL	LLAAVAALL	LLLPGPSAA	LMALPPCHAL	LYVDSLFFL
KLPNSVLGR	KTLTSVFQK	LLAGIGTVPI	LLLRSPAGV	LMASSPTSI	LYVDSLFFLc
KLQAPVQEL	KTPFVSPLL	LLAGPPGV	LLLSAEVQQHL	LMETHLSSK	MALENNYEV
KLQATVQEL	KTVDLILEL	LLASSMSSQL	LLMEGVPKSL	LMFWSPSHSCA	MAQKRIHAL
KLQEELNKV	KTVNELQNL	LLDDSLVSI	LLMEKEDYHSL	LMGDKSENV	MAVPPCCIGV

(Table 4.1 continued)

MEGEVWGL	NLFDTAEVYA	PLTSIISAV	RAPPTTPAL	RLLYPDYQI	RTFHHGVRV
MEIFIEVFSHF	NLFDTAEVYAA	PPSACSPRF	RASHPIVQK	RLMKQDFSV	RTGEVKWSV
MEKEDYHSL	NLFETPVEA	PTLDKVLEL	RAYQQALSR	RLNAALREK	RTIAPIIGR
MEVDPIGHLY	NLFLFLFAV	PTLDKVLEV	RCHELTVSL	RLPRIFCSC	RTIPTPLQPL
MFPEVKEKG	NLIKLAQKV	QCSGNFMGF	RELEETNQKL	RLQGISPKI	RTKQLYPEW
MGNIDSINCK	NLKLKLHSF	QFITSTNTF	REPVTKAEML	RLQREWHTL	RTLAEIAKV
MIAVFLPIV	NLLDSLEQYI	QGQHFLQKV	REQFLGALDL	RLQTPMQVGL	RTLDKVLEV
MIHDLCLAFPA	NLLEREFGA	QIAKGMSYL	RESEEESVSL	RLQVPVEAV	RTNWPNTGK
MIHDLCLVFL	NLLGRFELI	QIEGLKEEL	RFEEKHAYF	RLRAPEVFL	RTTEINFKV
MIMQGGFSV	NLLGRFELIGI	QILKGGSGT	RFKMFPEVK	RLRPLCCTA	RVFQGFFTGR
MLAVISCAV	NLPDKMFLPGA	QILPLHGPEA	RIAECILGM	RLSCPSPRA	RVHAYIISY
MLGDPVPTPT	NLQGSPVYV	QIRPIFSNR	RIDITLSSV	RLSCSSPRA	RVKAPNKSL
MLGTHTMEV	NLSALGIFST	QLARQQVHV	RIGQRQETV	RLSSCVPVA	RVLRQEVAAPL
MLLAVLYCL	NLSSAEVVV	QLCAKVPLL	RIKDFLRNL	RLTSTNPTM	RVLRQEVEAPL
MLLDKNIPI	NLVRDDGSAV	QLCPICRAPV	RILGPGLNK	RLTSTNPTT	RVPGVAPTL
MLLKTSEFL	NLWDLTDASVV	QLEERTWLL	RILMEHIHKLK	RLVDDFLLV	RVQEAVESMVK
MLLSVPLLLG	NLYPFVKTV	QLFEDNYAL	RINEFSISSF	RLVELAGQSLLK	RVRFFFPSL
MLMAQEALAFL	NMQDLVEDL	QLFNHTMFI	RIVQRIKDF	RLWQELSD	RVSLPTSPR
MLPSQPTLL	NMVAKVDEV	QLFNKHTMFI	RLAEYQAYI	RLWTTTRPRV	RVTSIRLFEV
MLTNSCVKL	NPATPASKL	QLGPTCLSSL	RLARLALVL	RLYDEKQQHI	RVWDLPGVLK
MLVGGSTLCV	NPIVVFHGY	QLGPVGGVF	RLASFYDWLP	RLYDEKQQHIVY	RWPSCQKKF
MLWSCTFCRI	NPKAFFSVL	QLGRISLLL	RLASSVLRCGK	RLYEMILKR	RYAMTVWYF
MLWSCTFCRM	NSELSCQLY	QLIMPGQEA	RLASYLDKV	RLYPWGVVEV	RYCNLEGPPI
MLYYPSVSR	NSQPVWLCL	QLLALLPSL	RLDFNLIRV	RMFPNAPYL	RYGSFSVTL
MMKMMCIKDL	NTDSPLRY	QLLDGFMITL	RLDQLLRHV	RMLPHAPGV	RYMPPAHRNF
MMLPSQPTL	NTYASPRFK	QLLDQVEQI	RLFAFVRFT	RMMEYGTTMV	RYQLDPKFI
MMLPSQPTLL	NTYASPRFKf	QLLIKAVNL	RLFFYRKSV	RMMLPSQPTL	RYQQWMERF
MMLPSQPTLLT	NVIRDAVTY	QLLKLNVPA	RLFVGSIPK	RMPEAAPPV	SACDVSVRV
MMLPSRPTL	NVLHFFNAPL	QLLNSVLTL	RLGGAALPRV	RMTDQEAIQ	SACDVSVRVV
MMLPSRPTLL	NVMPVLDQSV	QLMAFNHLV	RLGLQVRKNK	RMTDQEAIQDL	SAFPTTINF
MMLPSRPTLLT	NYARTEDFF	QLQGLQHNA	RLGNSLLLK	RNGYRALMDKS	SAGPPSLRK
MMQICLHHL	NYKHCFPEI	QLSLLMWIT	RLGPTLMCL	RPHVPESAF	SASVQRADTSL
MMQVCLHHL	NYKRCFPVI	QLSSGVSEIRH	RLGPVARTRV	RPKSNIVL	SAWISKPPGV
MMSEGGPPGA	NYNNFYRFL	QLVFGIEVV	RLIDLGVGL	RPKSNIVLL	SAYGEPRKL
MMYKDILLL	NYSVRYRPGL	QLVIQCEPL	RLIGDAAKNQV	RQAGDFHQV	SEHLDTQKELL
MPFATPMEA	PAFSYSFFV	QLYALPCVL	RLLASLQDL	RQFVTQLY	SEIWRDIDF
MPFATPMEAEL	PLADLSPFA	QMFFCFKEL	RLLCALTSL	RQKKIRIQL	SEIWRDIDFd
MPGEATETV	PLALEGSLQK	QMMQICLHHL	RLLDLAQEGL	RQKRILVNL	SELFRSGLDSY
MQLIYDSSL	PLDGGVAAA	QMMQVCLHHL	RLLIKKLPRV	RQLAQEQFFL	SESIKKKVL
MSLQRQFLR	PLFDFSWLSL	QQITKTEV	RLLKEYQEL	RQVGDFHQV	SESLKMIF
MTSALPIIQK	PLFQVPEPV	QQLDSKFLEQV	RLLPLLALL	RRFFPYYV	SFSYTLLSL
MTVDSLVNK	PLHCWAVLL	QRPYGYDQIM	RLLPLLALLAL	RRKWRRWHL	SGMGSTVSK
MVIGIPVYV	PLHCWVVLL	QVFPGLLERV	RLLPLWAAL	RRQRRSRRL	SHETVIIEL
MVKISGGPR	PLLALLALWG	QVLDLRLPSGV	RLLPLWAALPL	RRRWHRWRL	SHLVEALYLV
MVWESGCTV	PLLENVISK	QYSWFVNGTF	RLLQETELV	RSCGLFQKL	SIFDGRVVAK
MVYDLYKTL	PLPEAPLSL	RAGLQVRKNK	RLLSDEDVAL	RSDSGQQARY	SIFTWAGKAVL
MYIFPVHWQF	PLPPARNGGL	RALAETSYV	RLLSDEDVALM	RSKFRQIV	SIFTWAGQAVL
NCLKLLESL	PLPPARNGGLg	RALAKLLPL	RLLSDEDVEL	RSRRVLYPR	SILEDPPSI
NLAQDLATV	PLQPEQLQV	RALEEANADLEV	RLLSDEDVELM	RSYHLQIVTK	SIQNYHPFA
NLATYMNSI	PLTEYIQPV	RALRLTAFASL	RLLVPTQFV	RSYVPLAHR	SISVLISAL

(Table 4.1 continued)

SIVKIQSWFRM	SLMSWSAIL	SQGFSHSQM	THFPDETEI	TMTRVLQGV	VLHDDLLE
SLAAGVKLL	SLNYSGVKEL	SQKTYQGSY	TIADFWQMV	TPGNRAISL	VLHDDLLEA
SLAAYIPRL	SLPGGTAS	SQLTTLSFY	TIHDSIQYV	TPNQRQNVC	VLHELFGMDI
SLADEAEVYL	SLPKHSVTI	SQQAQLAAA	TILLGIFFL	TPRLPSSADVEF	VLHWDPETV
SLADTNSLAV	SLPPPGTRV	SRASRALRL	TIMIHDLCLA	TPRTPPPQ	VLLESAFPGGL
SLADTNSLAVV	SLPRGTSTPK	SRDSRGKPGY	TINPQVSKT	TQPGPLAPL	VLLESAFPGRL
SLAMLDLLHV	SLQALKVTV	SRFGGAVVR	TIPTPLQPL	TQPGPLVPL	VLLGMEGSV
SLASLLPHV	SLQDVPLAAL	SRFTYTALK	TIRYPDPVI	TRPWSGPYIL	VLLLVLAGV
SLAVVSTQL	SLQEEIAFL	SSADVEFCL	TLADFDPRV	TRVLAMAIY	VLLQAGSLHA
SLCPWSWRAA	SLQEKVAKA	SSDNYEHWLY	TLAKYLMEL	TSALPIIQK	VLLRHSKNV
SLDDYNHLV	SLQKRGIVEQ	SSDYVIPIGTY	TLDEKVAELV	TSDQLGYSY	VLMIKALEL
SLDDYNHLVTL	SLQPLALEG	SSFGRGFFK	TLDSQVMSL	TSEHSHFSL	VLNSLASLL
SLDKDIVAL	SLQRMVQEL	SSKALQRPV	TLDWLLQTPK	TSEKRPFMCAY	VLNSVASLL
SLEEEIRFL	SLQRTVQEL	SSLSLFFRK	TLEEITGYL	TSTTSLELD	VLPDVFIRC
SLEENIVIL	SLQSMVQEL	SSPGCQPPA	TLEGFASPL	TTINYTLWR	VLPDVFIRCV
SLFEGIDIYT	SLQSTVQEL	SSSGLHPPK	TLGEFLKL	TTLITNLSSV	VLPDVFIRCV
SLFEGVDFYT	SLRILYMTL	SSVPGVRLL	TLITDGMRSV	TTNAIDELK	VLQELNVTV
SLFGKLQLQL	SLSKILDTV	STALRLTAF	TLKCDCEIL	TVASRLGPV	VLQVGLPAL
SLFLGILSV	SLSPLQAEL	STAPPAHGV	TLKKYFIPV	TVFDAKRLIGR	VLQWLPDNRL
SLFPNSPKWTSK	SLSRFSWGA	STAPPVHNV	TLLASSMSSQL	TVSGNILTIR	VLQWLSDNRL
SLFRAVITK	SLVEELKKV	STDPQHHAY	TLLIGATIQV	TYACFVSNL	VLRDDLLEA
SLFVSNHAY	SLWGGDVVL	STIKFQMKK	TLLIGATIQVT	TYLPTNASL	VLRENTSPK
SLGEQQYSV	SLWSSSPMA	STLCQVEPV	TLLIGATMQV	TYSEKTTLF	VLRKEEEKL
SLGIMAIEL	SLWSSSPMAT	STLQGLTSV	TLLIGATMQVT	VAANIVLTV	VLRQEVAAPL
SLGSPVLGL	SLWSSSPMATT	STMPHTSGMNR	TLLLEGVMAA	VAELVHFLL	VLSVNVPDV
SLGWLFLLL	SLYHVYEVNL	STPPPGATRV	TLLNLPDKMFL	VAVKAPGFGD	VLTSESMHV
SLIAAAAFCLA	SLYKFSPFPL	STSQEIHSATK	TLLNQPDKMFL	VCGERGFFYT	VLVEGSTRI
SLIKQIPRI	SLYQLENYC	STVASRLGPV	TLLPATMNI	VCLHHLPFWI	VLVPPLPSL
SLKLLESLTPI	SLYSFPEPEA	STVASWLGPV	TLLSNIQGV	VEETPGWPTTL	VLWDRTFSL
SLLDRFLATV	SMCRFSPLTL	SVAQQLLNGK	TLMSAMTNL	VEGSGELFRW	VLYGPDAPTV
SLLGLALLAV	SMLIRNNFL	SVASLLPHV	TLPGYPPHV	VEIEERGVKL	VLYPRVVRR
SLLGQLSGQV	SMPPPGTRV	SVASTITGV	TLPPAWQPFL	VFLPCDSWNL	VLYRYGSFSV
SLLKFLAKV	SMPQGTFPV	SVGSVLLTV	TLPPRPDHI	VIMPCSWWV	VLYRYGSFSVTL
SLLLELEEV	SMSKEAVAI	SVHSLHIWSL	TLRTGEVKWSV	VISNDVCAQV	VMALENNYEV
SLLMWITQA	SMSSQLGRISL	SVKPASSSF	TLSSRVCCRT	VIVMLTPLV	VMIIVSSLAV
SLLMWITQC	SNDGPTLI	SVPQLPHSSSHW	TLTNIAMRPGL	VIWEVLNAV	VMLDKQKEL
SLLMWITQCFL	SPASSRTDL	SVQGIIIYR	TLTTGEWAV	VLAGGFFLL	VMNILLQYV
SLLNLPVWV	SPAVDKAQAEL	SVSPVVHVR	TLWVDPYEV	VLAGVGFFI	VMNILLQYVV
SLLNLPVWVLM	SPGSGFWSF	SVVKIQSWFRM	TLYEAVREV	VLASIEAEL	VPGWGIALL
SLLPAIVEL	SPHPVTALL	SVYDFFVWL	TLYNPERTITV	VLASIEAELPM	VPLDCVLYRY
SLLQHLIGL	SPLFQRSSL	SYLDKVRA	TMASTSVSRSA	VLASIEPEL	VPRSAATTL
SLLQSREYSSL	SPQNLRNTL	SYLDSGIHF	TMESMNGGKLY	VLASIEPELPM	VPYGSFKHV
SLLQSRGYSSL	SPRFSPITI	SYRNEIAYL	TMGGYCGYL	VLCSIDWFM	VRIGHLYIL
SLLSGDWVL	SPRPPLGSSL	SYTRLFLIL	TMHSLTIQM	VLDFRLPSGV	VRLGSLSTK
SLLSLPVWV	SPRWWPTCL	TALRLTAFASL	TMKIYSENLTL	VLDGLDVLL	VRSRRCLRL
SLLSLPVWVLM	SPSKAFASL	TCQPTCRSL	TMKLYSENLTL	VLEGMEVV	VSDFGGRSL
SLLSPLHCWA	SPSSNRIRNT	TEAASRYNL	TMLARLASA	VLFGLGFAI	VSLLSLPVWV
SLLSPLHCWAV	SPSVDKARAEL	TETEAIHVF	TMLGRRAPI	VLFSSDFRI	VTLLIGATIQV
SLLTSSKGQLQK	SPTSSRTSSL	TFDYLRSVL	TMLGRRPPI	VLFYLGQY	VTLLIGATMQV
SLMASSPTSI	SQFGGGSQY	TFPDLESEF	TMNGSKSPV	VLFYLGQYI	VTTDIQVKV

(Table 4.1 continued)

VVEGTAYGL	YLDPAQQNL	YVDPVITSI
VVHFFKNIV	YLEPGPVTA	YVFTLLVSL
VVLGVVFGI	YLEYRQVPV	YVIPIGTYGQM
VVMSWAPPV	YLFSEEITSG	YYNAFHWAI
VVMVNQGLTK	YLGSYGFRL	YYSVRDTLL
VVPCEPPEV	YLIELIDRV	YYWPRPRRY
VVPEDYWGV	YLLKPVQRI	RVASPTSGVK
VVQNFAKEFV	YLLLRVLNI	
VVTGVLVYL	YLLPAIVHI	
VVVGAVGVG	YLLPEAEEI	
VYDFFVWLHY	YLLQGMIAAV	
VYDYNCHVDL	YLMDTSGKV	
VYFFLPDHL	YLNDHLEPWI	
VYGIRLEHF	YLNKEIEEA	
VYLDKFIRL	YLQGMIAAV	
VYSDADIFL	YLQLVFGIEV	
VYVKGLLAKI	YLQQNTHTL	
WATLPLLCAR	YLSGANLNL	
WGPDPAAA	YLSGANLNLG	
WLDEVKQAL	YLSGANLNV	
WLDPNETNEI	YLVGNVCIL	
WLEYYNLER	YLVPQQGFFC	
WLLPLWAAL	YLYDRLLRI	
WLLPLWAALPL	YLYGQTTTY	
WLPFGFILI	YMDGTMSQV	
WLPKILGEV	YMFDVTSRV	
WLQYFPNPV	YMFPNAPYL	
WLSLKTLLSL	YMIAHITGL	
WLSLLFKKL	YMIDPSGVSY	
WMRLLPLLAL	YMIMVKCWMI	
WQYFFPVIF	YMIPSIRNSI	
WYEGLDHAL	YMMPVNSEV	
WYQTKYEEL	YMNGTMSQV	
YAVDRAITH	YMNSIRLYA	
YEDIHGTLHL	YPFKPPKV	
YEGSPIKVTL	YQGSYGFRL	
YGHSGQASGLY	YQLDPKFIV	
YGYDNVKEY	YRPRPRRY	
YIDEQFERY	YRYGSFSVTL	
YIFAVLLVCV	YSDHQPSGPYY	
YIGEVLVSV	YSLEYFQFV	
YLAMPFATPME	YSLKLIKRL	
YLAPENGYL	YSWMDISCWI	
YLCDKVIPG	YTCPLCRAPV	
YLCDKVVPG	YTDFHCQYV	
YLCSGSSYF	YTDFVGEGL	
YLCSGSSYFV	YTDQPSTSQIAY	
YLDLFGDPSV	YTLDRDSLYV	
YLDLLFQIL	YTMKEVLFY	
YLDLLFQILL	YVDFREYEYY	

Table 4.2: Custom library of tumor associated antigen source proteins.

ABCA1	BING4	CLTC	DUSP22	GNTK	IMP3
ABCA6	BIRC5	CLYBL	EEF2	GPC3	INPP5D
ABCC3	BIRC7	CML28	EFTUD2	GPCPD1	INS
ABCD3	BIRC8	CNMD	EGFR	GPNMB	INSM2
ABL1	BIRC9	COA1	EHD2	GPR143	INTS11
ACPP	BRAF	COL2A1	EIF2S3	HAO2	INTS13
ACRBP	BST2	COL4A3	EIF3D	HAUS3	IQGAP2
ACTB	BTBD2	COL6A2	ELAC2	HBD	IRS2
ACTN4	BTG1	CORO1A	ELAVL1	HCG	ITGAL
ADAM17	BTK	COX2	ELAVL4	HDAC1	ITGAM
ADAMTSL5	C18orf21	CPSF	EML6	HDGF	ITGB2
ADRP	C2CD4A	CPSF1	ENAH	HEPACAM	ITGB8
AFP	C5	CPVL	EPCAM	HHAT	KAAG1
AIM2	CA9	CR2	EPHA2	HIFPH3	KCNAB1
AIMP1	CACNG	CRABP1	ERAP1	HIST4H4	KDM2B
AKAP13	CADH3	CRNKL1	ERBB2	HIVEP1	KDM5B
ALDH1A1	CALCA	CSAG2	ERVK3-1	HLA-A	KDM5C
ALDOA	CALR	CSF1	ETV5	HLA-B	KDM5D
ALK	CAMP	CSF3R	EVI2B	HLA-DOB	KDR
ALYREF	CASP5	CSNK1A1	EZH2	HLA-DPA1	KIAA1551
AML1	CASP8	CSPG4	EZR	HMMR	KIF20A
AMZ2	CCDC110	CT83	FAM136A	HMOX1	KLK10
ANKRD30A	CCL3	CTAG1A	FASN	HMSD	KLK3
ANO7	CCL3L1	CTDP1	FBXW11	HNF4G	KLK4
ANXA1	CCLA2	CTNNB1	FCER1A	HNRNPL	KRAS
APOBEC3H	CCNA1	CTPS1	FDPS	HNRNPLL	KRI1
ARF1	CCNB1	CTSH	FGF5	HNRNPR	KRT16
ARHGAP15	CCND1	CYP1B1	FGF6	HOXD3	KRT18
ARHGAP25	CCNI	CYP21A2	FLT3	HPN	KRT6C
ARHGAP4	CD19	CYP2A6	FLT3LG	HPSE	KTN1
ARHGAP45	CD274	CYP2A7	FMOD	HSDL1	LAGE1
ARL4D	CD33	CYP2C8	FMR1NB	HSP90AB1	LAGE3
ART4	CD48	CYP2C9	FNDC3B	HSPA1A	LAS1L
ART5	CD69	CYP2D6	FOLH1	HSPA1B	LCK
ASH1L	CD79B	CYPB	FOXO1	HSPA1L	LCP2
ATIC	CDC5L	DAPK2	G3BP1	HSPA6	LGALS1
ATP2A3	CDCA7L	DCT	G6PC2	HSPB1	LGALS3BP
ATXN10	CDH13	DDX21	GAD2	HSPD1	LGSN
B2A2	CDK12	DDX3Y	GAGE1	ICAM3	LPGAT1
B3A2	CDK4	DDX5	GAS7	ICE	LRMP
BA46	CDKN1A	DKK1	GATA2	IDNK	LRRC8A
BAD	CDKN2A	DLAT	GC	IDO1	LTB
BAGE1	CDR2	DMD	GCGR	IER3	LY6K
BCAP31	CEACAM5	DMXL1	GEMIN4	IFG2BP3	LYN
BCHE	CELF6	DNAJC2	GFAP	IFI30	MAG
BCL2	CELSR1	DNMBP	GINS1	IFI6	MAGEA1
BCL2A1	CENPM	DNMT1	GLRX3	IGF2BP2	MAGEA12
BCL2L4	CEP55	DOCK2	GLS	IGF2BP3	MAGEB2
BFAR	CLCA2	DOK2	GNAO1	IL13RA2	MAGEC1
BID	CLP	DSE	GNL3L	IL2RG	MAGEC2

(Table 4.2 continued).

MAGEC2	NELFA	PSMB1	SIRT2	UBE2C
MAGED2	NFYC	PSMB10	SLC25A5	UBE2D2
MAGEE1	NISCH	PTHLH	SLC30A8	UGT2B17
MAGEF1	NLRP5	PTPN11	SLC41A3	UQCR10
MAGEF1	NOB1	PTPN21	SLC45A2	UQCRH
MALL	NONO	PTPRC	SLC45A3	USP11
MAP4K1	NPM1	PTPRN	SLCO2A1	USP9X
MARK3	NQO1	PTTG1IP	SNRNP70	USP9Y
MATN2	NRAS	PUM3	SNRPD1	UTY
MBP	NUDCD1	PWWP3A	SNX14	VEGFA
MC1R	NUF2	PXDN	SOX10	VENTXP1
MCF2	NUF3	RAB38	SP110	VGF
MCM5	NUP210	RAN	SPA17	VIM
MCMBP	NUP37	RASGRF1	SPARC	VIPR1
MDK	OCA2	RASGRP2	SPATA5L1	VPS13B
MDM2	OGT	RASSF10	SSX1	VSIG10L
MDN1	OS9	RBAF600	SSX2	WNK2
ME1	P2RX5	RBBP4	STAT1	WT1
MED23	PAK2	RBL2	STEAP1	XAGE1B
MED24	PARP10	RFA1	SUGT1	XBP1
MET	PARP3	RGS5	SUPT5H	ZFAND5
METTL21A	PASD1	RHOC	SYNGR1	ZFHX3
MFGE8	PAX3	RINT1	TAG1	ZFP36L1
MICA	PAX5	RNF19B	TALDO1	ZFY
MLANA	PCDH11Y	RNF43	TBC1D22A	ZMYM4
MMP2	PCDH20	RPA1	TCHH	ZNF395
MMP7	PDGFRA	RPL10A	TEK	
MOK	PFKM	RPL19	TEP1	
MPL	PGK1	RPS2	TERT	
MRPL19	PHB	RPS4Y1	TG	
MS4A1	PHRF1	RPSA	TGRBR2	
MSCP	PIM1	RUBCNL	THEM6	
MSLN	PLAC1	SAGE1	TMCO1	
MT-ATP6	PLIN2	SART1	TMED4	
MT-CO2	PLP1	SART3	TMSB10	
MTRR	PMEL	SASH1	TMSB4Y	
MUC1	POP1	SCGB2A2	TOP1	
MUC16	PP2A	SCGB2A7	TOP2A	
MUC5AC	PPFIBP1	SCRN1	TP53	
MUM2	PPIB	SEC31A	TP53I11	
MUM3	PPP1R3B	SELL	TPBG	
MYH1	PRAME	SELPLG	TPO	
MYH2	PRDM1	SEPT2	TRIM22	
MYH9	PRDX2	SEPT6	TRIM68	
MYO1G	PRDX5	SERPINB5	TTK	
N4BP2	PRELID1	SF1	TTN	
N4BP2L1	PRKCB	SFMBT1	TYMS	
NACA2	PRTN3	SGT1B	TYR	
NCF4	PSD4	SH3GLB2	TYRP1	
NECTIN4	PSMA3	SIRPD	UBD	

Chapter 5

Developing Antibodies Against Peptide-Orientation Specific Class II MHC-peptide Complexes

Abstract

Class II MHC-peptide complexes, which present peptides derived from extracellular proteins, are preloaded with class II-associated Ii peptide (CLIP). This peptide can be further processed into variants of different length and exchanged back into the peptide binding groove with HLA-DM. Interestingly, it's been shown that different CLIP variants can bind in different orientations. These CLIP MHC-peptide complexes are believed to be presented on the cell surface and may play a role in immunosurveillance of antigen presenting cells and may impact the T cell repertoire. However, current methods to study CLIP presentation and to distinguish variants are limited. Here, we describe the generation of antibodies that can distinguish between different orientated CLIP variants and bind at high affinity. These antibodies will help elucidate the presentation and biological role of variant CLIP MHC-peptide complexes.

Introduction

Unlike class I MHC-peptide complexes, class II present peptides derived from extracellular proteins that are degraded in the lysosome. In order to prevent premature loading of intracellular peptides and potential autoimmune responses, class II MHC molecules are folded in the ER with a standard invariant chain. This folded complex is trafficked to endosomes where this invariant chain is processed, leaving a free-standing peptide known as CLIP. In the endosome, the placeholder CLIP can be exchanged for processed antigenic peptides through HLA-DR catalysis. The resulting MHC-peptide complex can then be shuttled to the surface and displayed to $CD4^+$ T cells for surveillance of antigen presenting cells (APCs)[57].

Despite its role as a placeholder peptide, MHC-peptide complexes containing CLIP are often presented at the surface of APC's. Additionally, it is believed that CLIP presentation levels shape the T cell repertoire and can be influenced by variations in the N-terminal length of CLIP.

Interestingly, recent results have shown a phenomenon in which a shorter variant of CLIP can adopt a reverse orientation in the peptide-binding pocket of HLA-DR1, resulting in a potentially important T cell antigen[171]. Yet it is still unknown what immunological role this "inverted" CLIP MHC-peptide complex plays, if any, or if it is even presented at the surface of cells. Hence, developing tools to measure inverted CLIP presentation levels on antigen presenting cells, and under what contexts, is necessary.

Here, we describe the generation of antibodies that specifically recognize both the "canonical" and "inverted" CLIP HLA-DR1 MHC-peptide complexes. We engineered a covalently linked peptide Fc-fusion construct that was amendable to catch and release phage display selections. Using phage display, we were able to generate 9 Fabs that specifically recognized the canonical CLIP HLA-DR1 MHC-peptide complex and 2 Fabs that were specific to the inverted CLIP complex. Converting top antibodies for each complex into IgG's, Octet analysis revealed our antibodies were able to specifically recognize their respective MHC-peptide complex with subnanomolar affinity. These IgG's will be useful tools in the study of CLIP presentation and antigen presenting cell biology.

Results

In order to engineer HLA-DR1 MHC-peptide complex antigens for phage display, we fused the HLA-DR1 extracellular domain of the alpha subunit to a human IgG1 Fc domain with a TEV protease site in the linker connecting them. The HLA-DR1 extracellular domain beta subunit was co-expressed in a separate construct. Canonical CLIP MHC-peptide complexes additionally had an N-terminal $CLIP_{102\text{-}120}$ fused to the N-terminus of the alpha subunit with a thrombin cleavage site in the linker connecting them. Inverted CLIP MHC-peptide complexes had an N-terminal $CLIP_{106\text{-}120}$ fused to the N-terminus of the beta subunit with the same thrombin cleavage linker.

All HLA-DR1 Fc-fusions contain a C-terminal AviTag to biotinylate and immobilize constructs on streptavidin beads throughout the phage display process (**Figure 5.1A**). After the proteins were expressed and purified, thrombin was used to cut and release the bound peptide to allow for a free peptide in the peptide binding groove and no linker interfering in the peptide epitope (**Figure 5.1B**).

Using a Fab-phage library, we first performed a negative clearance using the opposite HLA-DR1 Fc-fusion than the one we were interested in selecting for, thereby removing any Fab-phage that bound elsewhere on the complex other than the peptide epitope. Taking the remaining phage, we performed a positive selection against the HLA-DR1 Fc-fusion of interest and eluted any bound phage with TEV protease cleavage to be amplified in *E.coli* (**Figure 5.2A & 5.2B**). After multiple rounds of selection, individual phage clones were screened via ELISA to determine specific binding to correct HLA-DR1 MHC-peptide complex. Antibodies that appeared to be specific and have a predicted affinity of <20 nM were carried forward (**Figures 5.2C & 5.2D).** Upon sequencing, we identified 9 unique Fab-phage clones specific to the canonical CLIP HLA-DR1 MHC-peptide complex and 2 unique Fab-phage clones specific to the inverted CLIP HLA-DR1 MHC-peptide complex. Octet analysis revealed many of these Fabs to be specific and to bind with high affinity to their respective MHC-peptide complex (**Figures 5.3 & 5.4**). When top performing Fabs (CCA5 for the canonical complex and ICD5 for the inverted complex) were converted to full length IgG's, affinity was improved to subnanomolar levels and specificity maintained (**Figure 5.5**). Hence, we successfully designed high affinity antibodies that can distinguish between the two different orientations of the CLIP variants. These tools will be important in the study for antigen presenting cells and uncovering the role CLIP MHC-peptide complexes play.

Discussion

CLIP variants of different lengths have been shown to bind to HLA-DR1 in different orientations in the peptide binding pocket of the MHC-peptide complex. Here, we generate antibodies that can specifically recognize two different variants of CLIP: one that adopts a "canonical" orientation and a shorter variant that adopts an "inverted" orientation. While $CLIP_{106\text{-}120}$ has been eluted from antigen presenting cells and identified via mass spectrometry, it is still unclear if the inverted CLIP MHC-peptide complex is generated and presented on the surface of cells[171]. These antibodies can be used not only to determine if this complex is displayed on cells, but what causes differing levels of CLIP presentation. For example, it has been hypothesized that cells with high levels of HLA-DM activity would present increased levels of the inverted CLIP MHC-peptide complex[171]. If so, how this molds T cell repertoires will be important in potentially understanding underlying mechanisms of autoimmunity and class II HLA-associated peptide processing and presentation.

Methods

Cloning

For canonical CLIP HLA-DR1, the covalently linked peptide and alpha subunit were cloned into a pFUSE (InvivoGen) vector with a human IgG1 Fc domain as previously described. The beta subunit chain of HLA-DR1 was cloned into the same vector but lacking the Fc domain. For inverted CLIP HLA-DR1, the covalently linked peptide and beta subunit were cloned into a pFUSE (InvivoGen) vector with a human IgG1 Fc domain as previously described.[26] The alpha subunit chain of HLA-DR1 was cloned into the same vector but lacking the Fc domain. Fabs were subcloned from the Fab-phagemid into an *E. coli* expression vector pBL347. The heavy

chain of the IgG was cloned from the Fab plasmid into a pFUSE (InvivoGen) vector with a murine IgG1 Fc domain. The light chain of the IgG was cloned from the Fab plasmid into the same vector but lacking the murine Fc domain.

Cell Culture

Expi293F-BirA cell lines were from frozen stocks maintained by the Wells lab and cultured in Expi293 growth media (Thermo Scientific). Cells were incubated for 5 days at 37ºC and 8% CO_2.

Protein expression and purification

HLA-DR1 Fc-fusions were expressed and purified from Expi293F-BirA cells using transient transfection (Expifectamine, Thermo Scientific). Enhancers were added 20 hrs after transfection. Cells were incubated in media containing 1 μM biotin for 5 days at 37ºC and 8% CO_2. Media was then harvested by centrifugation at 4,000xg for 20 min. Fc-fusions were purified by Protein A affinity chromatography and buffer exchanged into 50 mM Tris, 10 mM $CaCl_2$ pH 8.0. Purified protein was subsequently processed using an Thrombin CleanCleave™ Kit (Sigma Aldrich) for 4 hours. Immobilized thrombin was removed and cleaved MHC-peptide complex was buffer exchanged into PBS pH 7.4, then stored in 10% glycerol at -80°C and assessed by SDS-PAGE.

Fabs were expressed in E. coli C43 (DE3) Pro+ as previously described using an optimized autoinduction medium and purified by protein A affinity chromatography[50]. Fabs were subsequently buffer exchanged into PBS pH 7.4 and stored in 10% glycerol at -80°C and assessed by SDS-PAGE.

IgGs were expressed and purified from Expi293F-BirA cells using transient transfection (Expifectamine, Thermo Fisher Scientific). Enhancers were added 20 hours after transfection. Cells were incubated for 5 days at 37ºC and 8% CO_2. Media was then harvested by centrifugation at 4,000xg for 20 min. IgGs were purified by Ni-NTA affinity chromatography and buffer exchanged into PBS pH 7.4 and stored in 10% glycerol at -80°C and assessed by SDS-PAGE.

Phage display selection

All phage selections were done according to previously established protocols. Briefly, selections with antibody phage library were performed using biotinylated HLA-DR1 Fc-fusion antigens captured with streptavidin-coated magnetic beads (Promega). Prior to each selection, the phage pool was incubated with 1 μM of the opposing HLA-DR1 Fc-fusion immobilized on streptavidin beads in order to deplete the library of any binders to the beads or Fc-tag. In total, four rounds of selection were performed with decreasing amounts of HLA-DR1 Fc-fusion antigens (100 nM, 50 nM, 10 nM and 10 nM). To reduce the deleterious effects of nonspecific binding phage, we employed a 'catch and release' strategy, where HLA-DR1 Fc-fusion binding Fab-phage were selectively eluted from the magnetic beads by the addition of 50 μg/mL TEV protease. Individual phage clones from the fourth round of selection were analyzed for binding by ELISA.

Fab-phage ELISA

For each phage clone, four different conditions were tested – Direct: HLA-DR1 Fc-fusion of interest, Competition: HLA-DR1 Fc-fusion with an equal concentration of Fc-fusion in solution, Negative selection: Opposing HLA-DR1 Fc-fusion, and Control: PBSTB. 384-well Nunc Maxisorp flat-bottom clear plates (Thermo Fisher Scientific) were coated with 0.5 μg/mL of

NeutrAvidin in PBS overnight at 4°C and subsequently blocked with PBSTB. Plates were washed 3x with PBS containing 0.05% Tween-20 (PBST) and were washed similarly between each of the steps. 20 nM biotinylated HLA-DR1 Fc-fusions were diluted in PBSTB and immobilized on the NeutrAvidin-coated wells for 30 minutes at room temperature, then blocked with PBSTB + 10 μM biotin for 10 minutes. For the competition samples, phage supernatant was diluted 1:5 into PBSTB with 20 nM HLA-DR1 Fc-fusion (same construct as what was immobilized) 30 minutes prior to addition to the plate. For the direct samples, phage supernatant was diluted 1:5 in PBSTB. Competition and direct samples were added to the plate for 30 minutes at room temperature. Bound phage was detected by incubation with anti-M13-horseradish peroxidase conjugate (Sino Biologics, 1:5000) for 30 minutes, followed by the addition of TMB substrate (VWR International). The reaction was quenched with the addition of 1 M phosphoric acid and the absorbance at 450 nm was measured using a Tecan M200 Pro spectrophotometer. Clones with high binding to HLA-DR1 Fc-fusion, low binding to PBSTB/opposing HLA-DR1 Fc-fusion, and competition signal <0.5*direct binding signal were carried forward.

Bio-layer Interferometry

BLI measurements were made using an Octet RED384 (ForteBio) instrument. MHC-peptide complex was immobilized on a streptavidin biosensor and loaded for 200 seconds. After blocking with 10 μM biotin, purified binders in solution were used as the analyte. PBSTB was used for all buffers. Data were analyzed using the ForteBio Octet analysis software and kinetic parameters were determined using a 1:1 monovalent binding model.

Figures and Tables

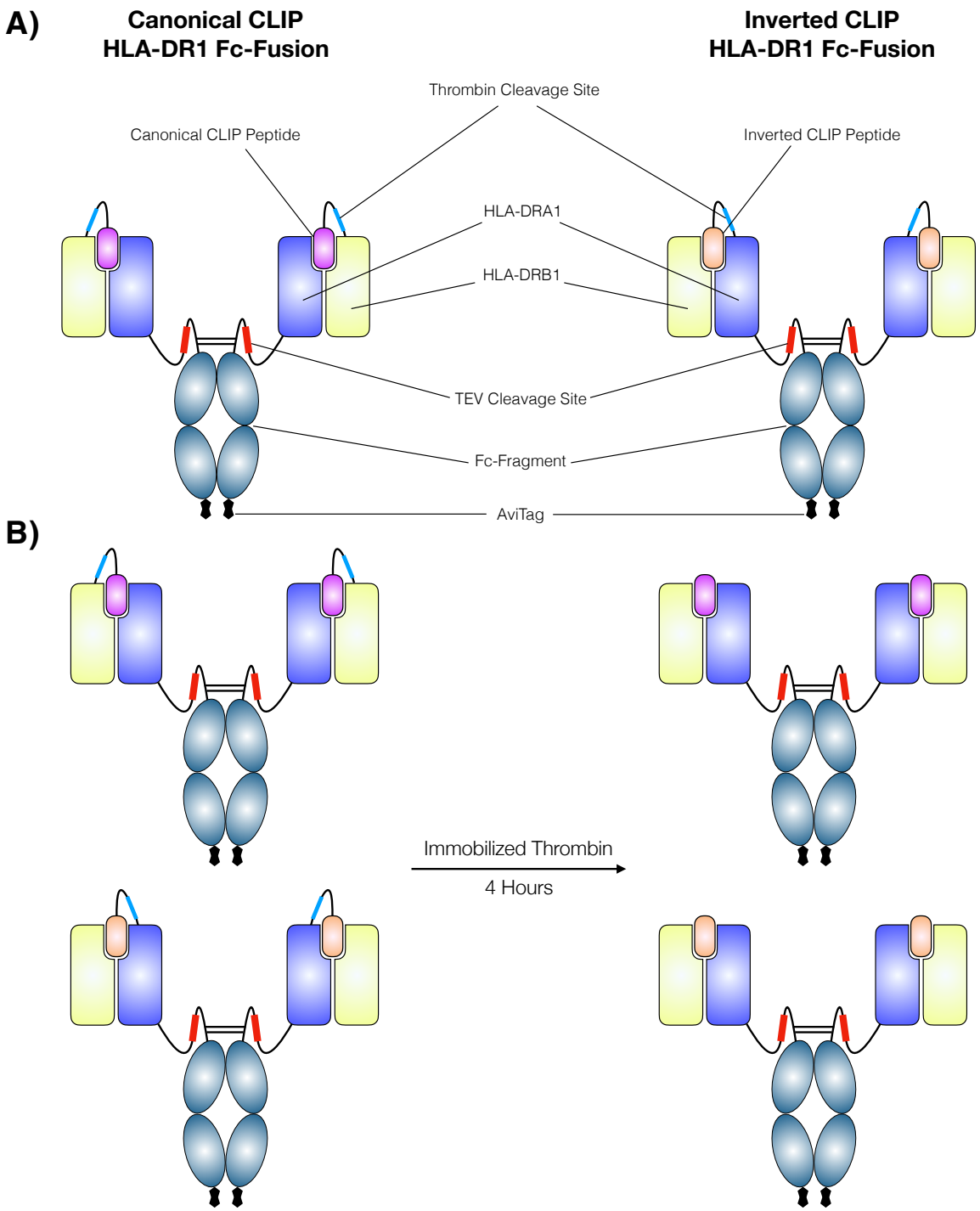

Figure 5.1: Schematic of CLIP HLA-DR1 Fc-fusion constructs. A) Design of CLIP HLA-DR1 MHC-peptide complex constructs for phage display selection. B) Thrombin cleavage of the linker in MHC-peptide complexes.

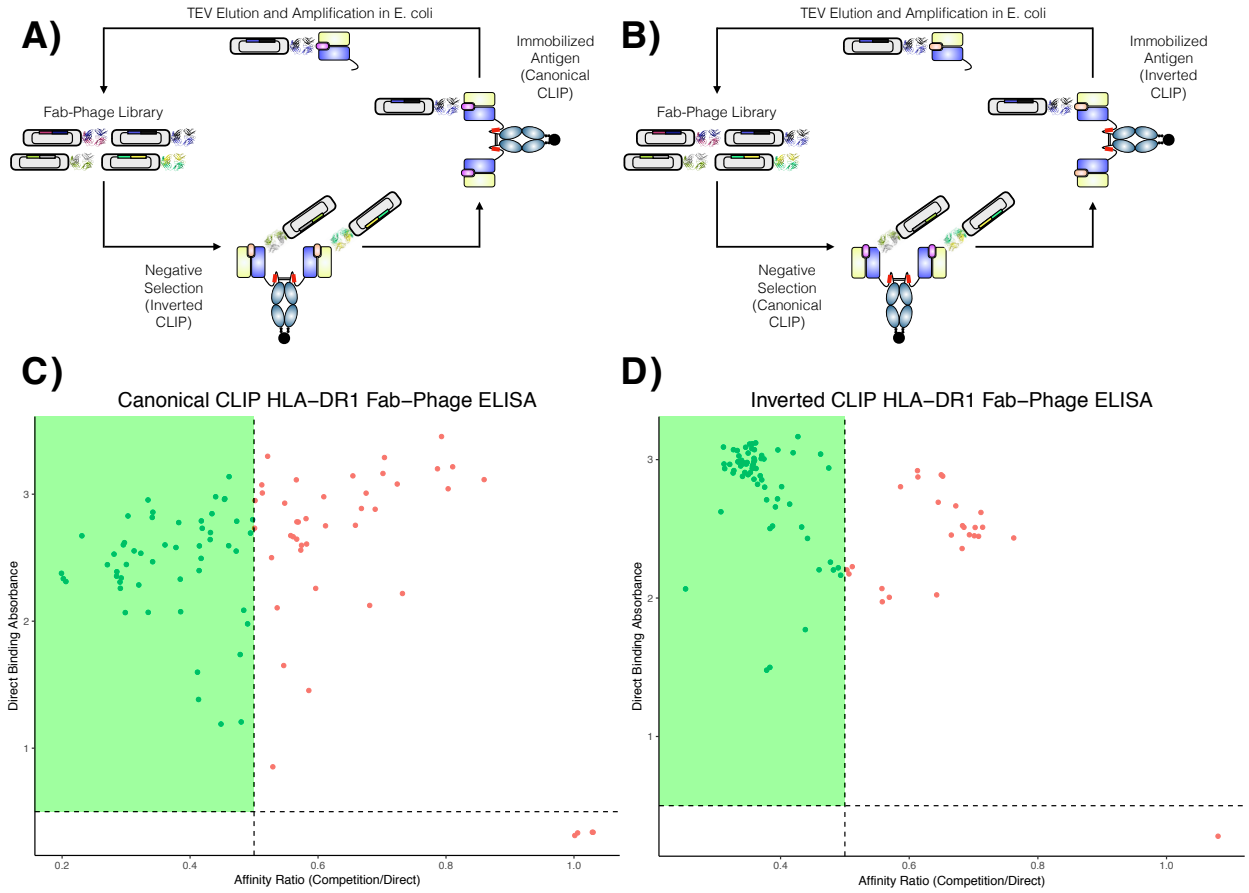

Figure 5.2: Fab-phage display strategy for differential selection of CLIP HLA-DR1 MHC-peptide complexes. A) Selection strategy for the "canonical" CLIP MHC-peptide complex. B) Selection strategy for the "inverted" CLIP MHC-peptide complex. C) Single colony ELISA screen of Fab-phage clones against the "canonical" CLIP MHC-peptide complex. D) Single colony ELISA screen of Fab-phage clones against the "inverted" CLIP MHC-peptide complex.

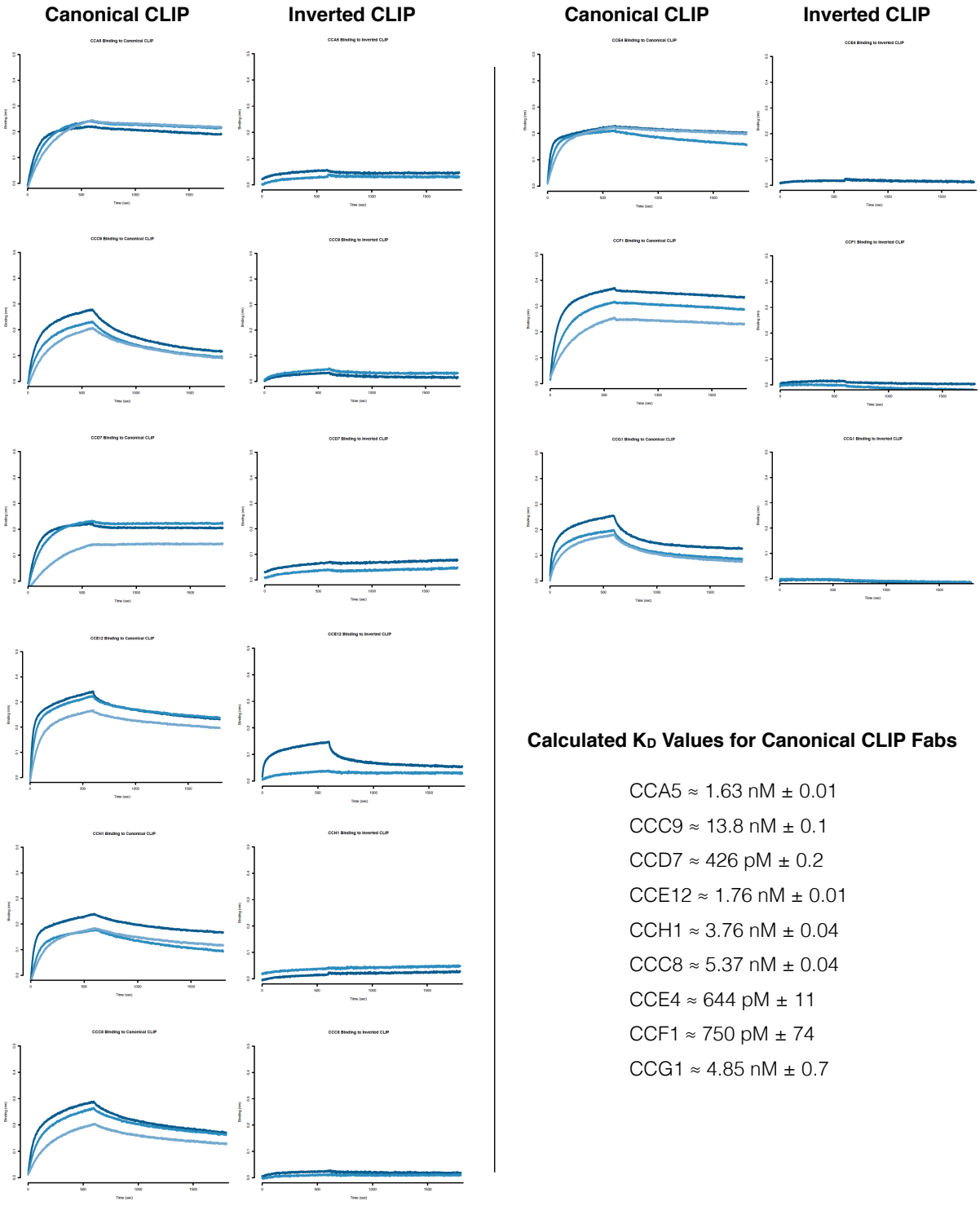

Calculated K_D Values for Canonical CLIP Fabs

CCA5 ≈ 1.63 nM ± 0.01

CCC9 ≈ 13.8 nM ± 0.1

CCD7 ≈ 426 pM ± 0.2

CCE12 ≈ 1.76 nM ± 0.01

CCH1 ≈ 3.76 nM ± 0.04

CCC8 ≈ 5.37 nM ± 0.04

CCE4 ≈ 644 pM ± 11

CCF1 ≈ 750 pM ± 74

CCG1 ≈ 4.85 nM ± 0.7

Figure 5.3: Octet binding of unique Fab hits from our of our ELISA data targeting the canonical CLIP HLA-DR1 MHC-peptide complex. Concentrations for assessing binding to the canonical CLIP MHC-peptide complex are 200 nM, 100 nM, and 50 nM in descending order. Concentrations for assessing binding to the inverted CLIP MHC-peptide complex are 200 nM and 100 nM in descending order.

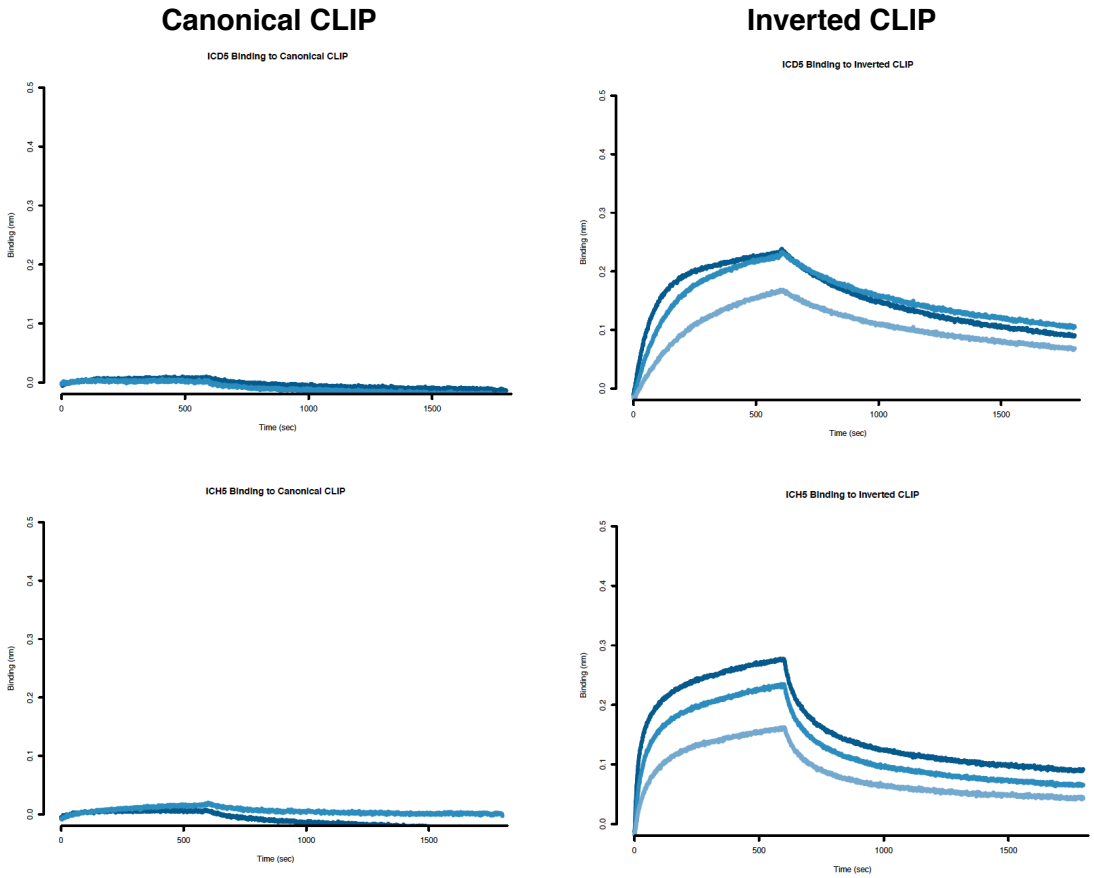

Calculated K_D Values for Inverted CLIP Fabs

ICD5 ≈ 15.4 nM ± 0.1

ICH5 ≈ 80.4 nM ± 0.2

Figure 5.4: Octet binding of unique Fab hits from our of our ELISA data targeting the inverted CLIP HLA-DR1 MHC-peptide complex. Concentrations for assessing binding to the canonical CLIP MHC-peptide complex are 200 nM and 100 nM in descending order. Concentrations for assessing binding to the inverted CLIP MHC-peptide complex are 200 nM, 100 nM, and 50 nM in descending order.

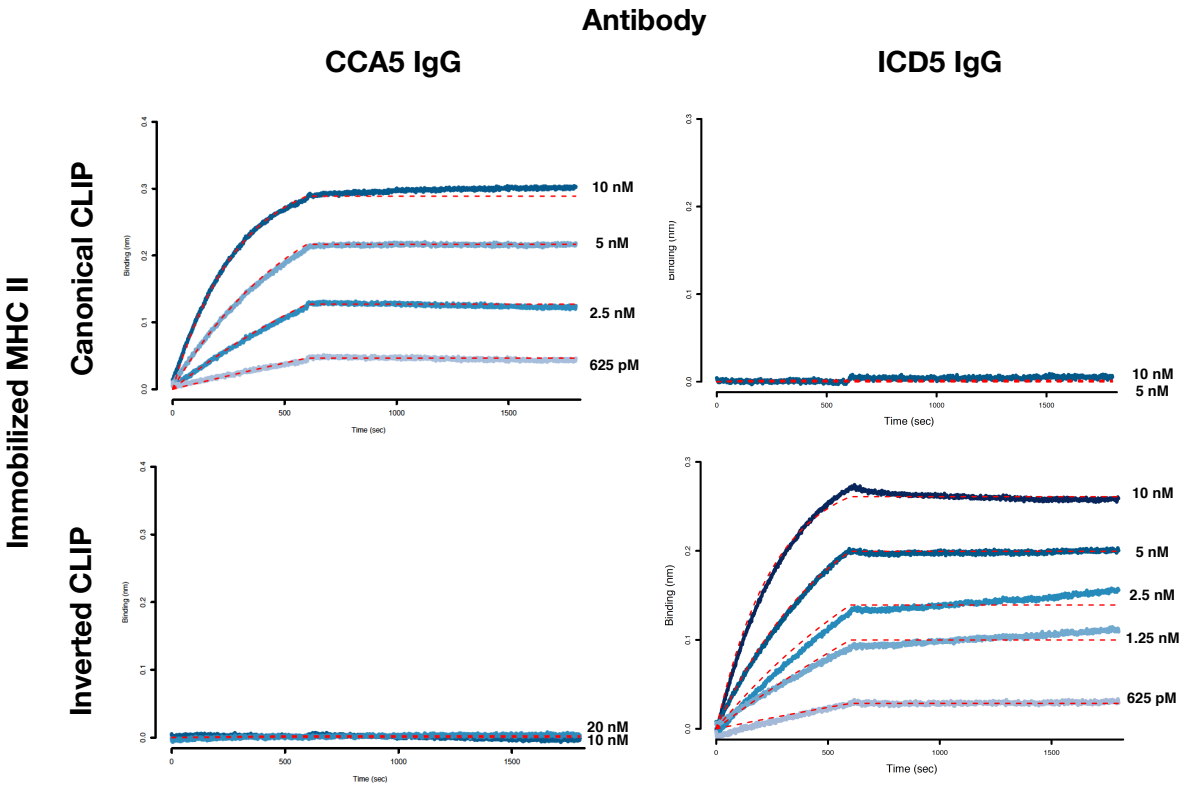

Figure 5.5: Octet binding of CCA5 and ICD5 IgG's against variant CLIP HLA-DR1 MHC-peptide complexes.

References

1. Campisi, J. & d'Adda di Fagagna, F. Cellular senescence: when bad things happen to good cells. *Nat. Rev. Mol. Cell Biol.* **8**, 729–740 (2007).
2. Gorgoulis, V. *et al.* Cellular Senescence: Defining a Path Forward. *Cell* **179**, 813–827 (2019).
3. Masutomi, K. *et al.* Telomerase maintains telomere structure in normal human cells. *Cell* **114**, 241–253 (2003).
4. Ohtani, N., Yamakoshi, K., Takahashi, A. & Hara, E. The p16INK4a-RB pathway: molecular link between cellular senescence and tumor suppression. *J. Med. Investig. JMI* **51**, 146–153 (2004).
5. Rodier, F. *et al.* Persistent DNA damage signalling triggers senescence-associated inflammatory cytokine secretion. *Nat. Cell Biol.* **11**, 973–979 (2009).
6. Serrano, M., Lin, A. W., McCurrach, M. E., Beach, D. & Lowe, S. W. Oncogenic ras provokes premature cell senescence associated with accumulation of p53 and p16INK4a. *Cell* **88**, 593–602 (1997).
7. Wiley, C. D. *et al.* Mitochondrial Dysfunction Induces Senescence with a Distinct Secretory Phenotype. *Cell Metab.* **23**, 303–314 (2016).
8. Coppé, J.-P. *et al.* Senescence-associated secretory phenotypes reveal cell-nonautonomous functions of oncogenic RAS and the p53 tumor suppressor. *PLoS Biol.* **6**, 2853–2868 (2008).
9. Kuilman, T. & Peeper, D. S. Senescence-messaging secretome: SMS-ing cellular stress. *Nat. Rev. Cancer* **9**, 81–94 (2009).

10. Orjalo, A. V., Bhaumik, D., Gengler, B. K., Scott, G. K. & Campisi, J. Cell surface-bound IL-1alpha is an upstream regulator of the senescence-associated IL-6/IL-8 cytokine network. *Proc. Natl. Acad. Sci. U. S. A.* **106**, 17031–17036 (2009).
11. Acosta, J. C. *et al.* A complex secretory program orchestrated by the inflammasome controls paracrine senescence. *Nat. Cell Biol.* **15**, 978–990 (2013).
12. Iannello, A., Thompson, T. W., Ardolino, M., Lowe, S. W. & Raulet, D. H. p53-dependent chemokine production by senescent tumor cells supports NKG2D-dependent tumor elimination by natural killer cells. *J. Exp. Med.* **210**, 2057–2069 (2013).
13. Sagiv, A. *et al.* NKG2D ligands mediate immunosurveillance of senescent cells. *Aging* **8**, 328–344 (2016).
14. Kay, M. M. Mechanism of removal of senescent cells by human macrophages in situ. *Proc. Natl. Acad. Sci. U. S. A.* **72**, 3521–3525 (1975).
15. Burton, D. G. A. & Faragher, R. G. A. Cellular senescence: from growth arrest to immunogenic conversion. *Age Dordr. Neth.* **37**, 27 (2015).
16. Muñoz-Espín, D. & Serrano, M. Cellular senescence: from physiology to pathology. *Nat. Rev. Mol. Cell Biol.* **15**, 482–496 (2014).
17. Akbar, A. N. & Gilroy, D. W. Aging immunity may exacerbate COVID-19. *Science* **369**, 256–257 (2020).
18. Saez-Atienzar, S. & Masliah, E. Cellular senescence and Alzheimer disease: the egg and the chicken scenario. *Nat. Rev. Neurosci.* **21**, 433–444 (2020).
19. Palmer, A. K. *et al.* Cellular Senescence in Type 2 Diabetes: A Therapeutic Opportunity. *Diabetes* **64**, 2289–2298 (2015).
20. van Deursen, J. M. The role of senescent cells in ageing. *Nature* **509**, 439–446 (2014).

21. Zhu, Y. *et al.* The Achilles' heel of senescent cells: from transcriptome to senolytic drugs. *Aging Cell* **14**, 644–658 (2015).
22. Childs, B. G., Durik, M., Baker, D. J. & van Deursen, J. M. Cellular senescence in aging and age-related disease: from mechanisms to therapy. *Nat. Med.* **21**, 1424–1435 (2015).
23. Roy, A. L. *et al.* A Blueprint for Characterizing Senescence. *Cell* **183**, 1143–1146 (2020).
24. Sharpless, N. E. & Sherr, C. J. Forging a signature of in vivo senescence. *Nat. Rev. Cancer* **15**, 397–408 (2015).
25. Leung, K. K. *et al.* Multiomics of azacitidine-treated AML cells reveals variable and convergent targets that remodel the cell-surface proteome. *Proc. Natl. Acad. Sci.* **116**, 695–700 (2019).
26. Kim, K. M. *et al.* Identification of senescent cell surface targetable protein DPP4. *Genes Dev.* **31**, 1529–1534 (2017).
27. Xu, W. *et al.* [The profile of IGF2R gene expression and H3 histone modifications in replicative cell senescence]. *Sichuan Da Xue Xue Bao Yi Xue Ban* **45**, 6–9 (2014).
28. Ruscetti, M. *et al.* NK cell-mediated cytotoxicity contributes to tumor control by a cytostatic drug combination. *Science* **362**, 1416–1422 (2018).
29. Collado, M. *et al.* Senescence in premalignant tumours. *Nature* **436**, 642–642 (2005).
30. Antonangeli, F. *et al.* Natural killer cell recognition of in vivo drug-induced senescent multiple myeloma cells. *Oncoimmunology* **5**, e1218105 (2016).
31. Rapisarda, V. *et al.* Integrin Beta 3 Regulates Cellular Senescence by Activating the TGF-β Pathway. *Cell Rep.* **18**, 2480–2493 (2017).
32. Schinzel, R. T. *et al.* The Hyaluronidase, TMEM2, Promotes ER Homeostasis and Longevity Independent of the UPRER. *Cell* **179**, 1306-1318.e18 (2019).

33. Oh-hashi, K., Imai, K., Koga, H., Hirata, Y. & Kiuchi, K. Knockdown of transmembrane protein 132A by RNA interference facilitates serum starvation-induced cell death in Neuro2a cells. *Mol. Cell. Biochem.* **342**, 117–123 (2010).

34. Leung, K. K. *et al.* Broad and thematic remodeling of the surfaceome and glycoproteome on isogenic cells transformed with driving proliferative oncogenes. *Proc. Natl. Acad. Sci.* **117**, 7764–7775 (2020).

35. Castonguay, R. *et al.* Kinetic Characterization and Identification of the Acylation and Glycosylation Sites of Recombinant Human γ-Glutamyltranspeptidase. *Biochemistry* **46**, 12253–12262 (2007).

36. Fafián-Labora, J. A., Rodríguez-Navarro, J. A. & O'Loghlen, A. Small Extracellular Vesicles Have GST Activity and Ameliorate Senescence-Related Tissue Damage. *Cell Metab.* **32**, 71-86.e5 (2020).

37. Hornsby, M. *et al.* A High Through-put Platform for Recombinant Antibodies to Folded Proteins. *Mol. Cell. Proteomics MCP* **14**, 2833–2847 (2015).

38. Lee, S. & Schmitt, C. A. The dynamic nature of senescence in cancer. *Nat. Cell Biol.* **21**, 94–101 (2019).

39. Rayess, H., Wang, M. B. & Srivatsan, E. S. Cellular senescence and tumor suppressor gene p16. *Int. J. Cancer* **130**, 1715–1725 (2012).

40. de Keizer, P. L. J. The Fountain of Youth by Targeting Senescent Cells? *Trends Mol. Med.* **23**, 6–17 (2017).

41. Demaria, M. *et al.* An essential role for senescent cells in optimal wound healing through secretion of PDGF-AA. *Dev. Cell* **31**, 722–733 (2014).

42. Baker, D. J. *et al.* Clearance of p16Ink4a-positive senescent cells delays ageing-associated disorders. *Nature* **479**, 232–236 (2011).

43. Ogrodnik, M. *et al.* Obesity-Induced Cellular Senescence Drives Anxiety and Impairs Neurogenesis. *Cell Metab.* **29**, 1061-1077.e8 (2019).

44. Bussian, T. J. *et al.* Clearance of senescent glial cells prevents tau-dependent pathology and cognitive decline. *Nature* **562**, 578–582 (2018).

45. Farr, J. N. *et al.* Targeting cellular senescence prevents age-related bone loss in mice. *Nat. Med.* **23**, 1072–1079 (2017).

46. Palmer, A. K. *et al.* Targeting senescent cells alleviates obesity-induced metabolic dysfunction. *Aging Cell* **18**, e12950 (2019).

47. Childs, B. G. *et al.* Senescent intimal foam cells are deleterious at all stages of atherosclerosis. *Science* **354**, 472–477 (2016).

48. Jeon, O. H. *et al.* Local clearance of senescent cells attenuates the development of post-traumatic osteoarthritis and creates a pro-regenerative environment. *Nat. Med.* **23**, 775–781 (2017).

49. Xu, M. *et al.* Targeting senescent cells enhances adipogenesis and metabolic function in old age. *eLife* **4**, e12997 (2015).

50. Ogrodnik, M. *et al.* Cellular senescence drives age-dependent hepatic steatosis. *Nat. Commun.* **8**, 15691 (2017).

51. Chinta, S. J. *et al.* Cellular Senescence Is Induced by the Environmental Neurotoxin Paraquat and Contributes to Neuropathology Linked to Parkinson's Disease. *Cell Rep.* **22**, 930–940 (2018).

52. Schafer, M. J. *et al.* Cellular senescence mediates fibrotic pulmonary disease. *Nat. Commun.* **8**, 14532 (2017).

53. Baar, M. P. *et al.* Targeted Apoptosis of Senescent Cells Restores Tissue Homeostasis in Response to Chemotoxicity and Aging. *Cell* **169**, 132-147.e16 (2017).

54. Baker, D. J. *et al.* Naturally occurring p16(Ink4a)-positive cells shorten healthy lifespan. *Nature* **530**, 184–189 (2016).

55. Demaria, M. *et al.* Cellular Senescence Promotes Adverse Effects of Chemotherapy and Cancer Relapse. *Cancer Discov.* **7**, 165–176 (2017).

56. Harding, C. V. Class I MHC presentation of exogenous antigens. *J. Clin. Immunol.* **16**, 90–96 (1996).

57. Neefjes, J., Jongsma, M. L. M., Paul, P. & Bakke, O. Towards a systems understanding of MHC class I and MHC class II antigen presentation. *Nat. Rev. Immunol.* **11**, 823–836 (2011).

58. Falk, K., Rötzschke, O., Stevanović, S., Jung, G. & Rammensee, H. G. Allele-specific motifs revealed by sequencing of self-peptides eluted from MHC molecules. *Nature* **351**, 290–296 (1991).

59. Nelde, A., Rammensee, H.-G. & Walz, J. S. The Peptide Vaccine of the Future. *Mol. Cell. Proteomics MCP* **20**, 100022 (2021).

60. Hawkins, O. E. *et al.* Identification of breast cancer peptide epitopes presented by HLA-A*0201. *J. Proteome Res.* **7**, 1445–1457 (2008).

61. Jain, R., Rawat, A., Verma, B., Markiewski, M. M. & Weidanz, J. A. Antitumor activity of a monoclonal antibody targeting major histocompatibility complex class I-Her2 peptide complexes. *J. Natl. Cancer Inst.* **105**, 202–218 (2013).

62. Neefjes, J. & Ovaa, H. A peptide's perspective on antigen presentation to the immune system. *Nat. Chem. Biol.* **9**, 769–775 (2013).

63. Khodadoust, M. S. *et al.* Antigen presentation profiling reveals recognition of lymphoma immunoglobulin neoantigens. *Nature* **543**, 723–727 (2017).

64. Klechevsky, E. *et al.* Antitumor activity of immunotoxins with T-cell receptor-like specificity against human melanoma xenografts. *Cancer Res.* **68**, 6360–6367 (2008).

65. Dao, T. *et al.* Targeting the intracellular WT1 oncogene product with a therapeutic human antibody. *Sci. Transl. Med.* **5**, 176ra33 (2013).

66. Veomett, N. *et al.* Therapeutic efficacy of an Fc-enhanced TCR-like antibody to the intracellular WT1 oncoprotein. *Clin. Cancer Res. Off. J. Am. Assoc. Cancer Res.* **20**, 4036–4046 (2014).

67. Dao, T. *et al.* Therapeutic bispecific T-cell engager antibody targeting the intracellular oncoprotein WT1. *Nat. Biotechnol.* **33**, 1079–1086 (2015).

68. Pereira, B. I. *et al.* Senescent cells evade immune clearance via HLA-E-mediated NK and CD8+ T cell inhibition. *Nat. Commun.* **10**, 2387 (2019).

69. Chen, X., Barton, L. F., Chi, Y., Clurman, B. E. & Roberts, J. M. Ubiquitin-independent degradation of cell-cycle inhibitors by the REGgamma proteasome. *Mol. Cell* **26**, 843–852 (2007).

70. Li, J., Poi, M. J. & Tsai, M.-D. Regulatory mechanisms of tumor suppressor P16(INK4A) and their relevance to cancer. *Biochemistry* **50**, 5566–5582 (2011).

71. Lu, Y., Ma, W., Li, Z., Lu, J. & Wang, X. The interplay between p16 serine phosphorylation and arginine methylation determines its function in modulating cellular apoptosis and senescence. *Sci. Rep.* **7**, 41390 (2017).

72. Vyas, J. M., Van der Veen, A. G. & Ploegh, H. L. The known unknowns of antigen processing and presentation. *Nat. Rev. Immunol.* **8**, 607–618 (2008).

73. Nielsen, M., Andreatta, M., Peters, B. & Buus, S. Immunoinformatics: Predicting Peptide–MHC Binding. *Annu. Rev. Biomed. Data Sci.* **3**, 191–215 (2020).

74. Trowsdale, J. & Knight, J. C. Major histocompatibility complex genomics and human disease. *Annu. Rev. Genomics Hum. Genet.* **14**, 301–323 (2013).

75. Boegel, S., Löwer, M., Bukur, T., Sahin, U. & Castle, J. C. A catalog of HLA type, HLA expression, and neo-epitope candidates in human cancer cell lines. *Oncoimmunology* **3**, e954893 (2014).

76. Abelin, J. G. *et al.* Mass Spectrometry Profiling of HLA-Associated Peptidomes in Mono-allelic Cells Enables More Accurate Epitope Prediction. *Immunity* **46**, 315–326 (2017).

77. Spencer, C. T. *et al.* Viral infection causes a shift in the self peptide repertoire presented by human MHC class I molecules. *Proteomics Clin. Appl.* **9**, 1035–1052 (2015).

78. Høydahl, L. S., Frick, R., Sandlie, I. & Løset, G. Å. Targeting the MHC Ligandome by Use of TCR-Like Antibodies. *Antibodies Basel Switz.* **8**, E32 (2019).

79. Holland, C. J. *et al.* Specificity of bispecific T cell receptors and antibodies targeting peptide-HLA. *J. Clin. Invest.* **130**, 2673–2688 (2020).

80. Douglass, J. *et al.* Bispecific antibodies targeting mutant RAS neoantigens. *Sci. Immunol.* **6**, eabd5515 (2021).

81. Hsiue, E. H.-C. *et al.* Targeting a neoantigen derived from a common TP53 mutation. *Science* **371**, eabc8697 (2021).

82. Stone, J. D., Aggen, D. H., Schietinger, A., Schreiber, H. & Kranz, D. M. A sensitivity scale for targeting T cells with chimeric antigen receptors (CARs) and bispecific T-cell Engagers (BiTEs). *Oncoimmunology* **1**, 863–873 (2012).

83. Amor, C. *et al.* Senolytic CAR T cells reverse senescence-associated pathologies. *Nature* **583**, 127–132 (2020).

84. Zhao, Q. *et al.* Affinity maturation of T-cell receptor-like antibodies for Wilms tumor 1 peptide greatly enhances therapeutic potential. *Leukemia* **29**, 2238–2247 (2015).

85. Koerber, J. T., Hornsby, M. J. & Wells, J. A. An improved single-chain Fab platform for efficient display and recombinant expression. *J. Mol. Biol.* **427**, 576–586 (2015).

86. Morris, E. *et al.* Generation of tumor-specific T-cell therapies. *Blood Rev.* **20**, 61–69 (2006).

87. Ewald, J. A., Desotelle, J. A., Wilding, G. & Jarrard, D. F. Therapy-induced senescence in cancer. *J. Natl. Cancer Inst.* **102**, 1536–1546 (2010).

88. Rodier, F. *et al.* DNA-SCARS: distinct nuclear structures that sustain damage-induced senescence growth arrest and inflammatory cytokine secretion. *J. Cell Sci.* **124**, 68–81 (2011).

89. Tonnessen-Murray, C. A. *et al.* Chemotherapy-induced senescent cancer cells engulf other cells to enhance their survival. *J. Cell Biol.* **218**, 3827–3844 (2019).

90. Hubackova, S. *et al.* Selective elimination of senescent cells by mitochondrial targeting is regulated by ANT2. *Cell Death Differ.* **26**, 276–290 (2019).

91. Yosef, R. *et al.* Directed elimination of senescent cells by inhibition of BCL-W and BCL-XL. *Nat. Commun.* **7**, 11190 (2016).

92. He, S. & Sharpless, N. E. Senescence in Health and Disease. *Cell* **169**, 1000–1011 (2017).

93. Chang, J. *et al.* Clearance of senescent cells by ABT263 rejuvenates aged hematopoietic stem cells in mice. *Nat. Med.* **22**, 78–83 (2016).

94. Zhu, Y. *et al.* Identification of a novel senolytic agent, navitoclax, targeting the Bcl-2 family of anti-apoptotic factors. *Aging Cell* **15**, 428–435 (2016).

95. Hickson, L. J. *et al.* Senolytics decrease senescent cells in humans: Preliminary report from a clinical trial of Dasatinib plus Quercetin in individuals with diabetic kidney disease. *EBioMedicine* **47**, 446–456 (2019).

96. Kirkland, J. L., Tchkonia, T., Zhu, Y., Niedernhofer, L. J. & Robbins, P. D. The Clinical Potential of Senolytic Drugs. *J. Am. Geriatr. Soc.* **65**, 2297–2301 (2017).

97. Zhang, P. *et al.* Senolytic therapy alleviates Aβ-associated oligodendrocyte progenitor cell senescence and cognitive deficits in an Alzheimer's disease model. *Nat. Neurosci.* **22**, 719–728 (2019).

98. Le Roux, I., Konge, J., Le Cam, L., Flamant, P. & Tajbakhsh, S. Numb is required to prevent p53-dependent senescence following skeletal muscle injury. *Nat. Commun.* **6**, 8528 (2015).

99. Chiche, A. *et al.* Injury-Induced Senescence Enables In Vivo Reprogramming in Skeletal Muscle. *Cell Stem Cell* **20**, 407-414.e4 (2017).

100. Krizhanovsky, V. *et al.* Senescence of activated stellate cells limits liver fibrosis. *Cell* **134**, 657–667 (2008).

101. Muñoz-Espín, D. *et al.* Programmed cell senescence during mammalian embryonic development. *Cell* **155**, 1104–1118 (2013).

102. Helman, A. *et al.* p16(Ink4a)-induced senescence of pancreatic beta cells enhances insulin secretion. *Nat. Med.* **22**, 412–420 (2016).

103. Grosse, L. *et al.* Defined p16High Senescent Cell Types Are Indispensable for Mouse Healthspan. *Cell Metab.* **32**, 87-99.e6 (2020).

104. Hall, B. M. *et al.* p16(Ink4a) and senescence-associated β-galactosidase can be induced in macrophages as part of a reversible response to physiological stimuli. *Aging* **9**, 1867–1884 (2017).

105. Hyrenius-Wittsten, A. *et al.* SynNotch CAR circuits enhance solid tumor recognition and promote persistent antitumor activity in mouse models. *Sci. Transl. Med.* **13**, eabd8836 (2021).

106. Kloss, C. C., Condomines, M., Cartellieri, M., Bachmann, M. & Sadelain, M. Combinatorial antigen recognition with balanced signaling promotes selective tumor eradication by engineered T cells. *Nat. Biotechnol.* **31**, 71–75 (2013).

107. Cho, J. H., Collins, J. J. & Wong, W. W. Universal Chimeric Antigen Receptors for Multiplexed and Logical Control of T Cell Responses. *Cell* **173**, 1426-1438.e11 (2018).

108. Choi, B. D. *et al.* CAR-T cells secreting BiTEs circumvent antigen escape without detectable toxicity. *Nat. Biotechnol.* **37**, 1049–1058 (2019).

109. Rodenko, B. *et al.* Generation of peptide-MHC class I complexes through UV-mediated ligand exchange. *Nat. Protoc.* **1**, 1120–1132 (2006).

110. Stopfer, L. E. *et al. MEK inhibition enhances presentation of targetable MHC-I tumor antigens in mutant melanomas*. 2022.01.10.475285 https://www.biorxiv.org/content/10.1101/2022.01.10.475285v1 (2022) doi:10.1101/2022.01.10.475285.

111. Caron, E. *et al.* Analysis of Major Histocompatibility Complex (MHC) Immunopeptidomes Using Mass Spectrometry*. *Mol. Cell. Proteomics* **14**, 3105–3117 (2015).

112. Pollock, S. B. *et al.* Sensitive and Quantitative Detection of MHC-I Displayed Neoepitopes Using a Semiautomated Workflow and TOMAHAQ Mass Spectrometry. *Mol. Cell. Proteomics* **20**, (2021).

113. Purcell, A. W., Ramarathinam, S. H. & Ternette, N. Mass spectrometry–based identification of MHC-bound peptides for immunopeptidomics. *Nat. Protoc.* **14**, 1687–1707 (2019).

114. Sarkizova, S. *et al.* A large peptidome dataset improves HLA class I epitope prediction across most of the human population. *Nat. Biotechnol.* **38**, 199–209 (2020).

115. Hilton, H. G. *et al.* The Intergenic Recombinant HLA-B∗46:01 Has a Distinctive Peptidome that Includes KIR2DL3 Ligands. *Cell Rep.* **19**, 1394–1405 (2017).

116. Martinko, A. J. *et al.* Targeting RAS-driven human cancer cells with antibodies to upregulated and essential cell-surface proteins. *eLife* **7**, e31098 (2018).

117. Czajkowsky, D. M., Hu, J., Shao, Z. & Pleass, R. J. Fc-fusion proteins: new developments and future perspectives. *EMBO Mol. Med.* **4**, 1015–1028 (2012).

118. Yuen, A. & Díaz, B. The impact of hypoxia in pancreatic cancer invasion and metastasis. *Hypoxia* **2**, 91–106 (2014).

119. Jan, Y.-H. *et al.* Adenylate kinase 4 modulates oxidative stress and stabilizes HIF-1α to drive lung adenocarcinoma metastasis. *J. Hematol. Oncol.J Hematol Oncol* **12**, 12 (2019).

120. Godet, I. *et al.* Fate-mapping post-hypoxic tumor cells reveals a ROS-resistant phenotype that promotes metastasis. *Nat. Commun.* **10**, 4862 (2019).

121. Knaup, K. X. *et al.* Hypoxia regulates the sperm associated antigen 4 (SPAG4) via HIF, which is expressed in renal clear cell carcinoma and promotes migration and invasion in vitro. *Mol. Carcinog.* **53**, 970–978 (2014).

122. Gonçalves, S. *et al.* COX2 regulates senescence secretome composition and senescence surveillance through PGE2. *Cell Rep.* **34**, 108860 (2021).

123. Catherman, A. D. *et al.* Large-scale Top-down Proteomics of the Human Proteome: Membrane Proteins, Mitochondria, and Senescence. *Mol. Cell. Proteomics* **12**, 3465–3473 (2013).

124. Meier, F. *et al.* diaPASEF: parallel accumulation–serial fragmentation combined with data-independent acquisition. *Nat. Methods* **17**, 1229–1236 (2020).

125. Davies, H. *et al.* Mutations of the BRAF gene in human cancer. *Nature* **417**, 949–954 (2002).

126. Muñoz-Couselo, E., Adelantado, E. Z., Ortiz, C., García, J. S. & Perez-Garcia, J. NRAS-mutant melanoma: current challenges and future prospect. *OncoTargets Ther.* **10**, 3941–3947 (2017).

127. Falchook, G. S. *et al.* Activity of the oral MEK inhibitor trametinib in patients with advanced melanoma: a phase 1 dose-escalation trial. *Lancet Oncol.* **13**, 782–789 (2012).

128. Flaherty, K. T. *et al.* Improved Survival with MEK Inhibition in BRAF-Mutated Melanoma. *http://dx.doi.org/10.1056/NEJMoa1203421* https://www.nejm.org/doi/10.1056/NEJMoa1203421 (2012) doi:10.1056/NEJMoa1203421.

129. Sullivan, R. J., LoRusso, P. M. & Flaherty, K. T. The Intersection of Immune-Directed and Molecularly Targeted Therapy in Advanced Melanoma: Where We Have Been, Are, and Will Be. *Clin. Cancer Res.* **19**, 5283–5291 (2013).

130. Long, G. V. *et al.* COMBI-d: A randomized, double-blinded, Phase III study comparing the combination of dabrafenib and trametinib to dabrafenib and trametinib placebo as first-line therapy in patients (pts) with unresectable or metastatic BRAFV600E/K mutation-positive cutaneous melanoma. *J. Clin. Oncol.* **32**, 9011–9011 (2014).

131. Dummer, R. *et al.* Binimetinib versus dacarbazine in patients with advanced NRAS-mutant melanoma (NEMO): a multicentre, open-label, randomised, phase 3 trial. *Lancet Oncol.* **18**, 435–445 (2017).

132. Lim, S. Y., Menzies, A. M. & Rizos, H. Mechanisms and strategies to overcome resistance to molecularly targeted therapy for melanoma. *Cancer* **123**, 2118–2129 (2017).

133. Robert, C. *et al.* Five-Year Outcomes with Dabrafenib plus Trametinib in Metastatic Melanoma. *N. Engl. J. Med.* **381**, 626–636 (2019).

134. Larkin, J. *et al.* Combined Nivolumab and Ipilimumab or Monotherapy in Untreated Melanoma. *N. Engl. J. Med.* **373**, 23–34 (2015).

135. Hodi, F. S. *et al.* Nivolumab plus ipilimumab or nivolumab alone versus ipilimumab alone in advanced melanoma (CheckMate 067): 4-year outcomes of a multicentre, randomised, phase 3 trial. *Lancet Oncol.* **19**, 1480–1492 (2018).

136. Martins, F. *et al.* Adverse effects of immune-checkpoint inhibitors: epidemiology, management and surveillance. *Nat. Rev. Clin. Oncol.* **16**, 563–580 (2019).

137. Weiss, S. A., Wolchok, J. D. & Sznol, M. Immunotherapy of Melanoma: Facts and Hopes. *Clin. Cancer Res. Off. J. Am. Assoc. Cancer Res.* **25**, 5191–5201 (2019).

138. Boni, A. *et al.* Selective BRAFV600E inhibition enhances T-cell recognition of melanoma without affecting lymphocyte function. *Cancer Res.* **70**, 5213–5219 (2010).

139. Hu-Lieskovan, S. *et al.* Improved antitumor activity of immunotherapy with BRAF and MEK inhibitors in BRAFV600E melanoma. *Sci. Transl. Med.* (2015) doi:10.1126/scitranslmed.aaa4691.

140. Brea, E. J. *et al.* Kinase Regulation of Human MHC Class I Molecule Expression on Cancer Cells. *Cancer Immunol. Res.* **4**, 936–947 (2016).

141. Homet Moreno, B., Mok, S., Comin-Anduix, B., Hu-Lieskovan, S. & Ribas, A. Combined treatment with dabrafenib and trametinib with immune-stimulating antibodies for BRAF mutant melanoma. *OncoImmunology* **5**, e1052212 (2016).

142. Kirchberger, M. C. *et al.* MEK inhibition may increase survival of NRAS-mutated melanoma patients treated with checkpoint blockade: Results of a retrospective multicentre analysis of 364 patients. *Eur. J. Cancer* **98**, 10–16 (2018).

143. Ascierto, P. A. *et al.* Dabrafenib, trametinib and pembrolizumab or placebo in BRAF-mutant melanoma. *Nat. Med.* **25**, 941–946 (2019).

144. Ribas, A. *et al.* PD-L1 blockade in combination with inhibition of MAPK oncogenic signaling in patients with advanced melanoma. *Nat. Commun.* **11**, 6262 (2020).

145. Vella, L. J. *et al.* The kinase inhibitors dabrafenib and trametinib affect isolated immune cell populations. *Oncoimmunology* **3**, e946367 (2014).

146. Jaeger, A. M. *et al.* Rebalancing Protein Homeostasis Enhances Tumor Antigen Presentation. *Clin. Cancer Res.* **25**, 6392–6405 (2019).

147. Murphy, J. P. *et al.* Multiplexed Relative Quantitation with Isobaric Tagging Mass Spectrometry Reveals Class I Major Histocompatibility Complex Ligand Dynamics in Response to Doxorubicin. *Anal. Chem.* **91**, 5106–5115 (2019).

148. Stopfer, L. E., Mesfin, J. M., Joughin, B. A., Lauffenburger, D. A. & White, F. M. Multiplexed relative and absolute quantitative immunopeptidomics reveals MHC I repertoire alterations induced by CDK4/6 inhibition. *Nat. Commun.* **11**, 2760 (2020).

149. Liddy, N. *et al.* Monoclonal TCR-redirected tumor cell killing. *Nat. Med.* **18**, 980–987 (2012).

150. Lowe, D. B. *et al.* TCR-like antibody drug conjugates mediate killing of tumor cells with low peptide/HLA targets. *mAbs* **9**, 603–614 (2017).

151. Lai, J. *et al.* Elimination of melanoma by sortase A-generated TCR-like antibody-drug conjugates (TL-ADCs) targeting intracellular melanoma antigen MART-1. *Biomaterials* **178**, 158–169 (2018).

152. Stopfer, L. E. *et al.* Absolute quantification of tumor antigens using embedded MHC-I isotopologue calibrants. *Proc. Natl. Acad. Sci. U. S. A.* **118**, e2111173118 (2021).

153. Gonzalez-Galarza, F. F. *et al.* Allele frequency net database (AFND) 2020 update: gold-standard data classification, open access genotype data and new query tools. *Nucleic Acids Res.* **48**, D783–D788 (2020).

154. Middleton, M. R. *et al.* Tebentafusp, A TCR/Anti-CD3 Bispecific Fusion Protein Targeting gp100, Potently Activated Antitumor Immune Responses in Patients with Metastatic Melanoma. *Clin. Cancer Res.* **26**, 5869–5878 (2020).

155. Gobin, S. J. P., Zutphen, M. van, Woltman, A. M. & Elsen, P. J. van den. Transactivation of Classical and Nonclassical HLA Class I Genes Through the IFN-Stimulated Response Element. *J. Immunol.* **163**, 1428–1434 (1999).

156. Castro, F., Cardoso, A. P., Gonçalves, R. M., Serre, K. & Oliveira, M. J. Interferon-Gamma at the Crossroads of Tumor Immune Surveillance or Evasion. *Front. Immunol.* **9**, (2018).

157. Zhang, Y., Chen, Y., Liu, Z. & Lai, R. ERK is a negative feedback regulator for IFN-γ/STAT1 signaling by promoting STAT1 ubiquitination. *BMC Cancer* **18**, 613 (2018).

158. Yang, L. & Ding, J. L. MEK1/2 Inhibitors Unlock the Constrained Interferon Response in Macrophages Through IRF1 Signaling. *Front. Immunol.* **10**, 2020 (2019).

159. Goel, S. *et al.* CDK4/6 inhibition triggers anti-tumour immunity. *Nature* **548**, 471–475 (2017).

160. Stopfer, L. E., Mesfin, J. M., Joughin, B. A., Lauffenburger, D. A. & White, F. M. Multiplexed relative and absolute quantitative immunopeptidomics reveals MHC I repertoire alterations induced by CDK4/6 inhibition. *Nat. Commun.* **11**, 2760 (2020).

161. Stopfer, L. E., Conage-Pough, J. E. & White, F. M. Quantitative Consequences of Protein Carriers in Immunopeptidomics and Tyrosine Phosphorylation MS2 Analyses. *Mol. Cell. Proteomics* **20**, (2021).

162. Johnson, L. A. *et al.* Gene therapy with human and mouse T-cell receptors mediates cancer regression and targets normal tissues expressing cognate antigen. *Blood* **114**, 535–546 (2009).

163. Parkhurst, M. R. *et al.* T Cells Targeting Carcinoembryonic Antigen Can Mediate Regression of Metastatic Colorectal Cancer but Induce Severe Transient Colitis. *Mol. Ther.* **19**, 620–626 (2011).

164. Morgan, R. A. *et al.* Cancer Regression and Neurological Toxicity Following Anti-MAGE-A3 TCR Gene Therapy. *J. Immunother.* **36**, 133–151 (2013).

165. Stopfer, L. E., D'Souza, A. D. & White, F. M. 1,2,3, MHC: a review of mass-spectrometry-based immunopeptidomics methods for relative and absolute quantification of pMHCs. *Immuno-Oncol. Technol.* **11**, (2021).

166. Yarmarkovich, M. *et al.* Cross-HLA targeting of intracellular oncoproteins with peptide-centric CARs. *Nature* **599**, 477–484 (2021).

167. Chaganty, B. K. R. *et al.* Trastuzumab upregulates expression of HLA-ABC and T cell costimulatory molecules through engagement of natural killer cells and stimulation of IFNγ secretion. *OncoImmunology* **5**, e1100790 (2016).

168. Iwai, T. *et al.* Topoisomerase I inhibitor, irinotecan, depletes regulatory T cells and up-regulates MHC class I and PD-L1 expression, resulting in a supra-additive antitumor effect when combined with anti-PD-L1 antibodies. *Oncotarget* **9**, 31411–31421 (2018).

169. Ridgway, J. B. B., Presta, L. G. & Carter, P. 'Knobs-into-holes' engineering of antibody CH3 domains for heavy chain heterodimerization. *Protein Eng. Des. Sel.* **9**, 617–621 (1996).

170. Browne, C. M. *et al.* A Chemoproteomic Strategy for Direct and Proteome-Wide Covalent Inhibitor Target-Site Identification. *J. Am. Chem. Soc.* **141**, 191–203 (2019).

171. Günther, S. *et al.* Bidirectional binding of invariant chain peptides to an MHC class II molecule. *Proc. Natl. Acad. Sci.* **107**, 22219–22224 (2010).

Publishing Agreement

It is the policy of the University to encourage open access and broad distribution of all theses, dissertations, and manuscripts. The Graduate Division will facilitate the distribution of UCSF theses, dissertations, and manuscripts to the UCSF Library for open access and distribution. UCSF will make such theses, dissertations, and manuscripts accessible to the public and will take reasonable steps to preserve these works in perpetuity.

I hereby grant the non-exclusive, perpetual right to The Regents of the University of California to reproduce, publicly display, distribute, preserve, and publish copies of my thesis, dissertation, or manuscript in any form or media, now existing or later derived, including access online for teaching, research, and public service purposes.

DocuSigned by:
Rettko, Nicholas
C9DE9CE96F8B4D6...
Author Signature

1/25/2022
Date